Glass-to-crystal transition in a chiral pharmaceutical system

Quentin Viel

Normandie Université

THÈSE

Pour obtenir le diplôme de doctorat

Spécialité Physique-Chimie

Préparée au sein de l'Université de Rouen Normandie

De l'Amorphe au Cristal : Etude d'un Composé Pharmaceutique Chiral

Présentée et soutenue par

Quentin VIEL

Thèse soutenue publiquement le 16 Juin 2017 devant le jury composé de		
M. Marc DESCAMPS	Pr. UMET Université de Lille 1	Rapporteur
M. François PUEL	Pr. LGPM CentraleSupélec Paris	Rapporteur
Mme. Géraldine GOUHIER	Pr. COBRA Université de Rouen Normandie	Examinatrice
Mme. Emeline DUDOGNON	MCF. UMET Université de Lille 1	Examinatrice
M. Éric DARGENT	Pr. GPM Université de Rouen Normandie	Directeur de thèse
M. Samuel PETIT	Pr. SMS Université de Rouen Normandie	Co-directeur de thèse

Thèse dirigée par Éric DARGENT et Samuel PETIT, laboratoires GPM UMR 6634 et SMS EA 3233

UNIVERSITÉ DE ROUEN NORMANDIE

ED PSIME

SMS Sciences et Méthodes Séparatives

GPM

Normandie Université

PhD THESIS

In view to obtain the degree of Doctor of Philosophy in Science

Specialty: Physical Chemistry

Submitted to the Faculty of Science-University of Rouen Normandie

Glass-to-crystal Transition in a Chiral Pharmaceutical System

Presented and defended by

Quentin VIEL

Defended the June, 16th 2017 in front of the dissertation committee composed of		
Mr. Marc DESCAMPS	Pr. UMET Université de Lille 1	Reviewer
Mr. François PUEL	Pr. LGPM CentraleSupélec Paris	Reviewer
Mrs. Géraldine GOUHIER	Pr. COBRA Université de Rouen Normandie	Examiner
Mrs. Emeline DUDOGNON	MCF. UMET Université de Lille 1	Examiner
Mr. Eric DARGENT	Pr. GPM Université de Rouen Normandie	Advisor
Mr. Samuel PETIT	Pr. SMS Université de Rouen Normandie	Co-advisor

Supervised by Eric DARGENT and Samuel PETIT, GPM UMR 6634 and SMS EA 3233 laboratories

UNIVERSITÉ DE ROUEN NORMANDIE

ED PSIME

SMS Sciences et Méthodes Séparatives

GPM

A ma famille et à mes amis

Remerciements

Ces quelques lignes permettront de rendre hommage aux personnes qui ont contribué à l'accès puis à l'aboutissement de cette thèse. J'exprimerai donc ici ma profonde gratitude en mentionnant votre nom ou en laissant un témoignage, une anecdote, une description et/ou mon ressenti en ce qui vous concerne.

Mes tous premiers remerciements sont adressés aux deux responsables scientifiques du projet au nom que j'apprécie particulièrement : AC/DC (Amorphous to Crystals/Defective Crystals). Je pense donc à Eric Dargent et Gérard Coquerel.

En ce qui concerne le professeur Eric Dargent, directeur de ma thèse, et maintenant vice-président de l'université de Rouen : je te remercie pour le respect, la droiture, et l'endurance au travail qui sont des valeurs qui me sont chères… J'ai sincèrement apprécié de travailler ensemble, sur une thématique qui s'éloignait de la spécificité du Lecap (maintenant Eircap). Tu as su rester ouvert d'esprit et disponible même parfois sur tes horaires de repos. Un grand merci.

Pour le professeur Gérard Coquerel, et directeur du laboratoire SMS : votre passion et votre engagement dans ce que vous faites me marquera toujours. Je vous remercie d'avoir participé grandement à susciter mon intérêt sur votre discipline scientifique.

Pour le professeur Samuel Petit, co-directeur de ma thèse : je te remercie pour ta rigueur sur le plan scientifique (et sur l'anglais), ce qui ne m'a pas fait passer de très bons moments lors de ces trois années et demi, mais ce qui m'a fait grandir... Je n'oublierai pas les réunions des deux premières années de thèse ou tu partageais tes connaissances et ta passion lors des interprétations des résultats que j'apportais.

Je remercie également Yohann Cartigny (MCF) qui a participé aux réunions que je mentionne ci-dessus et qui a été de très bon conseil lors des relectures de mes travaux. Je tiens à remercier chaleureusement Clément Brandel (doctorant à mon arrivée au laboratoire et MCF maintenant) pour m'avoir grandement aidé sur certains aspects scientifiques, et pour avoir mené un travail de haute qualité sur la DPL sur lequel j'ai pu m'appuyer pour apporter ma contribution.

Je veux maintenant remercier les membres de mon jury de thèse : le professeur Marc Descamps, le professeur François Puel, la professeure Geraldine Gouhier et la maitre de conférences Emeline Dudognon. Vos commentaires et vos questions étaient vraiment constructifs, ce qui a rendu cette soutenance encore plus intéressante.

Pour les deux collaborateurs européens :
En Italie à l'université de Pise, je souhaiterais remercier trois personnes spécialement : Daniele Prevosto (anciennement MCF ou équivalent), Simone Capaccioli (professeur) et Allisson Saiter (MCF). J'ai adoré mon passage en Italie, certes les résultats étaient peu concluants mais très prometteurs en un mois de travail (c'est souvent comme ça avec la DPL), mais on se sait jamais ce qu'il peut se passer par la suite… Je n'oublie pas les techniciens ou ingénieurs de recherches qui étaient très sympas au sein du laboratoire.

Au Portugal à l'université de Coimbra : je remercie chaleureusement Ermelinda Eusébio et Joao Canotilho qui sont des gens très accueillants et d'une rare gentillesse. Les observations que j'ai pu faire sur la recristallisation de la DPL par microscopie ont fait avancer mes travaux de façon exponentielle… Un grand merci et j'espère que les collaborations continueront avec vous.

Je remercie ici sincèrement les stagiaires qui ont participé à faire évoluer ma thèse : Manon, Laura, Aurélien, Maxime, j'espère que vous aurez autant de chance que moi à rencontrer de bonnes personnes dans vos futurs parcours.

En ce qui concerne maintenant les personnes des laboratoires, d'abord au SMS : merci aux permanents pour vos contributions scientifiques : Valérie Dupray (Raman,…), Nicolas Couvrat (TG-DSC, DSC, RX température…), Morgane Sanselme (RX,…), Gabin Gbabode (RX, spray drying,…), Marie Vaccaro, Pascal Cardinael et Valérie Agasse (Chromato !). Et un grand merci aux doctorants qui ont réussi à créer puis faire perdurer une bonne ambiance de groupe : les anciens : Clément B., Simon C., Florent S., Julien M., JC, Curator, Grace. Les actuels : Choup FX, DSJ de Fort l'Ircof, Bubu de Sète, Manon de Barentin (^^), Mr. Bienvenu ATTAWA, Lina, Nihad... Bon courage aux doctorants du Projet CORE, et notamment à celle qui me succède Lina Harfouche.

J’ai également une grosse pensée pour Framboisouille qui part du laboratoire prochainement. Merci d’avoir toujours été là quand on en avait besoin.

Pour le LECAP : Tant d’années passées avec vous, mes remerciements sont nombreux… Ils sont adressés d’abord aux permanents : Laurent Delbreilh, Antonella Esposito, Allisson Saiter, Nicolas Delpouve avec lesquels j’ai appris, échangé, évolué, grandi sur le plan humain et scientifique… J’ai une pensée pour Jean Marc S. et Joe Turner qui m’ont permis d’avoir accès au rêve américain… (Personne ne le sait… personne n’ira… mais Lincoln au Nebraska … ça déchire en fait ! ;)). Place aux doctorants maintenant : Je remercie les anciens Arturo, Bidur, Tino, Emilie B., Akram, Nicolas D., Larissa, Angélique M., Florian H., Khadidja, Mélanie L., Lucie, … et puis les actuels : Xav, Steven, Selim, Nagihan, Aurélie, Sareh, Bienvenu (encore lui ^^). Bon courage à vous tous, vous avez de quoi faire de très bonnes thèses chacun ! Merci au trio magique du LECAP depuis de nombreuses années : Marie-Sylvie, Marie-Rose, Eric Dontzoff. J’ai une pensée pour la personne qui s’occupe du nettoyage au laboratoire avec qui l’échange d’un sourire franc et sincère et d’une petite conversation quotidienne m’a permis de conserver une humeur positive même dans les périodes plus dures. C’est dingue comme ce genre de gestes simples permet de tenir… (allez hop une petite citation de Mother Teresa : “Peace begins with a smile…”).

Ma famille et mes amis ont été un vrai socle et sont les seuls responsables de ma résilience à encaisser les coups (j’ai quand même fait du full contact pendant la thèse pour essayer d’en parer à l’avenir). Mille mercis à eux.

Et maintenant je passe à mes acolytes, mes compagnons de route, mes anciens colocataires, Emilie et Boujamir avec qui j’ai évolué depuis pas mal d’années. Que je suis heureux de vous voir bien dans vos vies respectives ! Je n’oublierai pas de citer Etienne 3so1/2 qui a été moins présent lors de la thèse (parce que Paris) mais qui l’est aux moments importants… Même si les routes se séparent un petit peu pour nous tous, on les recroisera régulièrement autour d’une table, d’un voyage,… on commence en Belgique ?

Je termine par ce dont je suis le plus heureux : Mélanie … Merci pour ton amour et ton soutient durant toute cette année… On continue en Belgique ?

Table of contents

Introduction

Introduction

Most of the active pharmaceutical ingredients are organic molecules formulated in a solid form so as to ensure a robust physical stability. During the last few decades, the field of crystal engineering, *i.e.* the rationalization and prediction of the structure-property relationships, has gained prominence. Along with the improvement of analytical techniques, the understanding and prediction of crystal structures become more and more accurate. Combined with the use of phase diagrams, this knowledge allows the design of appropriate crystallization procedures transposable at the industrial scale, so as to produce physically stable solid forms. Among the huge number of publications dealing with solid-state behavior of low molecular weight organic molecules, borderline cases have however been encountered and challenge the general understanding of crystallography, polymorphism, phase transition theories and chiral discrimination mechanisms.

In the present work, we investigate a chiral pharmaceutical drug, namely diprophylline (DPL), which is a theophylline (TPH) derivative. This chiral drug, displaying broncho- and vasodilator properties used in the treatment of pulmonary diseases, presents a borderline behavior, at least for crystallization aspects. The polymorphic landscape of this chiral compound is rather complex since the phase diagram between the two enantiomers present stable racemic compounds and enantiomeric forms but also metastable polymorphs and solid solutions that crystallize as function of kinetic condition as well as enantiomeric composition.

As the molecular mobility of amorphous DPL has never been meticulously investigated by taking into account those previous specific results, it appeared suitable to reconsider the polymorphic behavior of both racemic (50 percent of each enantiomer) and enantiopure (100 percent of one enantiomer) compositions of this system by studying carefully the kinetic transitions with respect to the global molecular mobility. Among the numerous available strategies designed for the transformation of a crystalline drug into a more soluble equivalent one (*i.e.* milling, spray drying …), amorphous DPL samples could be obtained by the most common one, the melt quenching procedure. Although it was proved that an amorphous state of DPL can be obtained by cooling the melt, only a single enantiomeric composition (*i.e.* racemic) was studied, which let still the characterization of amorphous DPL uncomplete.

Since more than 50 percent of the pharmaceutical compounds are chiral, the detailed understanding of the effect of enantiomeric composition in the amorphous state is of

fundamental interest. As a consequence, the chiral pharmaceutical drug DPL appeared to be a good model compound in the comprehension of the glass-to-crystal pathway.

Starting from the previous studies focusing on the metastable equilibria between the enantiomers of DPL, and considering the benefits of the molecular mobility investigation in the pharmaceutical field, a fundamental problematic arises:
Considering the whole panel of enantiomeric compositions, are there preliminary signs of these metastable forms in the amorphous state?

After introducing some generalities, Chapter I presents the concepts useful for the understanding of the relationships between molecular mobility in the glassy and/or the supercooled liquid states and crystallization from a disordered state. Distinct experimental cases available in the literature are reported with, at the end, a special emphasis on chiral molecules.

Thereafter, Chapter II is devoted to the comparative study of the relaxation behaviors of the racemic mixture and pure enantiomer of DPL in the amorphous state. After presenting the preparation and characterization of our samples, the devitrification process at various enantiomeric compositions is discussed. Additionally, a special insight is provided about the impact of chemical purity on the relaxation behavior of both the glassy and supercooled liquid states.

Finally, Chapter III depicts the preparation and characterization of crystalline phases of DPL obtained from an amorphous state. In the continuity of the study of molecular motions characterized in the amorphous state (Chapter II), our investigations focused on the exact role of enantiomeric composition as well as the chemical purity during DPL recrystallization.

Along the manuscript and in the conclusion, the results obtained for the various enantiomeric compositions of DPL will be discussed with two objectives:

i) Understanding if there is a signature in the amorphous state of the first crystals obtained that influence the glass-to-crystal pathway.

ii) Proposing a set of considerations that could help rationalizing other borderline cases (*e.g.* chemical purity impact, surface effects, …).

Chapter I

Generalities

I-1. Preamble

The matter can arrange into three states: liquid, solid and gas. If the constitutive atoms of a solid are arranged in a strict and periodic array (long range order), it is defined as a "crystal". Otherwise, if only a short range order is present, the material is said "amorphous". Intermediate situations may occur in case of liquid crystals (*e.g.* "smectic" and "nematic") which present long-range order in less than 3 dimensions [1].

I-2. Fundamentals: the Amorphous State

I-2-1. Amorphous State and Supercooled Melt

I-2-1-1. Amorphous state

a. General information about structural aspects

Historically, although silicate glasses have been a part of human technology for millennia, it has only been known since 1920s that any supercooled liquid can be turned into an amorphous solid state by further reduction of temperature. In addition to silicates, materials having widely varying types of intramolecular interactions, including metallic alloys, organic liquids and salt solutions, or polymers can also be glass formers.

Amorphous materials are genuine solids and share the essential attributes of the solid state with crystals. However, there is a fundamental distinction between the amorphous and crystalline states. In perfect crystals, atoms are arranged in a strict and periodic array in three dimensions to an infinite extent. In amorphous solids, long-range order is absent and there is no translational periodicity, as known for crystals. The lack of long-range order (or periodicity) for amorphous solids is clearly distinguishable by X-Ray diffraction through the presence of a broad halo pattern, while sharp Bragg peaks are present for crystalline samples (Figure 1).

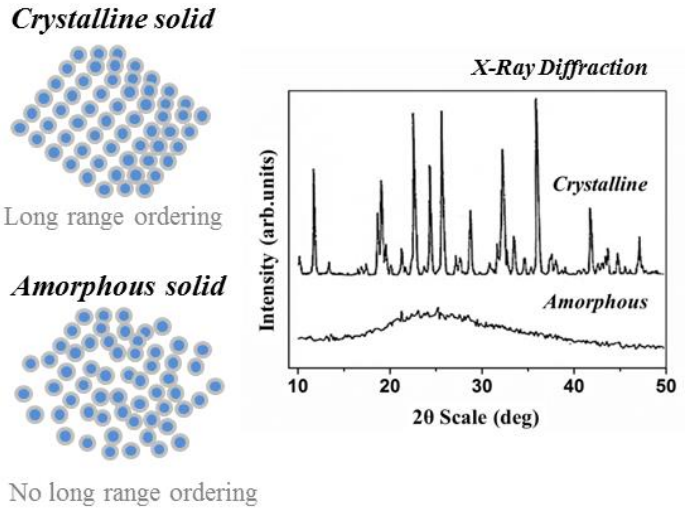

Figure 1. Schematic view of amorphous and crystalline solids. The right part of the figure corresponds to the typical X-ray patterns of crystalline and amorphous materials.

b. Amorphous and "polyamorphism" in pharmaceutics

In pharmaceutical drug systems, the attractive and valuable property of the amorphous state is its higher apparent solubility (and higher dissolution rate) compared to the crystalline counterpart [2]–[6]. However, the poor physical stability of a glassy state may raise substantial problems for drugs processing and/or scale-up [7], [8].

A theoretical concept consists in postulating the existence of multiple amorphous states in a one-component system (denoted "polyamorphism"), defined as more than one type of disorder in the solid state [9]. Polyamorphism was first found to exist in water [10] and then in inorganic materials [11], [12]. Nowadays, there is little evidence that small organic materials are concerned about polyamorphism [9], [13]. Several studies of Indomethacin have proven that "distinct" amorphous states can be generated by using different amorphization techniques on the same system [14], [15], including melt-quenching, ball milling, spray drying, and cryo-milling.

I-2-1-2. Description of the techniques used to generate an amorphous material

According to the Turnbull's viewpoint about amorphous state preparation, *"nearly all materials can, if cooled fast enough and far enough, be prepared as amorphous solids"* [16]. Quenching is indeed the oldest technique for producing amorphous solids. However, in the past

50 years, the industrial and scientific communities have proposed alternative methods for producing amorphous materials as presented in Table 1.

Table 1. Experimental techniques used to generate amorphous materials.

ROUTE to the AMORPHOUS STATE				
CRYSTAL	**LIQUID**	**VAPOR**	**SOLUTION**	**CHEMICAL**
Grinding *Compression*	*Melt-quenching* *Melt-extrusion*	*Vapor deposition* *Sublimation*	*Spray-drying* *Lyophylization*	*Gelation* *Dehydratation* *Precipitation*

I-2-1-3. Physical and chemical methods

In this section are listed the physical methods to create an amorphous solid: (i) The rapid cooling from the liquid state (melt-quenching) is the most common method. Recently, hyper-quenching method with a cooling rate at 4000 $K.s^{-1}$ could be reached by using fast calorimetry (only with a limited amount of sample ≈ ng) [17]. It allowed amorphization of materials that possess strong crystallization abilities; (ii) Mechanical milling corresponds to the alternative technique of the quench method, particularly for molecular compounds which undergo thermal degradation at the melting point. Besides, it is also of interest for compounds that are poorly soluble in polar and nonpolar solvents. Grinding is basically performed at room temperature, but "cryogrinding" which consists in freezing the material during the process was found more efficient for pharmaceuticals; (iii) Compression of liquids is a recent technique. It is based on the fact that pressurization of liquids gives similar effects as cooling of liquids; (iv) Vapor deposition represents a powerful technique. The basics of this method consists in vaporizing the material on a substrate kept at a temperature far below the glass transition temperature (T_g), (v) Spray drying is a process developed in industrial community, consisting in evaporating a solution (in the form of spray) in order to generate an amorphous hot dried medium. (vi) Compression of crystals is a very promising method allowing the system to convert into an amorphous solid without passing through the liquid state. The amorphous state is obtained by supplying high energy in the form of compression of the crystalline structure in order to destroy the ordered arrangement [18].

Chemical methods are also used in some specific cases: (vii) Gelation consists in transforming a sample into a gel, followed by removal of extra components and leading to an

amorphous state. (viii) Precipitation by chemical reactions can also produce an amorphous form (ix) Dehydration consists in removing water from a hydrated crystalline material (at a certain T) resulting, because of a destructive mechanism, in a disorder anhydrous sample that cannot reorganize into a crystalline ordered structure. In this thesis, the amorphous state of our samples was only obtained by the melt quenching technique.

I-2-1-4. Glassy and supercooled liquid states

a. Phenomenology of the glass transition

"It is a critical physical property which can dramatically influence its chemical stability, physical stability, and viscoelastic properties." Hancock and Zografi [19]*, 1994*

When a liquid is cooled from the highest temperatures, two scenarios are possible: if a slow cooling is applied to the system, crystallization may occur. Since crystallization is a first-order transition, it is manifested as an abrupt decrease in molar volume as illustrated in Figure 2. Because the crystallization process may take some time, it is also possible to supercool a liquid below its melting point in order to retain its liquid character. Any liquid which does not crystallize at the melting temperature (hereafter T_m) enters into a metastable state designated as "supercooled liquid". As shown in Figure 2, further cooling of this supercooled liquid leads to the glass formation manifested by a change in the slope V(T) in the vicinity of the glass temperature, T_g. It is important to emphasize that the glass transition temperature depends on the cooling rate ($q_{A-} > q_{B-}$). Fast cooling rate produces the "Glass A" (dark blue), with the glass transition temperature T_{gA}, while slower cooling rate leads to "Glass B" (light blue) with the glass transition temperature T_{gB}. The intersection of the extrapolation of the liquid state curve and the curve of the crystalline state corresponds to the "*Kauzmann temperature*", T_K [20], at which the difference in entropy becomes zero (often discussed via thermodynamic laws arguments, *i.e. Kauzmann paradox* [21], [22]).

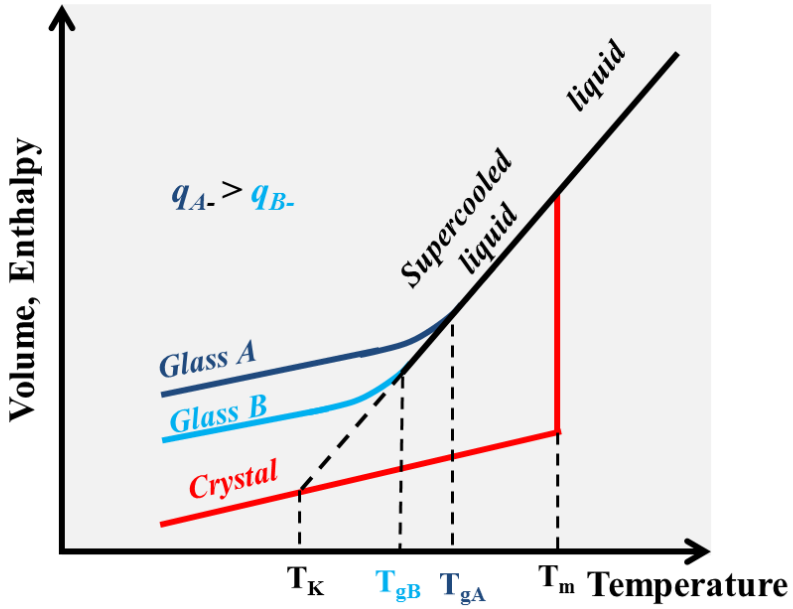

Figure 2. Schematic representation of the temperature dependence of system volume for a liquid that can both crystallize and form a glass. The thermodynamic and dynamic properties of a glass depend on the cooling rate, Glass A was formed with higher cooling rate than Glass B. T_K is the Kauzmann temperature, T_{gA} and T_{gB} indicate the glass transition temperatures for both cooling rates. T_m= melting temperature.

Figure 3 shows typical behaviors of the heat capacity (C_p) in the vicinity of the glass transition. From the liquid to the glass formation (path **1**), the specific heat capacity drops off the supercooled liquid at T_g to a lower value. When reheating (path **2**), the glass transition phenomenon is recovered by an enthalpy peak (*e.g.* with $q_{A-} < q_{A+}$, and $q_{B-} < q_{B+}$), resulting from the fact that below T_g, the system slowly equilibrates with time (thermodynamic variables change). Thus, thermodynamic properties of the glassy state depend on the cooling rate of the liquid, and generally on how the glass was formed. It is notwithstanding that the change of T_g caused by different cooling rates does not exceed 3-5 K in classical DSC [23] (see Appendix AI-5 for DSC), while it could be dozens in fast calorimetry [17]. For any material (including pharmaceutical compounds), the value of the glass transition temperature is commonly determined as the midpoint of the heat capacity increment during heating run. This behavior is a consequence of the kinetic nature and because of that, the glass transition temperature is not considered as a true thermodynamical phase transition [24].

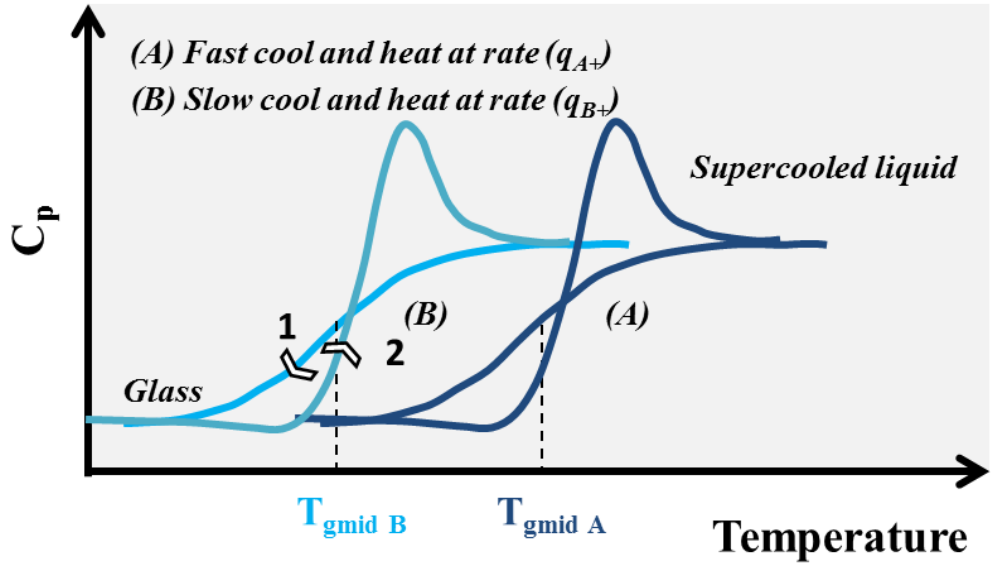

Figure 3. Schematic representation of the temperature dependence of the specific heat recorded in the glass transition region for different heating and cooling rates (Curves A and B). Path 1 corresponds to the liquid to glass formation and path 2 corresponds to the reheating from the glassy state.

b. Models of the glass transition

While so far, only the kinetics of the glass transition has been discussed, several models and theories were nonetheless proposed to explain the fundamental nature of the glass transition in glass-forming systems. However, none of them describes entirely all aspects of this phenomenon. Theories based on thermodynamic arguments will be briefly introduced hereafter.

Free-Volume models:

Doolittle and Cohen proposed the free-volume model [25], [26]. Basic assumptions behind this theory are: (i) molecules need vacant space in their surroundings to be able to rearrange (ii) free volume is continuously redistributed (without any expense of local free energy).

In view of this concept, Doolittle developed the following equation to describe the relation between the non-Arrhenius temperature dependence of viscosity (relaxation time τ) and free volume [25]:

$$\eta = A\exp\left(B\frac{V-V_f}{V_f}\right) \quad (Eq\ I)$$

where η corresponds to the viscosity (relaxation time), A and B are the fitting parameters, V is the total specific volume and V_f is free volume (free space available per molecule).

The Adam-Gibbs's model:

Adam-Gibbs approach is one of the most popular entropy based model [27]. It is based on the assumption that the rearrangements over energy barriers of molecular units must be "cooperative", involving a number of molecular units that necessarily increases with decreasing temperature. It is assumed that these molecules which move in cooperative manners are contained in distinguishable, independent and equivalent regions called "Cooperative Rearranging Region" (CRR). Hence, the relaxation time of the system depends on the configurational entropy S_c :

$$\tau = \tau_0 \exp\left(\frac{C}{TS_c(T)}\right) \quad (Eq\ II)$$

Where τ_0 and C are constants.

Two Order Parameter Model (TOP)

Tanaka proposed more recently a two-order-parameter model to understand the liquid-glass transition [28], [29]. It is based on the idea that there always exists two competing orderings in any liquid: (i) long-range density ordering toward crystallization (ii) short-range bond ordering toward the formation of locally favored structures due to the incompatibility in their symmetry. The essential difference between the TOP model and the others (*i.e.* Free Volume and Adam – Gibb's models) is that it considers crystallization as a key factor that plays a crucial role in liquid-glass transitions. According to this model, as approaching the glass transition, the effect of geometrical frustration between short-range and long-range orderings acts as impurities against crystallization and increases the free energy barrier for nucleation [30]. Hence, TOP model predicts stronger frustration for "stronger" liquids and weaker frustration for "fragile" liquids (see section I-2-2-3-b Fragility).

I-2-2. Relaxation phenomena in glass forming liquids of pharmaceutical systems

I-2-2-1. Context

Amorphous substances/dosages are recognized to have a faster dissolution rate and an increased biodisponibility, compared to their crystalline counterparts [3], [7], [31], [32]. However, amorphous drugs are thermodynamically unstable and may undergo recrystallization

during processing and/or formulation [7], [33]. The fundamental mechanisms related to the physical instability of glassy materials remain considerably unexplained and the scientific community tries to understand the physical factors that govern crystallization from the glassy state. One of the main factors determining the stability of amorphous materials is their molecular mobility [34]–[41]. To investigate its incidence, the study of the relaxation processes in the supercooled liquid and glassy state can be used. The experimental technique named Broadband Dielectric Spectroscopy (BDS - see Appendix AI-1) is utilized to determine the timescales of molecular motions of amorphous pharmaceuticals. It enables measurements of relaxation times over a wide frequency (ω) range of up to 16 decades at different temperatures (and/or different pressures). For this purpose, the investigated material is subjected to an external electrical field E(ω) and the following phenomena can occur [42]:

- dielectric dispersion ε'(ω) and absorption ε''(ω) caused by dipole relaxation arising from the reorientational motion of molecular dipoles (represented by the complex dielectric permittivity ε*(ω) = ε'(ω) - iε''(ω))
- electrical conduction arising from the translational motions of electric charges such as ions, electrons (described by the complex conductivity σ*(ω) = σ'(ω) + iσ''(ω))

I-2-2-2. Dielectric theoretical background

a. Debye Relaxation model

The nature of the dielectric dispersion and absorption induced by an electrical field in polar materials can be described by the Debye model of dipole relaxation. According to this model, the dielectric dispersion and absorption, respectively represented by a real part ε'(ω) and a imaginary part ε''(ω), are described as:

$$\varepsilon'(\omega) = \varepsilon_\infty + \left(\frac{\varepsilon_s - \varepsilon_\infty}{1 + (\omega\tau_D)^2}\right) \quad (Eq\ \text{III})$$

$$\varepsilon''(\omega) = (\varepsilon_s - \varepsilon_\infty)\frac{\omega\tau_D}{1 + (\omega\tau_D)^2} \quad (Eq\ \text{IV})$$

where ε_s and ε_∞ are dielectric constants in the limits of low and high frequency, respectively. Real and imaginary parts of the Debye function are both presented in Figure 4.

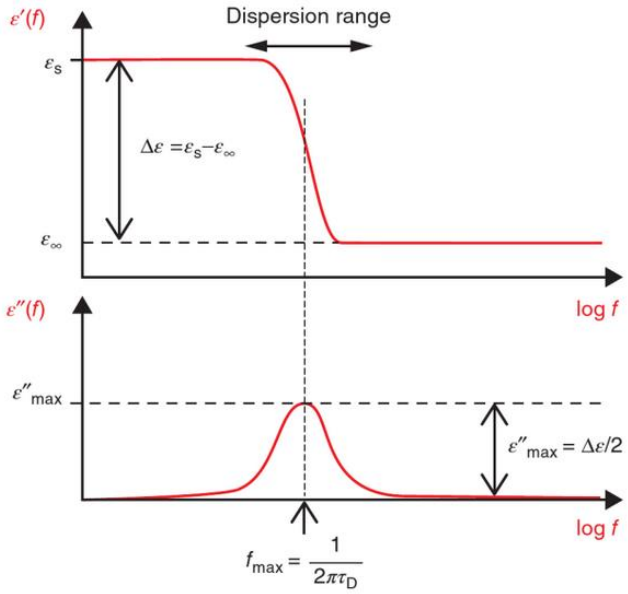

Figure 4. Schematic frequency dependence of the real and imaginary parts of complex dielectric permittivity for Debye dielectric relaxation. Figure was taken from [43].

The dielectric dispersion ε'(ω) decreases nearly in one step with increasing frequency, while the dielectric absorption ε''(ω) reaches a maximum at the frequency f_{max}, which is related to the characteristic relaxation time of the reorienting dipoles τ_D (= $1/2\pi f_{max}$). According to the Onsager model, the dielectric strength $\Delta\varepsilon = \varepsilon_S - \varepsilon_\infty \approx N\mu^2$, with N the number of relaxing dipoles per volume unit and μ the permanent dipole moment. The dielectric absorption ε''(ω) (loss peak) of the Debye relaxation is narrow and symmetric.

b. Non-Debye Relaxation models

Debye model turned out to successfully describe relaxation processes for systems in which dipoles do not interact with each other (*e.g.* gases or very simple liquids). However, this model cannot be longer applied to experimental results obtained from complex systems (including supercooled liquids) where cooperative movements occur. In the case of glass forming liquids, distributions of relaxation times exist in comparison with classical Debye relaxation. This means that the molecular motions of all dipoles in the material cannot be characterized by a single relaxation time τ_D. For the purpose of describing non-Debye relaxation processes in the experimental dielectric spectra, different empirical equations are used:

- **Cole-Cole (CC) function**

An asymmetrical loss peak and wider dispersion area in comparison with Debye formula can be described by Cole-Cole equation [44]:

$$\varepsilon''(\omega) = \varepsilon_\infty + \Delta\,\varepsilon \frac{1}{1+(i\omega\tau_{CC})^{1-\alpha}}\ (Eq\ \text{V})\ , \quad 0 \le \alpha < 1$$

Where α is a symmetric broadening parameter and $\tau_{CC} = 1/2\pi f_{max}$.

- **Cole-Davidson (CD) function**

For low molecular weight liquids and glass forming substances having asymmetric broadening of loss peak due to its high-frequency side, the Cole-Davidson function is used [45], [46]:

$$\varepsilon''(\omega) = \varepsilon_\infty + \frac{\Delta\varepsilon}{(1+(i\omega\tau_{CD}))^{\beta}}\ (Eq\ \text{VI})\ , \quad 0 \le \beta < 1$$

Where β is an asymmetric broadening parameter.

- **Havriliak-Negami Function**

A generalization of the CC and CD models was formulated by Havriliak and Negami [47], [48]**.** It describes broadened and asymmetric dielectric processes:

$$\varepsilon''(\omega) = \varepsilon_\infty + \Delta\,\varepsilon\ \frac{1}{\left[1+(i\omega\tau_{HN})^{1-\alpha_{HN}}\right]^{\beta_{HN}}}\ (Eq\ \text{VII})\ , \quad 0 \le \alpha < 1 \text{ and } 0 < \beta \le 1$$

- **Kohlrausch-Williams-Watts Function (KWW)**

To describe the relaxation functions in the time domain, the Kohlrausch-Williams-Watts (KWW) function is used [49]:

$$\varphi_{KWW}(t) = \exp\left(-\left(\frac{\mathrm{t}}{\tau_{KWW}}\right)^{\beta_{KWW}}\right)\ (Eq\ \text{VIII})$$

where τ_{KWW} is a characteristic relaxation time and β_{KWW} denotes the stretching parameter, with values varying from 0 to 1 ($\beta_{KWW} = 1$ when a single exponential process is recovered). A non-exponential relaxation in the time–domain corresponds to a non-Debye relaxation in the frequency domain. The description of the transformation of the KWW function from the time- to the frequency - domain is described in [50].

I-2-2-3. Relaxation phenomena: Above T_g

a. Primary "alpha relaxation"

In the supercooled liquid state ($T > T_g$), the structural α-relaxation corresponds to the dominant relaxation process, and is associated to the molecular rearrangement. The two characteristic features of the structural relaxation process are: (i) the non-Arrhenius temperature dependence of α-relaxation times while approaching T_g and (ii) its non-Debye character.

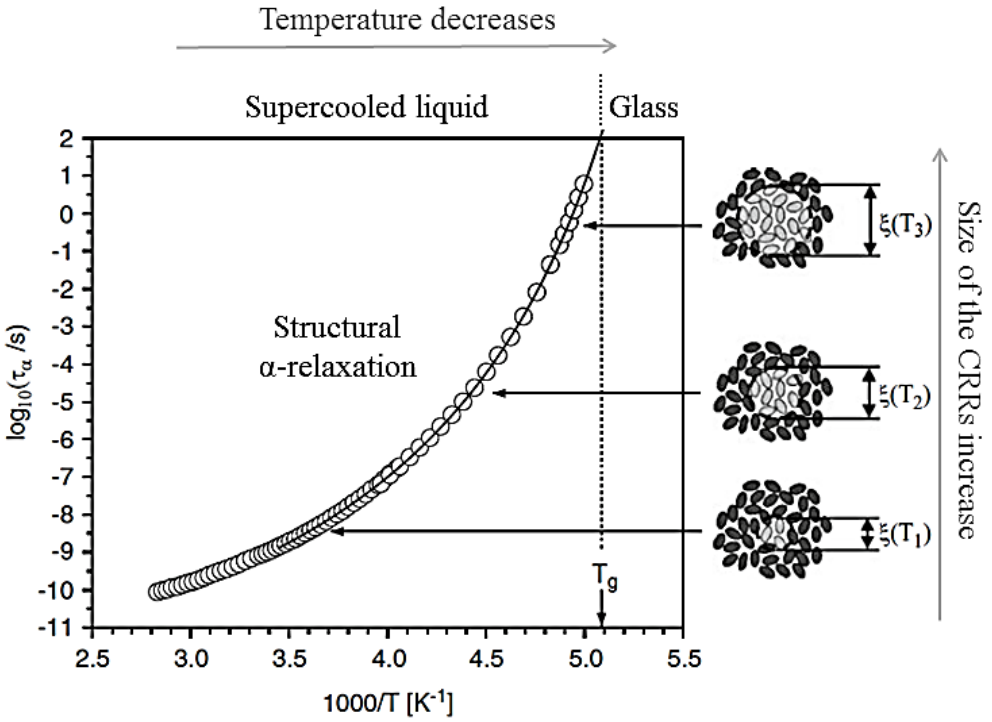

Figure 5. Non-Arrhenius temperature dependence of α-relaxation times of a glass forming liquid together with schematic illustration of increasing size of cooperatively rearranging regions during cooling (ξ is the so-called cooperativity length). Figure was adapted from [51].

During cooling, molecular motions of a supercooled liquid decrease significantly (Figure 5). The structural relaxation time (τ_α) increases non-linearly from values of the order of picoseconds up to hundreds of seconds in the vicinity of the glass transition [23], [52]. According to the Adam-Gibbs model (see section I.2.1.3.c), this slowdown in the molecular dynamics is caused by the decrease in the number of possible system configurations (S_c decreases see *Eq* II, so the size of the CRRs increases). To quantitatively describe the temperature dependence of α-relaxation times in the supercooled liquid, the Vogel-Fulcher-Tamman (VFT) equation can be used [53]–[55] :

$$\tau_\alpha = \tau_\infty \exp\left(\frac{DT_0}{T - T_0}\right) \quad (Eq\ \text{IX})$$

where τ_∞, T_0 and D are fitting parameters.

Noteworthy is the fact that the fundamental model proposed by Adam and Gibbs (see *eq* II) implies the VFT equation, when defining the configuration entropy as $S_c = a(T-T_K)/T$, where *a* is a constant and T_K is the Kauzmann temperature. With the interpretation that $T_0 = T_K$, the Adam-Gibbs equation leads to the VFT equation.

b. Fragility

Another important parameter that characterizes the non-Arrhenius temperature dependence of α-relaxation times while approaching T_g is the dynamic "*isobaric fragility*" parameter "*m*" (*steepness index*). Böhmer *et al.* proposed the following "m" definition [56]:

$$m = \left.\frac{d(\log \tau_\alpha)}{d\left(\frac{T_g}{T}\right)}\right|_{T=T_g} \equiv \frac{D\left(\frac{T_0}{T_g}\right)}{\left(1-\left(\frac{T_0}{T_g}\right)\right)^2 \ln(10)} \qquad (Eq\ \text{X})$$

Supercooled liquids can be classified into three categories by using the parameter *m* [57]: "fragile", "intermediate" and "strong". According to this terminology, "strong" liquids exhibit an Arrhenius dependence in the plot of log τ_α versus the scaled temperature T_g/T, whereas "fragile" liquids are characterized by a non-Arrhenius behavior (Figure 6). "Strong" glass formers are characterized by $m \leq 30$, and "fragile" glass formers have $m \geq 100$. The liquid is classified as "intermediate" glass former when *m* is ranged between 30 and 100.

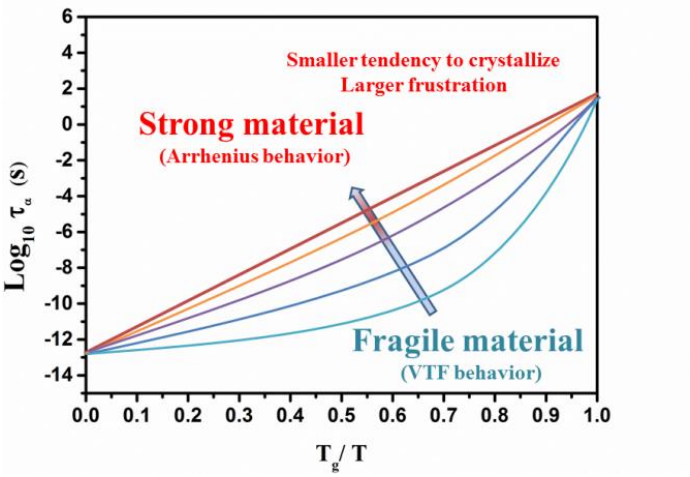

Figure 6. Schematic illustration of the Tanaka concept of frustration against crystallization. A strong material has smaller tendency to crystallize because of its large frustration against crystallization compared to fragile material.

In the current research field of formulation of amorphous drugs, the concept of fragility is of interest since it is considered as a key factor that correlates with the glass-forming ability and physical stability of amorphous systems [57]–[59]. Actually the parameter *m* is related to the average degree of molecular mobility in the structural relaxation near T_g. This is the reason why, at T_g, a "fragile" liquid has its molecular mobility that varies much faster than for "strong" liquids. Thus, "strong" liquids are considered more physically stable than "fragile" liquids.

c. Non-Debye character

The second characteristic feature of the structural relaxation process is its non-Debye character. Experimentally, it was proven that molecular relaxation processes in glass-forming materials are mostly non-exponential. By considering a pharmaceutical drug as an example (*i.e.* Indomethacin), it was shown that the structural relaxation process is broader ($\beta_{KWW} = 0.59$) than a single relaxation time process (($\beta_{KWW} = 1$), Figure 7, data from [60]).

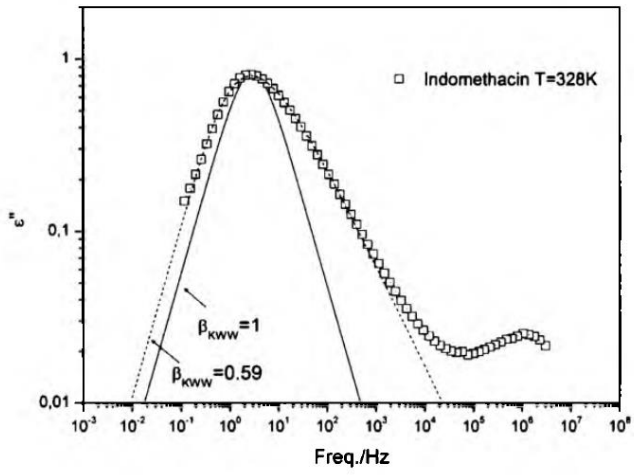

Figure 7. Dielectric loss ε'' of indomethacin versus frequency in supercooled liquid state (T= 328 K). Solid and dotted lines represents KWW fits with respectively β_{KWW} = 1 and β_{KWW} = 0.59. Figure was taken from [61]

Among the explanations of this non-Debye character, it was argued that it originates from the average relaxation time of molecules that relax exponentially, and with different relaxation times [62]. This broadening is believed to be due to a complex cooperative character of molecular rearrangements [63], [64]. Its fundamental origin is still open to discussion [65].

I-2-2-4. Relaxation phenomena: Below T_g

As temperature of supercooled liquid decreases, the α-relaxation process becomes very slow, and other relaxation processes emerge in the vicinity of T_g. They are usually termed as "secondary relaxations" and reflect fast local motions (with either inter or intramolecular origin), providing us information about the molecular dynamics in the glassy state. One of the main characteristic features of secondary relaxations is that they can be observed at very low temperatures, far below T_g. Consequently, they are considered as the main source of movement in the glassy state. The conventional designation of secondary relaxations consists in assigning Greek letters (β,γ,δ, etc…) in order of decreasing time scale. The temperature dependence of these secondary relaxation times (τ_β , τ_γ , τ_δ , etc…) in the glassy state is usually described by the Arrhenius equation:

$$\tau(T) = \tau_\infty \exp\left(\frac{\Delta E}{k_B T}\right) \quad (Eq\ XI)$$

where τ_∞ is a pre-exponential factor, ΔE represents the energy barrier of the studied secondary process, and k_B is the Boltzmann constant. However, in the liquid state, because of the strong

coupling between the structural and secondary processes, it is very difficult to characterize secondary relaxation times. In this case, the temperature dependence of the secondary relaxation times can be more complex (a single Arrhenius equation is not sufficient) [66].

Among the different secondary relaxation phenomena, the slowest one is called Johari-Goldstein (JG) relaxation (which has an intermolecular origin). It is assumed that this process is related to motions of entire molecules. In the 1970s the scientists Johari and Goldstein were the first to demonstrate the existence of a secondary relaxation in completely rigid molecules (*i.e.* Toluene, Chlorobenzene) [67]. Nowadays, the JG relaxation is believed to be a universal feature of all glass formers and serves as the precursor of the primary α-relaxation [68].

Other secondary relaxations (generally faster than the JG relaxation) exist and originate from intramolecular reorientations of some flexible parts of the molecules. Usually, these relaxations (*i.e.* β,γ,δ, etc) can be distinguished at higher frequencies than those at which the JG β-relaxation occurs. Hence, in the glassy state of a given glass former, more than one secondary relaxation process can exist, but with different molecular origins. In some cases, identification of the nature of secondary relaxations is very complex due to their distinct dielectric spectra manifestations. As an example, the JG relaxation process is assumed to have much lower magnitude than the structural α relaxation, and therefore, the secondary relaxation of intermolecular nature may not be visible in the dielectric spectra. By contrast with a well-pronounced relaxation peak, the high-frequency α-peak shows an *excess wing* (or "high-frequency wing"). Hence, Kudlik *et al* proposed formerly a classification of glass formers into two groups: A-type systems which exhibit an excess wing, and B-type systems with a discernable β-process [69]. Schematic illustrations of dielectric loss spectra ε'' for both types A and B glass formers are shown in Figure 8.

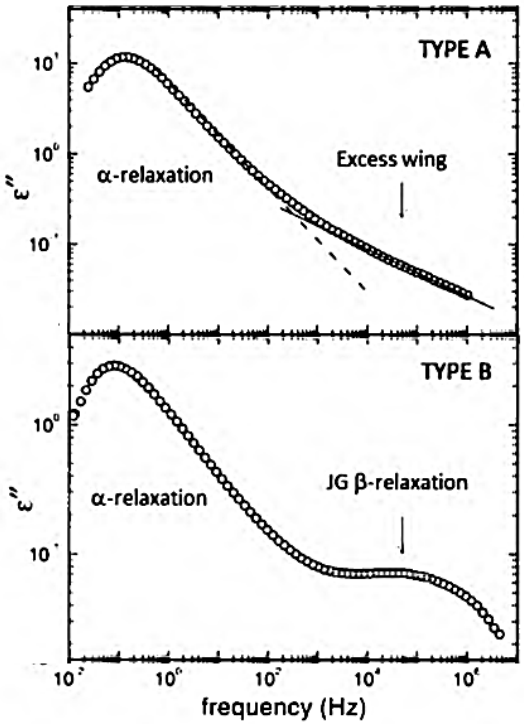

Figure 8. Dielectric spectra of Type A and Type B glass-forming systems. Solid line in the upper graph shows the additional power law with a weaker slope compared to a α-relaxation peak. Figure was adapted from [68]

In the past, the excess wing was interpreted as an inseparable part of the α-relaxation [70]. Nowadays, the excess wing is believed to be an unresolved JG relaxation, concealed by the most intense α-peak. The interpretation of both the excess wing and nature of secondary relaxations can be resolved by performing dielectric studies at elevated pressure (*e.g.* [71], [72]).

I-3. Crystallization from the Amorphous State

I-3-1. Relationship between molecular mobility and cold crystallization

Amorphous drugs can exhibit distinct recrystallization behaviors. Among cases reported in the literature, some of them are very good glass formers and present strong resistance to crystallization (*e.g.* Telmisartan [38]). Others are physically stable in their glassy form but recrystallize from the supercooled liquid state (*e.g.* Biclotymol [40], Sildenafil [73]). Some of them can recrystallize both easily in the liquid and glassy states (*e.g.* Celocoxib [59]). Thus, it is important to characterize the recrystallization behavior from the amorphous state of pharmaceutical systems in the vicinity of the glass transition (below and above T_g). Finding correlations between the molecular mobility and crystallization tendency could lead to a better understanding of the nucleation and crystal growth mechanisms.

I-3-2. Role of thermodynamics and kinetics

I-3-2-1. Outlines of crystallization in supercooled liquids

As described in the previous sections, when a liquid is cooled at a temperature lower than its melting point (T_m), it enters into a supercooled liquid state. During this cooling run, various phase transitions or physical changes can be observed: i) precipitation of a crystalline solid; ii) formation of a disordered solid (glass) which can crystallize if heating is subsequently applied to the system; iii) liquid-liquid separation followed by solidification of the components. These scenarios correspond to crystallization from the "liquid state" (or crystallization from the "melt") since a crystal growth process appears in the supercooled liquid state. However, crystallization may also occur in the glassy state (*e.g.* Celocoxib [59]). In this case, the process is termed "devitrification".

I-3-2-2. Nucleation and Crystal Growth

a. Homogenous nucleation

The crystallization from a homogenous liquid is triggered by the formation of molecular clusters. First attempts to describe the kinetics of homogenous nucleation is the Classical Nucleation Theory (CNT) [74], [75]. According to this model, homogenous nucleation proceeds via stochastic aggregation of molecules into nuclei presenting the same degree of order than the final crystal form. In the past, Landau and Lifshitz have estimated the probability P_n for the formation of a cluster containing *n* molecules:

$$P_n \sim \exp\left(\frac{\Delta G_n}{k_B T}\right) \quad (Eq\ \text{XII})$$

where ΔG_n ("n" for nucleation) represents the Gibbs energy variation of formation of the cluster, and k_B is the Boltzmann constant. This Gibbs energy variation includes a double contribution: the first term is representative of the molecular aggregation and the second one is related to the liquid/solid interface. Assuming a spherical shape of the clusters (with radius r), ΔG_n can be expressed as:

$$\Delta G_n = -\frac{4}{3}\pi r^3 \Delta g + 4\pi r^2 \gamma \quad (Eq\ \text{XIII})$$

where Δg is the Gibbs free energy variation per volume unit and γ is the interfacial energy per unit area. Figure 9 shows the typical behavior of the Gibbs energy variation as a function of nucleus size in case of homogenous nucleation.

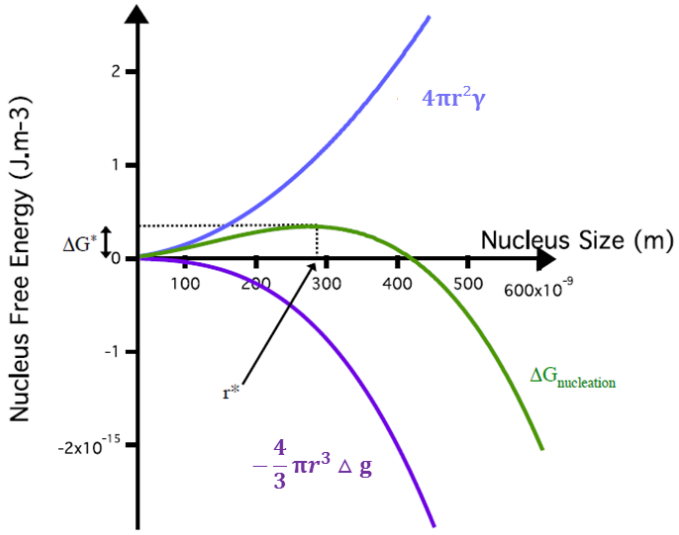

Figure 9. Illustration of the free energy change (green curve) associated with homogenous nucleation of a sphere of radius r (and assuming Δg = 7 kJ.m^{-3} and γ = 0.001 J.m^{-2} for the determination of the molecular aggregation (purple curve) and the liquid/solid interface (blue curve) contributions).

The formation of the nucleus becomes energetically favorable at the critical radius threshold r* when the contribution of the liquid/solid interface is not prevalent. After this, the growth of the nucleus stabilizes the system. This process of nucleation is driven by kinetics and the energy barrier ΔG_n*. It corresponds to the maximum of ΔG_n obtained for the radius of the nucleus r*, given by:

$$r^* = \frac{2\gamma}{\Delta g} \quad (Eq\ \text{XIV})$$

$$\Delta G_n^* = \frac{16\pi\gamma^3}{3(\Delta g)^2} \quad (Eq\ \text{XV})$$

When r < r*, $\Delta G_n > 0$, the aggregates will dissolve into single units, while for r > r*, $\Delta G_n < 0$ and the aggregates grow to form a crystal. For crystallization from the melt, the energy barrier height ΔG_n* for the nucleation process of a new solid form increases as supercooling increases. The supercooling represents the driving force for the occurrence of molecular aggregation ($\Delta\mu = \Delta S_m \Delta T$, where $\Delta\mu$ is the chemical potential variation, ΔS_m is the fusion entropy and $\Delta T = T_m$

- *T*). Therefore, Δg is more negative as ΔT increases, *i.e.* the height of the energy barrier decreases as the degree of supercooling increases.

From a thermodynamic point of view, when the temperature of a supercooled liquid decreases, crystal formation is favored since the driving force of nucleation increases. Inversely, from a kinetic point of view, the crystallization process encounters difficulties due to viscous retardation. The system reaches the maximum overall rate of crystallization when it reaches the temperature at which the positive contribution (*i.e.* representative of the supercooling) equalizes the negative contribution originated from molecular motions [76].

In case of heterogeneous nucleation, molecular aggregation occurs on foreign surfaces including dust, surface container or any solid particle. As a matter of fact, the presence of a solid phase reduces the activation energy of the process compared to the homogenous situation. Among the particular cases of heterogeneous nucleation, Yu and coworkers proposed the concept of cross-nucleation defined as a nucleation event taking place due to the presence of particles of an existing polymorph. The nascent crystals can be either more or less stable than "seeds", but the nascent crystals grow faster or at least as fast [77].

b. Crystal growth

Once a stable nuclei has reached r*, it will continue to grow until equilibration of the system. Crystal growth is generally described by the three following models: (i) continuous or normal growth (ii) two-dimensional growth, and (iii) or by screw dislocation [78]. The growth rate of crystals is mathematically formulated by U, as:

$$U = \frac{CT\omega}{\eta}\left[1 - \exp\left(-\frac{\Delta G_v}{k_B T}\right)\right] \quad (Eq\ \text{XVI})$$

Where *C* and ω are constants, T is the temperature, η is the viscosity of the system (reflects the molecular mobility), k_B is the Boltzmann constant and ΔG_v is the difference in the free energy between the amorphous and the crystalline phase. This formula indicates that the crystal growth rate is strongly related to the temperature T of the system. Figure 10 illustrates schematically the first approximation view of the crystallization process in glass forming systems [79]. It shows the nucleation/growth (I_0/G) and the viscosity variations as a function of temperature. Since nucleation is thermodynamically favored at higher degrees of supercooling and the growth at lower degrees of supercooling, the two processes overlap in a temperature range

(representing by the shaded area), *i.e.* crystallization can occur in the system. According to this first approach, crystal growth is appearing between the melting temperature T_m and the glass transition temperature T_g but, as already mentioned above, there exists some cases where nucleation may occur in the glassy state ($T < T_g$) (*e.g.* Celocoxib [59], Indomethacin [80], Nifedipine [81], [82]). Conversely, it was also observed that some materials can crystallize at temperatures just below the melt, where the thermodynamic driving force is small. Besides, viscosity approaches infinity when the molecular mobility is supposed to be zero at T_0 (the VTF zero mobility temperature).

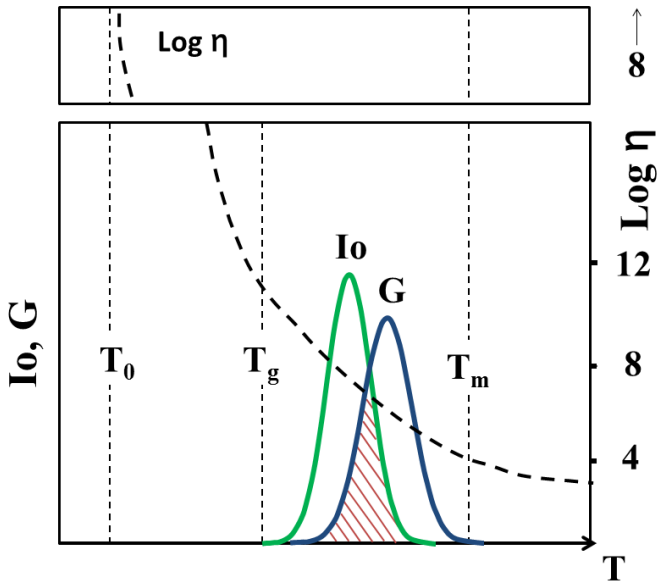

Figure 10. Schematic illustration of the nucleation/growth (I_0/G) and viscosity (η) processes in a supercooled liquid as function of temperature. T_0, T_g and T_m are respectively the VTF zero mobility temperature, the glass transition, and the melting temperature. The shaded area represents the overlap between the nucleation and growth processes.

I-3-2-3. Interfacial free enthalpy γ: disorder effect

In the field of nucleation/growth, the surface tension γ is assumed to be largely influenced by the difference in the degree of order (*i.e.* disorder) in the interfacial region between the amorphous phase and the crystallites. In the past, scientists pointed out that molecules in the liquid state have to increase their ordering close to the crystal boundary in order to allow an ordered embryo to grow [67]–[69]. This "ordering" (molecular reorientations) is the origin of the crystal/liquid interfacial free enthalpy. Hence, it is important to consider the potential role of the relative order in the surrounding liquid and the relative disorder in the crystal embryo.

Figure 11 shows the evolution of molecular ordering in the liquid at the interface together, with the evolution of the corresponding enthalpy *H* and entropy *S*. According to the Spaepen approach, entropy rises more slowly than enthalpy when a crystal changes into bulk liquid (negentropic model [83], [84]). Therefore, at the interface, an excess free energy γ rises, to satisfy the balance between enthalpy and entropy effects. Here, the maximum value of γ is $\triangle H_m = T_m \triangle S_m$ (bulk).

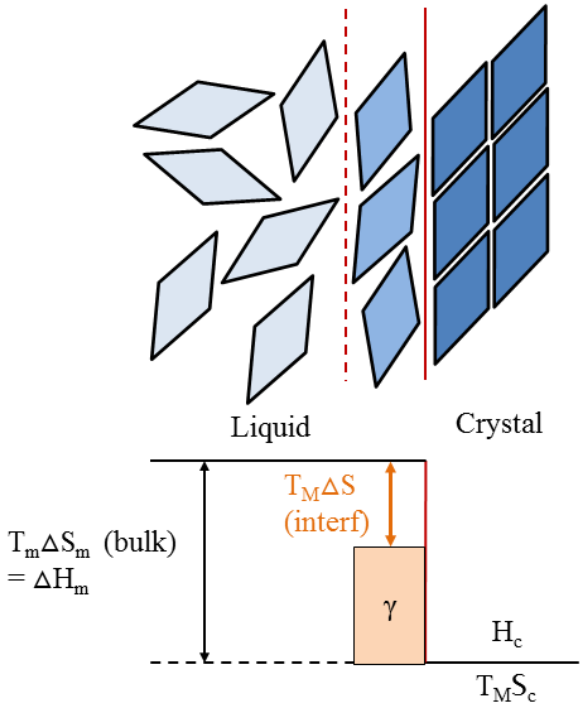

Figure 11. Schematic representation of the crystal/liquid interface (with its short range molecular ordering) with its entropy evolution, according to Spaepen approach [83], [84]

At the interface, the configuration entropy decreases ($\triangle$S (interface) < $\triangle$S (bulk)). Thus, Spaepen proposed to describe the interfacial free enthalpy by taking into account this difference for γ [83], [84]:

$$\gamma \sim \alpha T \triangle S_m \quad (Eq \text{ XVII})$$

With $\alpha = [\triangle S \text{ (bulk)} < \triangle S \text{ (interface)}] / \triangle S_m$

This formula indicates that the ease to undercool a system is strongly dependent on the surface tension γ. Let us consider a very disordered system having low melting entropy (*e.g.* plastic crystals [85], [86]), the corresponding surface tension γ will be low, and its undercooling ability is very poor. It is also for this reason that metastable polymorphic forms, which have

lower enthalpy than stable crystalline phases (and higher crystalline entropy); often nucleate first. This is in agreement with the "rule of stages" law proposed by Ostwald [87], [88], stating that the crystalline phases appearing first in the supercooled melt (or in solution) would be the least stable polymorphs.

I-3-2-4. Liquid-liquid phase separation

When a glass-forming liquid is cooled or reheated from T_g, another phenomenon can occur before any transformation (*i.e.* vitrification or crystallization): the supercooled single-phase liquid might separate into two or more distinct liquids. This concerns mainly viscous liquid mixtures [89] or mixtures of polymeric materials [90].

From a thermodynamic point of view, the stability condition to multicomponent systems is represented by the variation of Gibbs free energy ΔG_{mix} defined as:

$$\Delta G_{\mathrm{mix}} = \Delta H_{\mathrm{mix}} - T \Delta S_{\mathrm{mix}} \ (Eq \text{ XVIII})$$

Where ΔH_{mix} and ΔS_{mix} are, respectively, the differences in enthalpy and entropy between the mixed and unmixed states. In the case of two miscible liquids, the variation in Gibbs energy of mixing ΔG_{mix} as a function of composition is a downward-sloping convex curve (Figure 12 (a)). Alternatively, for partially miscible liquid mixtures, a convex upward curve on a certain composition range can be considered (Figure 12 (b)). The points b and b' indicate the equilibrium phase composition (binodal composition) [90], [91], whereas the points s and s' denote the local limit of stability (spinodal composition). The mixture is metastable between bs and b's', and becomes unstable between the points s and s'. The temperature diagram T-ρ shows the projection of the binodal and the spinodal in Figure 12 (c). The maximum point c represents the critical point (common to both curves). In this case, the nucleation of a critical size particle and its growth (via diffusion) takes place inside the binodal. Conversely, in the spinodal growth situation, a new phase grows (via decomposition) [92]. However, liquid-liquid phase separation can sometimes be a precursor state for devitrification.

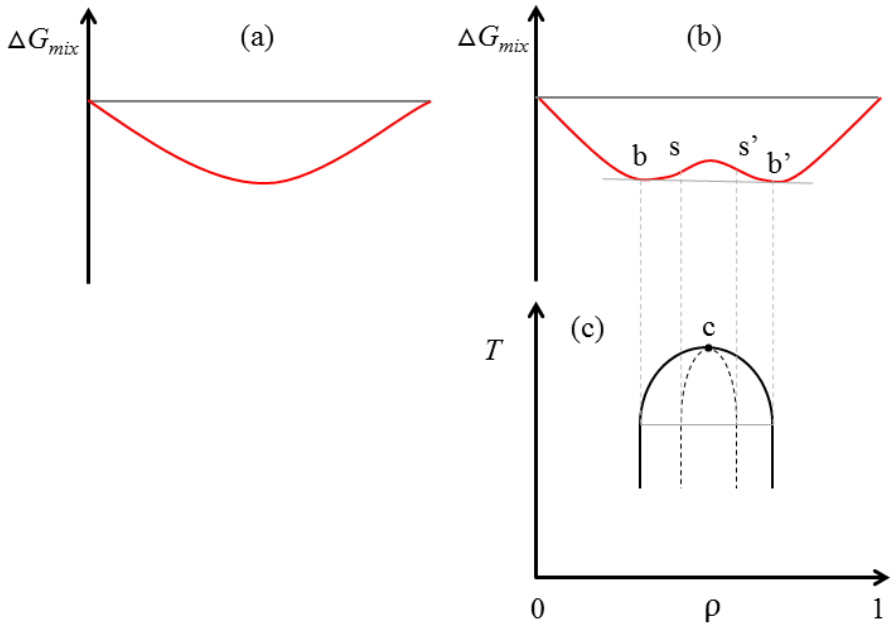

Figure 12. Schematic illustration of the spinodal decomposition of viscous liquids: (a) ΔG_{mix} evolution as a function of the density for two miscible liquids; (b) ΔG_{mix} evolution as a function of the density for two partially miscible liquid mixtures; (c) Temperature-density diagram. Figure was adapted from [92]

It is worth mentioning that the above theories are only approximations that give a qualitative understanding of the factors determining crystallization from the amorphous state. Furthermore, some of the factors described above (from *Eq* XII to *Eq* XVIII) are very difficult to obtain experimentally.

I-3-2-5. Factors influencing the tendency to crystallize

Hence, recrystallization from the amorphous state is affected by many parameters. Besides, these parameters often compete in a versatile way. Recently, Descamps *et al.* [43], [93] categorized these factors as follows:

- The thermodynamic drives the process.
- The molecular mobility facilitates the transformation (or reversely).
- The interface energy modulates the splitting of the nucleation and growth processes.
- The heterogeneities and cracks may amplify the rate of transformation. They result from modifications of interface energy [94] and surface mobility [95], [96].

Although molecular mobility is a key parameter affecting crystallization from the amorphous state, other parameters such as intra- or intermolecular interactions, impurities, effect of excipients, vitrification process also play a role. Nonetheless, additional work is

needed to assess which parameters may be of particular help to determine the physical stability of amorphous pharmaceutical drugs. It is worth mentioning that molecular compounds may exhibit a rich crystalline polymorphism with different structures and levels of disorders, and therefore the conditions of recrystallization are modified. This plays a key role in the phase selection during the nucleation/growth process.

I-4. Fundamentals of Polymorphism

I-4-1. Definition and Thermodynamic properties

I-4-1-1. Definition

Polymorphism can be defined as the ability of a compound to crystallize in two or more crystalline phases with distinct arrangements and/or conformations of the molecule in the crystal lattice [97]. Hence, polymorphs are distinct crystalline forms of exactly the same chemical composition. At least one-third of organic compounds and nowadays about 80% of the marketed drugs exhibit polymorphism [88], [98], [99]. The existence of distinct crystalline structures of the various polymorphs for a same compound often causes these solids to exhibit distinct physical and chemical properties [100]. However, theses distinctions disappear in the liquid and vapor phases.

With regard to polymorph stability and kinetics of transformation between two polymorphs, namely (P1) and (P2) (Figure 13), Gibbs free energy variation is expressed as:

$$\Delta G_{(\mathrm{P1}).(\mathrm{P2})}(T) = \Delta H_{(\mathrm{P1}).(\mathrm{P2})}(T) - T\,\Delta S_{(\mathrm{P1}).(\mathrm{P2})}(T) \quad (Eq\ \mathrm{XIX})$$

where $\Delta G_{(P1),(P2)}$ (= $G_{(P2)}$ - $G_{(P1)}$), $\Delta H_{(P1),(P2)}$ (= $H_{(P2)}$ - $H_{(P1)}$) and $\Delta S_{(P1),(P2)}$ (=$S_{(P2)}$ - $S_{(P1)}$) are respectively the free energy, enthalpy and entropy differences between polymorphs (P1) and (P2). In this example, let us consider the (P1) polymorph more thermodynamically stable than (P2). Figure 14 depicts the evolution of Gibbs free energy (G) and enthalpy (H), at constant pressure, as a function of temperature for a system composed of two polymorphic forms (P1) and (P2).

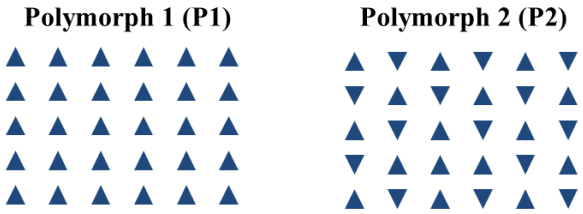

Figure 13. Schematic illustration of two distinct polymorphs (P1) and (P2) of a given molecular compound. (P1) is more stable than (P2).

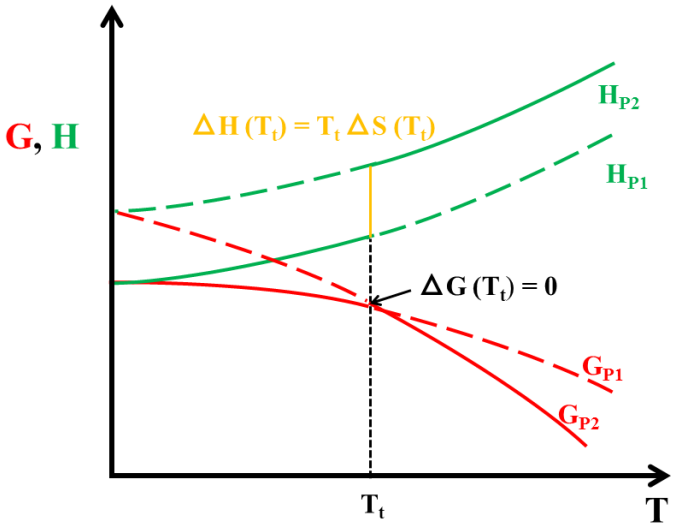

Figure 14. Gibbs free energy (G) and enthalpy (H), at constant pressure, as a function of temperature for a system composed of two polymorphic forms (P1) and (P2) (for enantiotropic system only)

Gibbs free energy (G) curves intersect at the transition temperature T_t. At this specific temperature, Gibbs free energies are identical for the two polymorphs P1 and P2: they are at equilibrium (*i.e.* $H_{P2} > H_{P1}$ at T_t, and $S_{P2}(T_t) > S_{P1}(T_t)$). Below the transition temperature T_t, $G_{P1} < G_{P2}$, *i.e.* the P1 phase is the most stable phase. Conversely, above T_t, polymorph P2 is the most stable phase ($G_{P1} > G_{P2}$). Thus, at a given pressure and temperature, only one stable polymorph exists. The other polymorphic forms are denoted metastable.

I-4-1-2. Enantiotropy and Monotropy

In the above situation, the two polymorphic forms are named enantiotropic; *i.e.* each of the polymorphic forms has a defined stability range. In the case of monotropy, only one of the two polymorphic forms is stable (the other being unstable). This is the reason why the Gibbs free energy curves do not cross below the melting temperature ($T_{f\,P1}$ and $T_{f\,P2}$). Figure 15 illustrates the evolution of Gibbs free energies of polymorphs P1 and P2 in both cases: enantiotropic and monotropic systems.

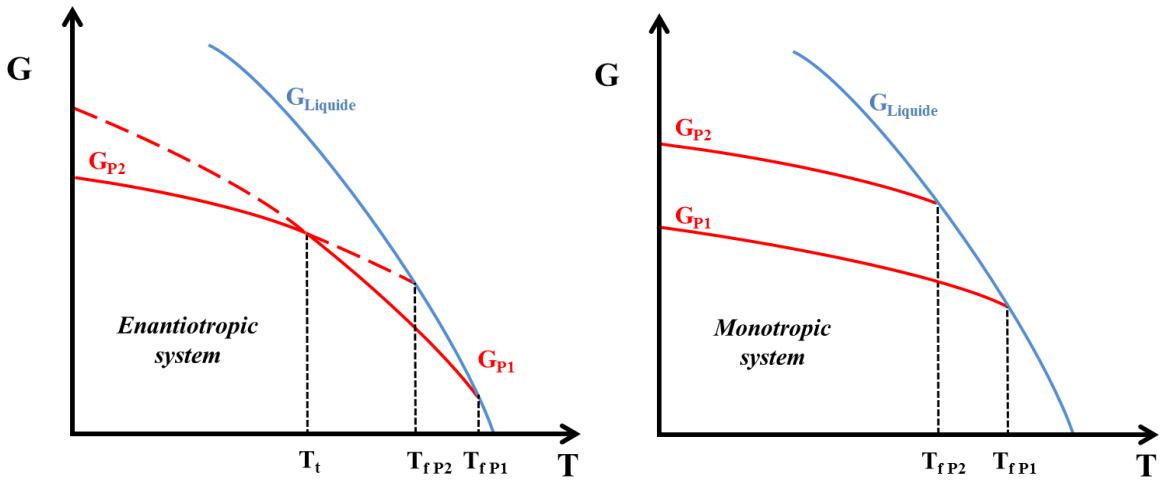

Figure 15. Gibbs free energy (G) as function of temperature of enantiotropic and monotropic systems.

In order to define an enantiotropic or monotropic character to a polymorphic system, Burger and Ramberger [101], [102] have proposed several thermodynamic rules, including the following:

(i) ***Heat of transition rule*:** If the transition between polymorphs upon heating is endothermic, then the two polymorphic forms are enantiotropically related. Conversely, if the transition is exothermic, both polymorphs are monotropically related.

(ii) ***Heat of fusion rule*:** If the polymorphic form which melts at higher temperature possesses a lower melting enthalpy, both polymorphs are enantiotropically related. Conversely, if the polymorphic form which melts at higher temperature possesses the higher melting enthalpy, polymorphs are monotropically related.

Although two polymorphs of a same compound share the same chemical composition, the spatial arrangement of atoms differs, which often results in significantly distinct physical properties. Structure-properties relationship of polymorphs has been the subject of intense research due to the crucial importance of polymorphism for industrial applications. In a pharmaceutical context, there is a substantial need to comprehensively characterize polymorphs of systems (Active Pharmaceutical Ingredient (API)), since their pharmacological properties may differ [97], [103], [104].

I-4-2. Polymorphism of conformationally flexible molecules

One of the particular cases of polymorphism encountered in the literature is related to the conformational flexibility of molecules [43], [105]. It introduces two potential complications in the crystallization process (either in the melt or with solvent): (i) a larger number of structural options is available in the crystallization media (melt or solution phases), leading to distinct close-packing motifs and molecular conformations[1] [103]. Figure 16 illustrates this phenomenon for a system with two competing pathways originating from distinct conformers and leading to distinct crystalline forms; (ii) the tendency for crystallization may be significantly reduced by the conformational flexibility, because of the presence of multiple conformers in the crystallizing media. Considering that the melt is a mixture of energetically similar conformers, the process of crystallization must select the "right" conformers from the "wrong" ones, a difficulty not encountered with rigid molecules. This situation is analogous to that faced by the crystallization of enantiomers from a racemic mixture [106]. In addition, the presence of other conformers in melt (or solution) has the same effect as impurities since they cause a depression of the melting or dissolution temperature [43] [107].

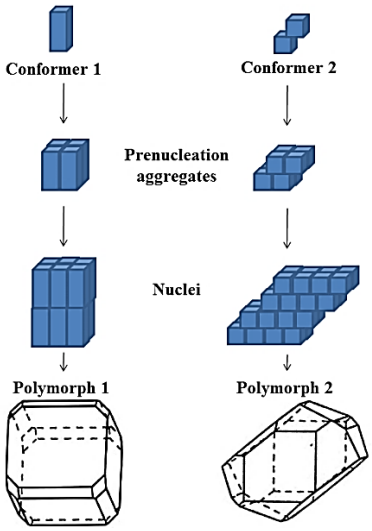

Figure 16. Schematic illustration of the crystallization of conformationally flexible molecules

[1] *By definition, a conformation is "the spatial arrangement of the atoms affording distinction between stereoisomers which can be interconverted by rotations around formally single bonds", not to confuse with a conformer which is « one of a set of stereoisomers, each of which is characterized by a conformation corresponding to a distinct potential energy minimum »* [100]

I-5. Chirality: Definition and Implication in Crystallization from the Amorphous State

I-5-1. Definitions

"I call any geometrical figure, or group of points, chiral, and say that it has chirality, if its image in a plane mirror, ideally realized, cannot be brought to coincide with itself" Lord Kelvin [108], *1884.*

The term *chiral*, first described by L.Kelvin, is originated from the greek "*χειρ",i.e.* hand, the most familiar chiral object. Thus, any object is chiral as soon as it is not superimposable to its mirror-image object. These two mirror-image objects are termed "enantiomers" derived from "ἐνάντιος", meaning "opposite". Conversely, if an object is not chiral, it is called "achiral" [109]. Molecules can also exhibit chirality, caused by the presence of stereogenic centers (*e.g.* asymmetric carbons), and this property is crucial for the manufacturing of APIs.

The Cahn-Ingold-Prelog rules (CIP, Figure 17) are used for naming enantiomers of a chiral compound unambiguously. The method is formally known as R/S nomenclature (*(R)*-rectus and *(S)*-sinister). The latter was determined by Bijvoet *et al.* in 1950 [110].

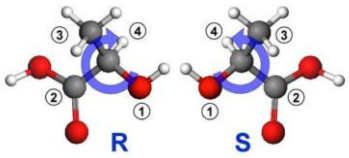

Figure 17. Absolute configuration of 2-hydroxypropanoic acid according to the CIP rule. (R)-rectus and (S)-sinister enantiomers are displayed.

Before the work of Bijvoet, other nomenclatures were also employed, D and L, rather specific to sugar chemistry; or can be either (+)-dextrogyre or (-)-levrogyre, with respect to the angle of deviation of the transmitted polarized light applied on a mixture of pure enantiomers (in solution). Hereafter *(R)* and *(S)* notations will be used to name both enantiomers of a chiral system.

Currently, the mechanisms involved in organic chemistry are not stereoselective and the synthesis of pure enantiomers requires the use of asymmetric precursors or specific additives.

Indeed, mixtures of enantiomers are often obtained and thus, the proportion of each enantiomer in a system is defined by the enantiomeric composition, also called "enantiomeric excess"[2],

$$ee = \frac{n_R - n_S}{n_R + n_S} \times 100 \ (Eq \text{ XX})$$

When ee = 0%, the sample is denoted "racemic" and consists of an equimolar mixture of both enantiomers. If ee = 100%, only one enantiomer is present in the sample, the latter is called "enantiopure". If 0% < ee < 100%, the sample has a scalemic composition [111]. Various techniques are employed to measure the enantiomeric composition of a sample, including chiral chromatography or polarimetry combined with refractometry. (The apparatus used in this work are described in Appendix AI-2).

I-5-2. Crystallization and heterogeneous equilibria

Prior to any description of the heterogeneous equilibria involving enantiomers, it is necessary to remind thermodynamic formalism. For this, let us consider a system composed of two enantiomers (without possible variation of the enantiomeric composition within the timescale of the experiment). If the system consists of a single achiral phase (Φ, *e.g.* liquid state), the chemical potentials of each enantiomer are identical:

$$\mu_R^{\Phi} = \mu_S^{\Phi} \ (Eq \text{ XXI})$$

If, however, the system presents a pair of symmetrical phases (Φ and Φ', *e.g.* two solid forms), the chemical potential of the first enantiomer in Φ is identical to that of the second enantiomer in Φ':

$$\mu_R^{\Phi} = \mu_S^{\Phi}, \mu_R^{\Phi'} = \mu_S^{\Phi} \ (Eq \text{ XXII})$$

When a system of *n* achiral independent components and $\frac{n'}{2}$ pairs of enantiomers (thus, n' chiral components) is composed of achiral phases Φ and at least one pair of symmetrical phases $\frac{\Phi'}{2}$, in this case, the Gibbs-Scott phase rule prevails [112] (at the expense of the Gibbs phase rule).

$$v = \frac{n_2}{2} + n_1 + 2 - \frac{\varphi_2}{2} - \varphi_1 \ (Eq \text{ XXIII})$$

[2] *Another designation to express enantiomeric compositions is the ratio between the two enantiomers X : $X_{(S)}$ = $m_{(S)} / (m_{(S)} + m_{(R)})$ or $n_{(S)} / (n_{(S)} + n_{(R)})$*

where n_1 and φ_1 are respectively the number of independent components and the number of phases that are not symmetrical. Conversely, n_2 and φ_2 are the number of independent components and the number of phases that are symmetrical (applicable only if $\varphi_2 \geq 2$ [113]).

Among the 230 crystalline space groups (SG), only 65 are chiral, thus limiting the crystallization of a single enantiomer [114]. In addition, crystal structures of two opposite enantiomers are specular images and the associated scalar properties of the crystalline materials (*e.g.* solubility, density, melting point) are identical while vectorial properties (*e.g.* optical properties) are of opposite signs.

The mirror symmetry between two enantiomers is also observable in phase diagrams. As a matter of fact, a vertical mirror exists along the racemic section in all phase diagrams between enantiomers. As illustrated in the textbook of Jacques *et al.* [106], three types of solid/liquid equilibrium phase diagram are encountered in case of mixture of enantiomers:

(i) According to the Cambridge Structural Data base (CSD), more than 95% of chiral compounds crystallize as racemic compounds [115]. It is a stoichiometric defined compound made of an equimolar association of both enantiomers (Figure 18 (a)). Unlike enantiopure samples, the symmetry of the lattice in a racemic compound is typically centrosymmetric.

(ii) In approximately 5% of occurrences, the mixture of enantiomers crystallizes as a physical mixture of the two enantiomorphic solids (Figure 18 (b)). In this case, it is defined as a conglomerate [116].

(iii) In rare cases (less than 1%), the mixture of enantiomers crystallizes as a complete solid solution (or mixed crystals):[117] both enantiomers are randomly distributed in a crystal isomorphous to the enantiopure forms. Rozeboom. proposed to classify the solid solutions into three types (I, II, III) according to the melting behavior of the mixture [118] (Figure 18 (c)).

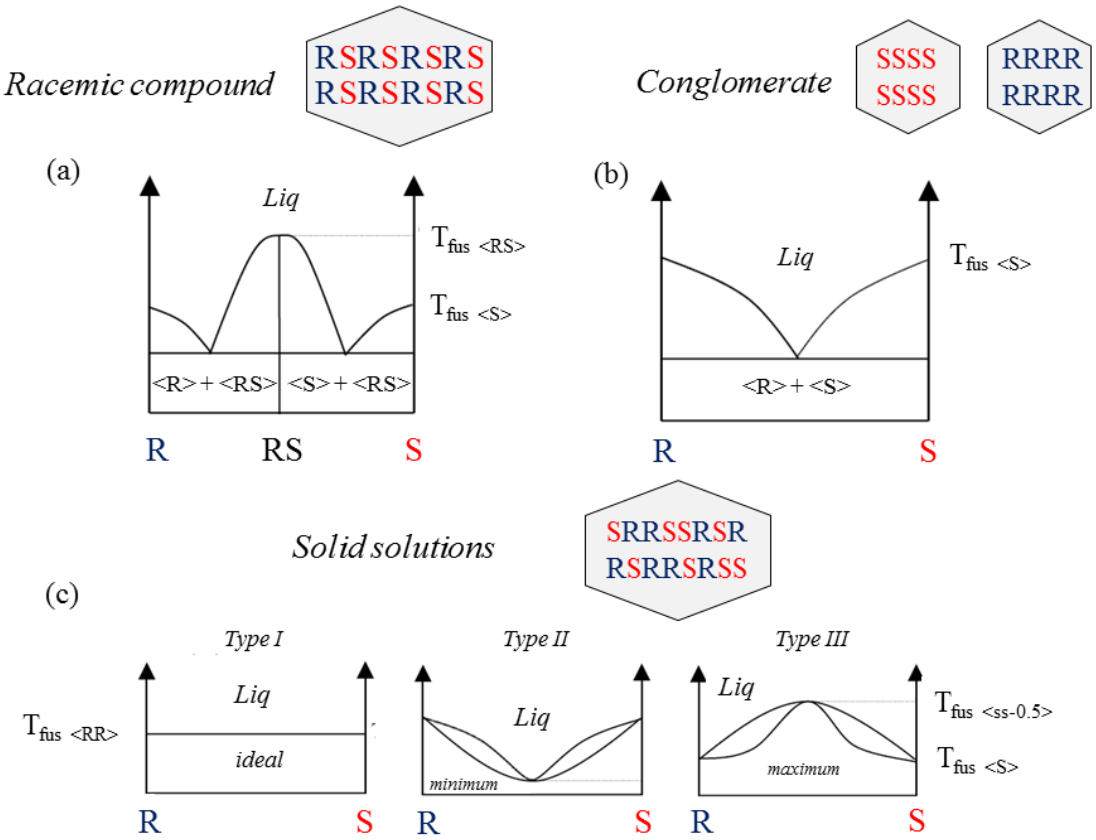

Figure 18. Schematic representation of the binary phase diagrams between enantiomers displaying the distinct equilibria: (a) racemic compound, (b) conglomerate, (c) three types of solid solutions (according to Roozeboom [118]).

The equilibria depicted in Figure 18 deal with only simple cases. Metastable equilibria and polymorphism of a given compound may occur and give rise to more complicated phase diagrams. As a matter of fact, the pure enantiomers or the racemic compound may be polymorphic [119]–[121], (*i.e.* enantiotropic or monotropic, see section I-4-1-2). In addition, concerning racemic compounds and conglomerates, the enantiomers may present domains of partial solid solutions [122]–[125]. A double polymorphism, *i.e.* the existence of several crystalline forms for both the pure enantiomers and the racemic compound, has been reported for the marketed drug named modafinil [126], [127].

I-5-3. Interest of chirality in disordered solids

I-5-3-1. Metastable Binary phase diagram

Many studies have been performed about polymorphism characterization in enantiomeric systems [112], [119], [121]-[124], [126]–[133]. However, these studies are rather focused on crystallization in solution and to a less extent on crystallization from the amorphous state. Among the exceptions are polymorphism studies of mixtures in the enantiomers of system {(1-x) mol L-limonene (4-isopropenyl-1-methyl-cyclohexene) + x mol D-limonene} [134]. The results were experimentally obtained by cooling the liquid mixtures to the amorphous state and then heating until they start to crystallize. It gave rise to two different solid-liquid phase diagrams. The diagram that corresponds to the thermodynamically stable situation involves the formation of racemic compound (Figure 19 (a)), whereas the other diagram obtained from amorphous state relies on the presence of mixed crystals (including a metastable solid solution, Figure 19 (b)). It clearly illustrates that whatever the enantiomeric excess of a mixture of enantiomers, the temperature of the glass transition remains constant.

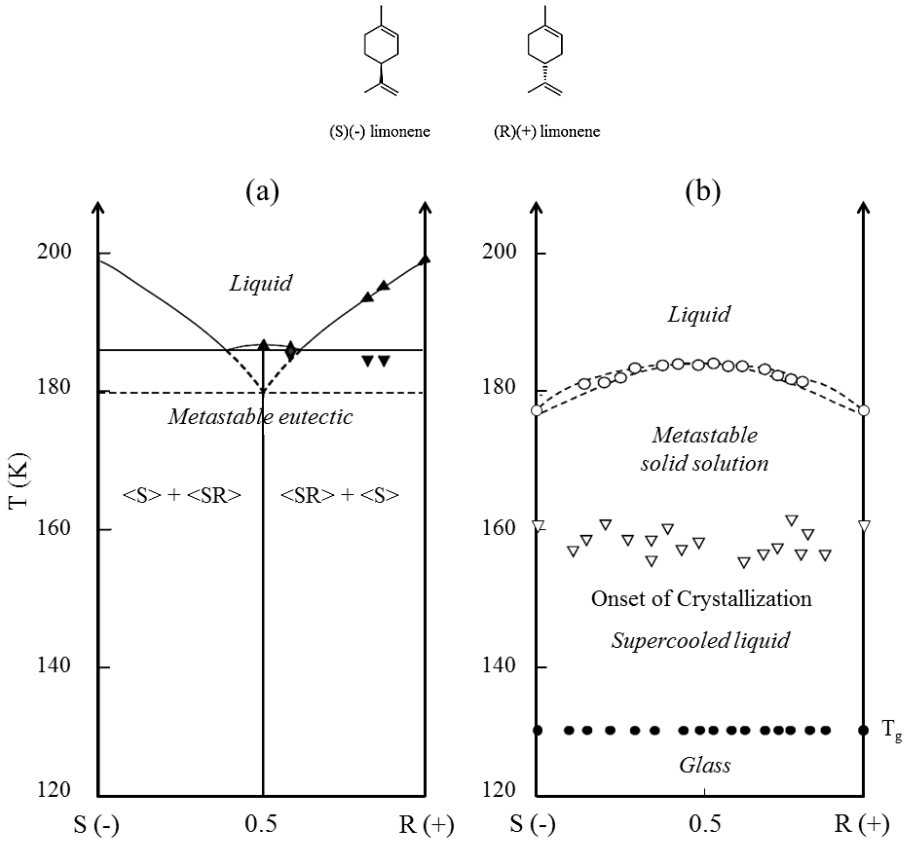

Figure 19. (a) Stable equibrilia between enantiomers of limonene. (b) Temperature of the glass transition temperature T_g versus enantiomeric composition and metastable equilibria exhibiting a single complete solid solution between chiral components. The upper part of the figure depicts the developed formulae of the enantiomers of limonene; Figure was adapted from [134].

A similar situation was observed for Carvone where undercooled mixtures d- and l-carvone, when heated in a calorimeter, crystallize as a solid solution [135]. Another interesting example, concerning only the racemic composition of ibuprofen is particularly illustrative of the resistance of an ordered racemic compound against nucleation in contrast to the relative ease of nucleation for a more disordered form at low temperature [93].

I-5-3-2. Chirality and Amorphous state

a. Prediction of glass transition temperatures in binary systems

Among the predicting laws of T_g in binary systems (Gordon-Taylor law [136] and its derivatives Kwei [137] and Couchman-Karasz laws [138]), the Gordon-Taylor law considering complete miscible mixtures of enantiomers could be adequately examined (excess entropy neglected) in any R-S binary system as follows:

$$T_g(x) = \frac{xT_{gS} + (1-x)KT_{gR}}{x + (1-x)K} \quad (Eq \text{ XXIV})$$

For each enantiomer, the glass transition temperatures (*i.e.* T_{gS} and T_{gR}) are identical and the constant K should be equal to 1 since it is defined as the ratio of the molar heat capacity increments of pure compounds [138] (*i.e.* ΔC_{pR} ,ΔC_{pS}). Thus, the glass transition temperatures T_g (x) should be independent of the enantiomeric composition x according to *Eq* XXII. This statement was experimentally confirmed by Gallis and coworkers on the study on the enantiomers of the limonene (Figure 19 (b)).

b. Relaxation between enantiomers

In the course of very recent studies (2015 - 2016) on the glass-to-crystal transition of a chiral API (Ketoprofen), [139], [140], Adrjanowicz *et al.* have demonstrated that the crystallization tendencies of supercooled S-enantiomer and racemic Ketoprofen studied along the same temperature/pressure conditions might be entirely different. Based on results of dielectric relaxation studies, they have demonstrated that the dynamics of a single enantiomer and the racemic mixture of enantiomers analyzed within the same range of thermodynamic conditions are similar, but not identical. Is this statement true for all chiral compounds? Additionally, the question of controlling crystallization abilities of glass-forming liquids still remains [141]. It is therefore essential to find model systems suitable to get deeper insights into the glass-to-crystal transition. In this work, the chiral drug Diprophylline was considered as a model compound.

References:

[1] Raynes, P. Liquid Crystals — Second Edition, by S. Chandrasekhar, Cambridge University Press, (1992). *Liq. Cryst. Today* **1993**, *3* (3), 7–7.

[2] Murdande, S. B.; Pikal, M. J.; Shanker, R. M.; Bogner, R. H. Solubility Advantage of Amorphous Pharmaceuticals: I. A Thermodynamic Analysis. *J. Pharm. Sci.* **2010**, *99* (3), 1254–1264.

[3] Hancock, B. C.; Parks, M. What Is the True Solubility Advantage for Amorphous Pharmaceuticals? *Pharm. Res.* **2000**, *17* (4), 397–404.

[4] Alonzo, D. E.; Gao, Y.; Zhou, D.; Mo, H.; Zhang, G. G. Z.; Taylor, L. S. Dissolution and Precipitation Behavior of Amorphous Solid Dispersions. *J. Pharm. Sci.* **2011**, *100* (8), 3316–3331.

[5] Alonzo, D. E.; Zhang, G. G. Z.; Zhou, D.; Gao, Y.; Taylor, L. S. Understanding the Behavior of Amorphous Pharmaceutical Systems during Dissolution. *Pharm. Res.* **2010**, *27* (4), 608–618.

[6] Newman, A.; Knipp, G.; Zografi, G. Assessing the Performance of Amorphous Solid Dispersions. *J. Pharm. Sci.* **2012**, *101* (4), 1355–1377.

[7] Yu, L. Amorphous Pharmaceutical Solids: Preparation, Characterization and Stabilization. *Adv. Drug Deliv. Rev.* **2001**, *48* (1), 27–42.

[8] Wojnarowska, Z.; Grzybowska, K.; Hawelek, L.; Dulski, M.; Wrzalik, R.; Gruszka, I.; Paluch, M.; Pienkowska, K.; Sawicki, W.; Bujak, P.; Paluch K.J., Tajber L.; Markowski J.; Molecular Dynamics, Physical Stability and Solubility Advantage from Amorphous Indapamide Drug. *Mol. Pharm.* **2013**, *10* (10), 3612–3627.

[9] Hancock, B. C.; Carlson, G. T.; Ladipo, D. D.; Langdon, B. A.; Mullarney, M. P. Comparison of the Mechanical Properties of the Crystalline and Amorphous Forms of a Drug Substance. *Int. J. Pharm.* **2002**, *241* (1), 73–85.

[10] Mishima, O.; Calvert, L. D.; Whalley, E. An Apparently First-Order Transition between Two Amorphous Phases of Ice Induced by Pressure. *Nature* **1985**, *314* (6006), 76–78.

[11] Grimsditch, M. Polymorphism in Amorphous SiO_2. *Phys. Rev. Lett.* **1984**, *52* (26), 2379–2381.

[12] Smith, K. H.; Shero, E.; Chizmeshya, A.; Wolf, G. The Equation of State of Polyamorphic Germania Glass: A two-domain description of the viscoelastic response. *J. Chem. Phys.* **1995**, *102* (17), 6851–6857.

[13] Zhu, M.; Wang, J.-Q.; Perepezko, J. H.; Yu, L. Possible Existence of Two Amorphous Phases of D-Mannitol Related by a First-Order Transition. *J. Chem. Phys.* **2015**, *142* (24), 244504-1– 244504-7.

[14] Karmwar, P.; Graeser, K.; Gordon, K. C.; Strachan, C. J.; Rades, T. Investigation of Properties and Recrystallisation Behaviour of Amorphous Indomethacin Samples Prepared by Different Methods. *Int. J. Pharm.* **2011**, *417* (1–2), 94–100.

[15] Savolainen, M.; Heinz, A.; Strachan, C.; Gordon, K. C.; Yliruusi, J.; Rades, T.; Sandler, N. Screening for Differences in the Amorphous State of Indomethacin Using Multivariate Visualization. *Eur. J. Pharm. Sci.* **2007**, *30* (2), 113–123.

[16] Turnbull, D. Under What Conditions Can a Glass Be Formed? *Contemp. Phys.* **1969**, *10* (5), 473–488.

[17] Dhotel, A.; Rijal, B.; Delbreilh, L.; Dargent, E.; Saiter, A. Combining Flash DSC, DSC and Broadband Dielectric Spectroscopy to Determine Fragility. *J. Therm. Anal. Calorim.* **2015**, *121* (1), 453–461.

[18] Šesták, J., Mareš, J. J., Hubík, P. *Glassy, Amorphous and Nano-Crystalline Materials*, Hot Topics in Thermal Analysis and Calorimetry; Springer Netherlands: Dordrecht, **2011**; Vol. 8.
[19] Hancock, B. C.; Zografi, G. The Relationship Between the Glass Transition Temperature and the Water Content of Amorphous Pharmaceutical Solids. *Pharm. Res.* **1994**, *11* (4), 471–477.
[20] Kauzmann, W. The Nature of the Glassy State and the Behavior of Liquids at Low Temperatures. *Chem. Rev.* **1948**, *43* (2), 219–256.
[21] Stillinger, F. H.; Debenedetti, P. G.; Truskett, T. M. The Kauzmann Paradox Revisited. *J. Phys. Chem. B* **2001**, *105* (47), 11809–11816.
[22] Stillinger, F. H.; Debenedetti, P. G. Phase Transitions, Kauzmann Curves, and Inverse Melting. *Biophys. Chem.* **2003**, *105* (2–3), 211–220.
[23] Ediger, M. D.; Angell, C. A.; Nagel, S. R. Supercooled Liquids and Glasses. *J. Phys. Chem.* **1996**, *100* (31), 13200–13212.
[24) Debenedetti, P. G.; Stillinger, F. H. Supercooled Liquids and the Glass Transition. *Nature* **2001**, *410* (6825), 259–267.
[25] Doolittle, A. K. Studies in Newtonian Flow. II. The Dependence of the Viscosity of Liquids on Free-Space. *J. Appl. Phys.* **1951**, *22* (12), 1471–1475.
[26] Cohen, M. H.; Grest, G. S. Liquid-Glass Transition, a Free-Volume Approach. *Phys. Rev. B* **1979**, *20* (3), 1077–1098.
[27] Adam, G.; Gibbs, J. H. On the Temperature Dependence of Cooperative Relaxation Properties in Glass-Forming Liquids. *J. Chem. Phys.* **1965**, *43* (1), 139–146.
[28] Tanaka, H. Two-Order-Parameter Description of Liquids. I. A General Model of Glass Transition Covering Its Strong to Fragile Limit. *J. Chem. Phys.* **1999**, *111* (7), 3163–3174.
[29] Tanaka, H. Two-Order-Parameter Model of the Liquid–glass Transition. I. Relation between Glass Transition and Crystallization. *J. Non-Cryst. Solids* **2005**, *351* (43–45), 3371–3384.
[30] Shintani, H.; Tanaka, H. Frustration on the Way to Crystallization in Glass. *Nat. Phys.* **2006**, *2* (3), 200–206.
[31] Kaushal, A. M.; Gupta, P.; Bansal, A. K. Amorphous Drug Delivery Systems: Molecular Aspects, Design, and Performance. *Crit. Rev. Ther. Drug Carrier Syst.* **2004**, *21* (3), 133–193.
[32] Babu, N. J.; Nangia, A. Solubility Advantage of Amorphous Drugs and Pharmaceutical Cocrystals. *Cryst. Growth Des.* **2011**, *11* (7), 2662–2679.
[33] Laitinen, R.; Löbmann, K.; Strachan, C. J.; Grohganz, H.; Rades, T. Emerging Trends in the Stabilization of Amorphous Drugs. *Int. J. Pharm.* **2013**, *453* (1), 65–79.
[34] Gupta, P.; Chawla, G.; Bansal, A. K. Physical Stability and Solubility Advantage from Amorphous Celecoxib: The Role of Thermodynamic Quantities and Molecular Mobility. *Mol. Pharm.* **2004**, *1* (6), 406–413.
[35] Bhugra, C.; Shmeis, R.; Pikal, M. J. Role of Mechanical Stress in Crystallization and Relaxation Behavior of Amorphous Indomethacin. *J. Pharm. Sci.* **2008**, *97* (10), 4446–4458.
[36] Shamblin, S. L.; Tang, X.; Chang, L.; Hancock, B. C.; Pikal, M. J. Characterization of the Time Scales of Molecular Motion in Pharmaceutically Important Glasses. *J. Phys. Chem. B* **1999**, *103* (20), 4113–4121.
[37] Shamblin, S. L.; Hancock, B. C.; Dupuis, Y.; Pikal, M. J. Interpretation of Relaxation Time Constants for Amorphous Pharmaceutical Systems. *J. Pharm. Sci.* **2000**, *89* (3), 417–427.

[38] Adrjanowicz, K.; Wojnarowska, Z.; Wlodarczyk, P.; Kaminski, K.; Paluch, M.; Mazgalski, J. Molecular Mobility in Liquid and Glassy States of Telmisartan Studied by Broadband Dielectric Spectroscopy. *Eur. J. Pharm. Sci. Off. J. Eur. Fed. Pharm. Sci.* **2009**, *38* (4), 395–404.
[39] Bhardwaj, S. P.; Arora, K. K.; Kwong, E.; Templeton, A.; Clas, S.-D.; Suryanarayanan, R. Correlation between Molecular Mobility and Physical Stability of Amorphous Itraconazole. *Mol. Pharm.* **2013**, *10* (2), 694–700.
[40] Schammé, B.; Couvrat, N.; Malpeli, P.; Delbreilh, L.; Dupray, V.; Dargent, É.; Coquerel, G. Crystallization Kinetics and Molecular Mobility of an Amorphous Active Pharmaceutical Ingredient: A Case Study with Biclotymol. *Int. J. Pharm.* **2015**, *490* (1–2), 248–257.
[41] Zhou, D.; Zhang, G. G. Z.; Law, D.; Grant, D. J. W.; Schmitt, E. A. Thermodynamics, Molecular Mobility and Crystallization Kinetics of Amorphous Griseofulvin. *Mol. Pharm.* **2008**, *5* (6), 927–936.
[42] Kremer, F., Schönhals, A., *Broadband Dielectric Spectroscopy*; Springer Berlin Heidelberg: Berlin, Heidelberg, **2003**.
[43] Descamps, M. *Disordered Pharmaceutical Materials*; John Wiley & Sons, 2016.
[44] Cole, K. S.; Cole, R. H. Dispersion and Absorption in Dielectrics I. Alternating Current Characteristics. *J. Chem. Phys.* **1941**, *9* (4), 341–351.
[45] Davidson, D. W.; Cole, R. H. Dielectric Relaxation in Glycerine. *J. Chem. Phys.* **1950**, *18* (10), 1417–1417.
[46] Davidson, D. W.; Cole, R. H. Dielectric Relaxation in Glycerol, Propylene Glycol, and n-Propanol. *J. Chem. Phys.* **1951**, *19* (12), 1484–1490.
[47] Havriliak, S.; Negami, S. A Complex Plane Analysis of α-Dispersions in Some Polymer Systems. *J. Polym. Sci. Part C Polym. Symp.* **1966**, *14* (1), 99–117.
[48] Havriliak, S.; Negami, S. A Complex Plane Representation of Dielectric and Mechanical Relaxation Processes in Some Polymers. *Polymer* **1967**, *8*, 161–210.
[49] Williams, G.; Watts, D. C. Non-Symmetrical Dielectric Relaxation Behaviour Arising from a Simple Empirical Decay Function. *Trans. Faraday Soc.* **1970**, *66* (0), 80–85.
[50] Williams, G.; Watts, D. C.; Dev, S. B.; North, A. M. Further Considerations of Non Symmetrical Dielectric Relaxation Behaviour Arising from a Simple Empirical Decay Function. *Trans. Faraday Soc.* **1971**, *67* (0), 1323–1335.
[51] Floudas, D. G.; Paluch, P. M.; Grzybowski, D. A.; Ngai, P. K. L. Polypeptide Dynamics. In *Molecular Dynamics of Glass-Forming Systems*; Advances in Dielectrics; Springer Berlin Heidelberg, **2011**; 149–168.
[52] Angell, C. A.; Ngai, K. L.; McKenna, G. B.; McMillan, P. F.; Martin, S. W. Relaxation in Glassforming Liquids and Amorphous Solids. *J. Appl. Phys.* **2000**, *88* (6), 3113–3157.
[53] Cyrot, M. A Possible Origin for the Vogel-Fulcher Law. *Phys. Lett. A* **1981**, *83* (6), 275–278.
[54] Fulcher, G. S. Analysis of Recent Measurements of the Viscosity of Glasses. *J. Am. Ceram. Soc.* **1925**, *8* (6), 339–355.
[55] Tammann, G.; Hesse, W. Die Abhängigkeit Der Viscosität von Der Temperatur Bie Unterkühlten Flüssigkeiten. *Z. Für Anorg. Allg. Chem.* **1926**, *156* (1), 245–257.
[56] Böhmer, R.; Ngai, K. L.; Angell, C. A.; Plazek, D. J. Nonexponential Relaxations in Strong and Fragile Glass Formers. *J. Chem. Phys.* **1993**, *99* (5), 4201–4209.
[57] Angell, C. A. Relaxation in Liquids, Polymers and Plastic Crystals—strong/Fragile Patterns and Problems. *J. Non-Cryst. Solids* **1991**, *131*, 13–31.
[58] Hancock, B. C.; Shamblin, S. L. Molecular Mobility of Amorphous Pharmaceuticals Determined Using Differential Scanning Calorimetry. *Thermochim. Acta* **2001**, *380* (2), 95–107.

[59] Grzybowska, K.; Paluch, M.; Grzybowski, A.; Wojnarowska, Z.; Hawelek, L.; Kolodziejczyk, K.; Ngai, K. L. Molecular Dynamics and Physical Stability of Amorphous Anti-Inflammatory Drug: Celecoxib. *J. Phys. Chem. B* **2010**, *114* (40), 12792–12801.
[60] Wojnarowska, Z.; Adrjanowicz, K.; Wlodarczyk, P.; Kaminska, E.; Kaminski, K.; Grzybowska, K.; Wrzalik, R.; Paluch, M.; Ngai, K. L. Broadband Dielectric Relaxation Study at Ambient and Elevated Pressure of Molecular Dynamics of Pharmaceutical: Indomethacin. *J. Phys. Chem. B* **2009**, *113* (37), 12536–12545.
[61] Adrjanowicz, K. The Role of Molecular Mobility in Governing the Physical Stability of Amorphous Pharmaceuticals, PhD Thesis, University of Silesia, **2012**.
[62] Richert, R. Relaxations in Complex Systems Homogeneous Dispersion of Dielectric Responses in a Simple Glass. *J. Non-Cryst. Solids* **1994**, *172*, 209–213.
[63] Williams, G. Proceedings of the International Discussion Meeting on Relaxations in Complex Systems Molecular Motion in Glass-Forming Systems. *J. Non-Cryst. Solids* **1991**, *131*, 1–12.
[64] Ngai, K. L. Dynamic and Thermodynamic Properties of Glass-Forming Substances. *J. Non-Cryst. Solids* **2000**, *275* (1–2), 7–51.
[65] Kawasaki, T.; Tanaka, H. Formation of a Crystal Nucleus from Liquid. *Proc. Natl. Acad. Sci. U. S. A.* **2010**, *107* (32), 14036–14041.
[66] Grzybowska, K.; Grzybowski, A.; Ziolo, J.; Rzoska, S. J.; Paluch, M. Anomalous Behavior of Secondary Dielectric Relaxation in Polypropylene Glycols. *J. Phys. Condens. Matter* **2007**, *19* (37), 376105-1–376105-11.
[67] Johari, G. P.; Goldstein, M. Viscous Liquids and the Glass Transition. II. Secondary Relaxations in Glasses of Rigid Molecules. *J. Chem. Phys.* **1970**, *53* (6), 2372–2388.
[68] Ngai, K. L.; Paluch, M. Classification of Secondary Relaxation in Glass-Formers Based on Dynamic Properties. *J. Chem. Phys.* **2004**, *120* (2), 857–873.
[69] Kudlik, A.; Benkhof, S.; Blochowicz, T.; Tschirwitz, C.; Rössler, E. The Dielectric Response of Simple Organic Glass Formers. *J. Mol. Struct.* **1999**, *479* (2–3), 201–218.
[70] Dixon, P. K.; Wu, L.; Nagel, S. R.; Williams, B. D.; Carini, J. P. Scaling in the Relaxation of Supercooled Liquids. *Phys. Rev. Lett.* **1990**, *65* (9), 1108–1111.
[71] Floudas, D. G.; Paluch, P. M.; Grzybowski, D. A.; Ngai, P. K. L. New Physics Gained by the Application of Pressure in the Study of Dynamics of Glass Formers. In *Molecular Dynamics of Glass-Forming Systems*; Advances in Dielectrics; Springer Berlin Heidelberg, **2011**, 89–120.
[72] Roland, C. M.; Hensel-Bielowka, S.; Paluch, M.; Casalini, R. Supercooled Dynamics of Glass-Forming Liquids and Polymers under Hydrostatic Pressure. *Rep. Prog. Phys.* **2005**, *68* (6), 1405–1478.
[73] Kolodziejczyk, K.; Grzybowska, K.; Wojnarowska, Z.; Dulski, M.; Hawelek, L.; Paluch, M. Isothermal Cold Crystallization Kinetics Study of Sildenafil. *Cryst. Growth Des.* **2014**, *14* (7), 3199–3209.
[74] Kalikmanov, V.I.; Classical Nucleation Theory. In *Nucleation Theory;* Springer Netherlands, **2013.**
[75] Heady, R.B.; Cahn, J.W. Experimental test of classical nucleation theory in a liquid-liquid miscibility gap system. *J. Chem. Phys.* **1973**, *58* (3), 896-910.
[76] Hancock, B. C.; Zografi, G. Characteristics and Significance of the Amorphous State in Pharmaceutical Systems. *J. Pharm. Sci.* **1997**, *86* (1), 1–12.
[77] Tao, J.; Yu, L. Kinetics of Cross-Nucleation between Polymorphs. *J. Phys. Chem. B* **2006**, *110* (14), 7098–7101.
[78] Gutzow, I. S.; Schmelzer, J. W. P. *The Vitreous State*; Springer Berlin Heidelberg: Berlin, Heidelberg, **2013**.

[79] Gutzow, I.; Avramov, I.; Kästner, K. XVth International Congress on Glass Glass Formation and Crystallization. *J. Non-Cryst. Solids* **1990**, *123* (1), 97–113.
[80] Yoshioka, M.; Hancock, B. C.; Zografi, G. Crystallization of Indomethacin from the Amorphous State below and above Its Glass Transition Temperature. *J. Pharm. Sci.* **1994**, *83* (12), 1700–1705.
[81] Aso, Y.; Yoshioka, S.; Kojima, S. Relationship between the Crystallization Rates of Amorphous Nifedipine, Phenobarbital, and Flopropione, and Their Molecular Mobility as Measured by Their Enthalpy Relaxation and ^{1}H NMR Relaxation Times. *J. Pharm. Sci.* **2000**, *89* (3), 408–416.
[82] Aso, Y.; Yoshioka, S.; Kojima, S. Explanation of the Crystallization Rate of Amorphous Nifedipine and Phenobarbital from Their Molecular Mobility as Measured by ^{13}C Nuclear Magnetic Resonance Relaxation Time and the Relaxation Time Obtained from the Heating Rate Dependence of the Glass Transition Temperature. *J. Pharm. Sci.* **2001**, *90* (6), 798–806.
[83] Spaepen, F. A Structural Model for the Solid-Liquid Interface in Monatomic Systems. *Acta Metall.* **1975**, *23* (6), 729–743.
[84] Spaepen, F.; Meyer, R. B. The Surface Tension in a Structural Model for the Solid-Liquid Interface. *Scr. Metall.* **1976**, *10* (3), 257–263.
[85] Haase, W. J. N. Sherwood (Ed.): The Plastically Crystalline State. John Wiley & Sons, *Berichte Bunsenges. Für Phys. Chem.* **1980**, *84* (11), 1192–1192.
[86] Suga, H.; Seki, S. Thermodynamic Investigation on Glassy States of Pure Simple Compounds. *J. Non-Cryst. Solids* **1974**, *16* (2), 171–194.
[87] Ostwald, W. *Studien Über Die Bildung Und Umwandlung Fester Körper. 1. Abhandlung: Übersättigung Und Überkaltung*, **1897**.
[88] Threlfall, T. Structural and Thermodynamic Explanations of Ostwald's Rule. *Org. Process Res. Dev.* **2003**, *7* (6), 1017–1027.
[89] Turnbull, D.; Bagley, B. G. Transitions in Viscous Liquids and Glasses. In *Changes of State*; Hannay, N. B., Ed.; Springer US: Boston, MA, **1975**, 513–554.
[90] Sillescu, H. Relaxation and Thermodynamics in Polymers-Glass Transition. By Ernst-Joachim Donth, Akademie Verlag, Berlin 1992, *Acta Polym.* **1994**, *45* (1), 56–56.
[91] Kelton, K. F. Crystal Nucleation in Liquids and Glasses. In *Solid State Physics*; Turnbull, H. E. and D., Ed.; Academic Press, **1991**, *45*, 75–177.
[92] Redinha, J. S.; Jesus, A. L. *Crystal Growth of Pharmaceuticals from Melt*, Crystallization and Materials Science of Modern Artificial and Natural Crystals, **2012**, *10***,** 225–248.
[93] Descamps, M.; Dudognon, E. Crystallization from the Amorphous State: Nucleation–Growth Decoupling, Polymorphism Interplay, and the Role of Interfaces. *J. Pharm. Sci.* **2014**, *103* (9), 2615–2628.
[94] Porter, D. A.; Easterling, K. E.; Sherif, M. *Phase Transformations in Metals and Alloys*, CRC press, **2009**.
[95] Zhu, L.; Brian, C. W.; Swallen, S. F.; Straus, P. T.; Ediger, M. D.; Yu, L. Surface Self-Diffusion of an Organic Glass. *Phys. Rev. Lett.* **2011**, *106* (25), 256103-1–256103-4.
[96] Capaccioli, S.; Ngai, K. L.; Paluch, M.; Prevosto, D. Mechanism of Fast Surface Self-Diffusion of an Organic Glass. *Phys. Rev. E* **2012**, *86* (5), 051503-1–051503-6.
[97] Hilfiker, R., *Polymorphism in the Pharmaceutical Industry*; Ed. Wiley-VCH: Weinheim, **2006**.
[98] Datta, S.; Grant, D. J. W. Crystal Structures of Drugs: Advances in Determination, Prediction and Engineering. *Nat. Rev. Drug Discov.* **2004**, *3* (1), 42–57.

[99] Grunenberg, A.; Henck, J.-O.; Siesler, H. W. Theoretical Derivation and Practical Application of Energy/Temperature Diagrams as an Instrument in Preformulation Studies of Polymorphic Drug Substances. *Int. J. Pharm.* **1996**, *129* (1–2), 147–158.
[100] Haleblian, J. K. Characterization of Habits and Crystalline Modification of Solids and Their Pharmaceutical Applications. *J. Pharm. Sci.* **1975**, *64* (8), 1269–1288.
[101] Burger, A.; Ramberger, R. On the Polymorphism of Pharmaceuticals and Other Molecular Crystals. I. *Microchim. Acta* **1979**, *72* (3–4), 259–271.
[102] Burger, A.; Ramberger, R. On the Polymorphism of Pharmaceuticals and Other Molecular Crystals. II. *Microchim. Acta* **1979**, *72* (3–4), 273–316.
[103] Bernstein, J. *Polymorphism in Molecular Crystals*; International Union of Crystallography monographs on crystallography; Oxford University Press: Oxford Clarendon Press ; New York, **2002**.
[104] Moulton, B.; Zaworotko, M. J. From Molecules to Crystal Engineering: Supramolecular Isomerism and Polymorphism in Network Solids. *Chem. Rev.* **2001**, *101* (6), 1629–1658.
[105] Yu, L.; Reutzel-Edens, S. M.; Mitchell, C. A. Crystallization and Polymorphism of Conformationally Flexible Molecules: Problems, Patterns, and Strategies. *Org. Process Res. Dev.* **2000**, *4* (5), 396–402.
[106] Snatzke, G.; Jacques, J.; Collet, A.; Wilen S. H.: Enantiomers, Racemates, and Resolutions, J. Wiley & Sons, Inc. *Berichte Bunsenges. Für Phys. Chem.* **1982**, *86* (11), 1087–1087.
[107] Moss, G. P. Basic Terminology of Stereochemistry (IUPAC Recommendations 1996). *Pure Appl. Chem.* **1996**, *68* (12), 2193–2222.
[108] Kelvin, W. T. *The Molecular Tactics of a Crystal*; Oxford, Clarendon Press, **1894**.
[109] Collet, A.; Crassous, J.; Dutasta, J.-P.; Guy, L. *Molécules chirales : Stéréochimie et propriétés*; EDP Sciences: Les Ulis; Paris, **2006**.
[110] Bijvoet, J. M.; Peerdeman, A. F.; van Bommel, A. J. Determination of the Absolute Configuration of Optically Active Compounds by Means of X-Rays. *Nature* **1951**, *168* (4268), 271–272.
[111] Bredikhin, A. A.; Bredikhina, Z. A.; Novikova, V. G.; Pashagin, A. V.; Zakharychev, D. V.; Gubaidullin, A. T. Three Different Types of Chirality-Driven Crystallization within the Series of Uniformly Substituted Phenyl Glycerol Ethers. *Chirality* **2008**, *20* (10), 1092–1103.
[112] Scott, R. L. Modification of the Phase Rule for Optical Enantiomers and Other Symmetric Systems. *J. Chem. Soc. Faraday Trans. 2 Mol. Chem. Phys.* **1977**, *73* (3), 356–360.
[113] Coquerel, G. Review on the Heterogeneous Equilibria between Condensed Phases in Binary Systems of Enantiomers. *Enantiomer* **2000**, *5* (5), 481–498.
[114] Brock, C. P.; Dunitz, J. D. Towards a Grammar of Crystal Packing. *Chem. Mater.* **1994**, *6* (8), 1118–1127.
[115] Chen, L.; Ma, H.; Liu, X.; xiang Jiang, S. Semipreparative Enantiomer Separation of Propranolol Hydrochloride by High-Performance Liquid Chromatography Using Cellulose Tris (3, 5-Dimethylphenylcarbamate) Chiral Stationary Phase. *J. Chromatogr. Sci.* **2008**, *46* (9), 767–771.
[116] Galland, A.; Dupray, V.; Lafontaine, A.; Berton, B.; Sanselme, M.; Atmani, H.; Coquerel, G. Preparative Resolution of (±)-Trans-1,2-Diaminocyclohexane by Means of Preferential Crystallization of Its Citrate Monohydrate. *Tetrahedron Asymmetry* **2010**, *21* (18), 2212–2217.
[117] Kitaigorodsky, P. D. A. I. Particle Packing in a Crystal. In *Mixed Crystals*; Springer Series in Solid-State Sciences; Springer Berlin Heidelberg, **1984**, 49–84.

[118] Bakhuis-Roozeboom, H. W. Löslichkeit Und Schmelzpunkt Als Kriteria Für Racemische Verbindungen, Pseudoracemische Mischkrystalle Und Inactive Conglomerate. *Berichte Dtsch. Chem. Ges.* **1899**, *32* (1), 537–541.
[119] Kaemmerer, H.; Lorenz, H.; Black, S. N.; Seidel-Morgenstern, A. Study of System Thermodynamics and the Feasibility of Chiral Resolution of the Polymorphic System of Malic Acid Enantiomers and Its Partial Solid Solutions. *Cryst. Growth Des.* **2009**, *9* (4), 1851–1862.
[120] Burger, A.; Rollinger, J. M.; Brüggeller, P. Binary System of (R)- and (S)-Nitrendipine--Polymorphism and Structure. *J. Pharm. Sci.* **1997**, *86* (6), 674–679.
[121] Reutzel-Edens, S. M.; Russell, V. A.; Yu, L. Molecular Basis for the Stability Relationships between Homochiral and Racemic Crystals of Tazofelone: A Spectroscopic, Crystallographic, and Thermodynamic Investigation. *J. Chem. Soc. Perkin Trans. 2* **2000**, 5, 913–924.
[122] Taratin, N. V.; Lorenz, H.; Kotelnikova, E. N.; Glikin, A. E.; Galland, A.; Dupray, V.; Coquerel, G.; Seidel-Morgenstern, A. Mixed Crystals in Chiral Organic Systems: A Case Study on (R)- and (S)-Ethanolammonium 3-Chloromandelate. *Cryst. Growth Des.* **2012**, *12* (12), 5882–5888.
[123] Renou, L.; Morelli, T.; Coste, S.; Petit, M.-N.; Berton, B.; Malandain, J.-J.; Coquerel, G. Chiral Discrimination at the Solid State of Methyl 2-(Diphenylmethylsulfinyl)acetate. *Cryst. Growth Des.* **2007**, *7* (9), 1599–1607.
[124] Wermester, N.; Aubin, E.; Pauchet, M.; Coste, S.; Coquerel, G. Preferential Crystallization in an Unusual Case of Conglomerate with Partial Solid Solutions. *Tetrahedron Asymmetry* **2007**, *18* (7), 821–831.
[125] Linol, J.; Morelli, T.; Petit, M.-N.; Coquerel, G. Inversion of the Relative Stability between Two Polymorphic Forms of (±) Modafinil under Dry High-Energy Milling: Comparisons with Results Obtained under Wet High-Energy Milling. *Cryst. Growth Des.* **2007**, *7* (9), 1608–1611.
[126] Neckebrock, O.; Courvoisier, L.; Graf, S.; Serrure, G.; Coquerel, G.; Rose, S.; Besselievre, C.; Mallet, F.; Langevelde, A. van. Method for the Production of Crystalline Forms and Crystalline Forms of Optical Enantiomers of Modafinil. US20060135621 A1, **2006**.
[127] Rollinger, J. M.; Burger, A. Polymorphism of Racemic Felodipine and the Unusual Series of Solid Solutions in the Binary System of Its Enantiomers. *J. Pharm. Sci.* **2001**, *90* (7), 949–959.
[128] de Diego, H. L.; Bond, A. D.; Dancer, R. J. Formation of Solid Solutions between Racemic and Enantiomeric Citalopram Oxalate. *Chirality* **2011**, *23* (5), 408–416.
[129] Stéphane Beilles, P. C. Preferential Crystallisation and Comparative Crystal Growth Study between Pure Enantiomer and Racemic Mixture of a Chiral Molecule: 5-Ethyl-5-Methylhydrantoin. *Chem. Eng. Sci.* **2001**, *56* (7), 2281–2294.
[130] Lorenz, H.; Sapoundjiev, D.; Seidel-Morgenstern, A. Enantiomeric Mandelic Acid SystemMelting Point Phase Diagram and Solubility in Water. *J. Chem. Eng. Data* **2002**, *47* (5), 1280–1284.
[131] Le Minh, T.; Von Langermann, J.; Lorenz, H.; Seidel-Morgenstern, A. Enantiomeric 3-Chloromandelic Acid System: Binary Melting Point Phase Diagram, Ternary Solubility Phase Diagrams and Polymorphism. *J. Pharm. Sci.* **2010**, *99* (9), 4084–4095.
[132] Dwivedi, S. K.; Sattari, S.; Jamali, F.; Mitchell, A. G. Ibuprofen Racemate and Enantiomers: Phase Diagram, Solubility and Thermodynamic Studies. *Int. J. Pharm.* **1992**, *87* (1–3), 95–104.

[133] Gallis, H. E.; Cees van Miltenburg, J.; Oonk, H. A. J. Polymorphism of Mixtures of Enantiomers: A Thermodynamic Study of Mixtures of D- and L-Limonene. *Phys. Chem. Chem. Phys.* **2000**, *2* (24), 5619–5623.
[134] Gallis, H. E.; Bougrioua, F.; Oonk, H. A. J.; van Ekeren, P. J.; van Miltenburg, J. C. Mixtures of D- and L-Carvone: I. Differential Scanning Calorimetry and Solid-Liquid Phase Diagram. *Thermochim. Acta* **1996**, *274*, 231–242.
[135] Gallis, H. E.; van Ekeren, P. J.; van Miltenburg, J. C.; Oonk, H. A. J. Mixtures of D- and L-Carvone: IV. Transformation from a Solid Solution to a Racemic Compound. *Thermochim. Acta* **1999**, *326* (1–2), 83–90.
[136] Gordon, J. M.; Rouse, G. B.; Gibbs, J. H.; Jr, W. M. R. The Composition Dependence of Glass Transition Properties. *J. Chem. Phys.* **1977**, *66* (11), 4971–4976.
[137] Lin, A. A.; Kwei, T. K.; Reiser, A. On the Physical Meaning of the Kwei Equation for the Glass Transition Temperature of Polymer Blends. *Macromolecules* **1989**, *22* (10), 4112–4119.
[138] Couchman, P. R.; Karasz, F. E. A Classical Thermodynamic Discussion of the Effect of Composition on Glass-Transition Temperatures. *Macromolecules* **1978**, *11* (1), 117–119.
[139] Adrjanowicz, K.; Kaminski, K.; Paluch, M.; Niss, K. Crystallization Behavior and Relaxation Dynamics of Supercooled *S* -Ketoprofen and the Racemic Mixture along an Isochrone. *Cryst. Growth Des.* **2015**, *15* (7), 3257–3263.
[140] Adrjanowicz, K.; Kaminski, K.; Tarnacka, M.; Szutkowski, K.; Popenda, L.; Bartkowiak, G.; Paluch, M. The Effect of Hydrogen Bonding Propensity and Enantiomeric Composition on the Dynamics of Supercooled Ketoprofen – Dielectric, Rheological and NMR Studies. *Phys. Chem. Chem. Phys.* **2016**, *18* (15), 10585–10593.
[141] Kaminski, K.; Adrjanowicz, K.; Wojnarowska, Z.; Dulski, M.; Wrzalik, R.; Paluch, M.; Kaminska, E.; Kasprzycka, A. Do Intermolecular Interactions Control Crystallization Abilities of Glass-Forming Liquids? *J. Phys. Chem. B* **2011**, *115* (40), 11537–11547.

Chapter II

The Relaxation Behavior of Diprophylline (DPL): Influence of Chemical Purity and Chirality

Foreword

The chiral drug Diprophylline (DPL hereafter, Figure 1), also known as dyphylline, is a representative of theophylline derivatives with broncho- and vasodilator properties that are used in the treatment of pulmonary diseases (*e.g.* bronchial asthma). The racemic solid (a 50/50 mixture of both enantiomers) is used in oral dosage forms. The biological activity of the *(R)* or *(S)* enantiomer has been found rather similar to that of the racemate [1]. The other information provided by the European Pharmacopoeia are given in Appendix III. Like theophylline [2] and other theophylline derivatives such as etophylline [3] and proxyphylline [4], the racemic mixture of DPL exhibits a rich polymorphic landscape [5]. The polymorphism of DPL has been reported by Brandstätter and Grimm in 1956 [6] for the first time, indicating the existence of three potential crystalline phases (at the racemic composition). In a later communication (in 1971), only two crystalline forms have been mentioned [7]. The rationalization of the polymorphic behavior of rac-DPL (crystalline forms obtained either by recrystallization from the melt and from solvent) has been proposed by Griesser *et al.* in 1999 [5]. The complete characterization of the two phases of the racemic composition has been performed in 2013 by Brandel *et al.* [8]. Besides, the crystallization behavior of DPL between enantiomers has carefully been investigated and its binary phase diagram is admittedly incomplete but reveals an interesting situation since annealing DPL supercooled melts with various enantiomeric compositions can induce the crystallization of stable or metastable enantiomeric and racemic compounds but also metastable solid solutions [8]. In addition, it has been proved in the past that a glassy state of DPL could be reached by cooling the melt using differential scanning calorimetry [9]. However a complete characterization of the amorphous state of DPL was never performed as only a single enantiomeric composition was studied. The following chapter is thus devoted to the characterization of the molecular mobility (below and above the glass transition temperature) of the amorphous state of DPL at various enantiomeric compositions.

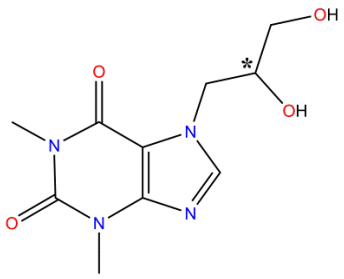

Figure 1. Developed formula of the API Diprophylline consisting of a heterocyclic part (theophylline moiety) bonded to a flexible propanediol substituent. The asymmetric carbon is shown with an asterisk.

II-1. Preparation of samples and characterization of racemic and enantiopure compositions of Diprophylline (DPL)

II-1-1. Preparation and characterization of enantiopure and racemic DPL crystalline phases

As described in a previous work [8], pure enantiomers can be synthesized as follows (Figure 2): 3.27 g of theophylline (purchased from Acros Organic, purity 99%) and 1.17 g of potassium hydroxyde (Acros organic, purity 85%) were dissolved at 70°C in 30 mL of distilled water. Then, 2.31 g of (*R*) or *(S)*-3-Chloro 1, 2-propanediol (Alpha Aesar, USA, purity 98%, 97% ee) were dissolved in distilled water (5mL) and added dropwise. The mixture was stirred during 24h at 70°C.

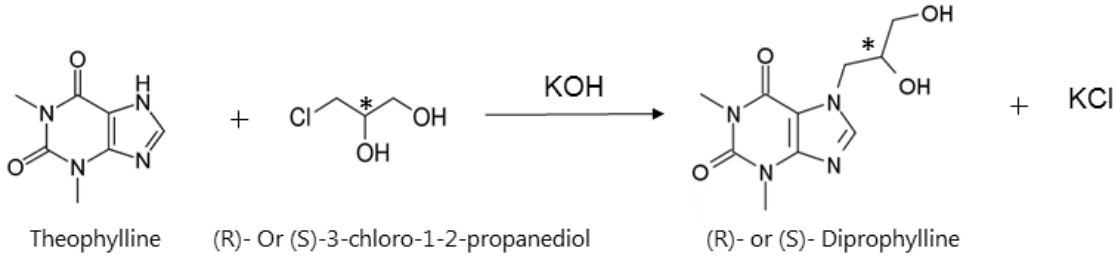

Figure 2. Chemical reaction used for the synthesis of (R)- or (S)-DPL.

Water was evaporated under reduced pressure, and the solid was obtained by drying in an oven at 50°C during 48h. Then, it was dissolved in 150 mL of ethanol (purity > 99.7%). The solution was heated at reflux for 3 hours in order to dissolve DPL whereas potassium chloride remains in suspension. After filtration, *(R)* - or (*S*) - DPL crystallized in the filtrate upon cooling to room temperature. Racemic DPL was purchased from Sigma-Aldrich (USA, purity 99%).

II-1-2. Melt-quenching protocol

Crystalline racemic and enantiopure DPL starting materials were analyzed by TG-DSC (see Appendix AI-6) which confirmed the presence of the thermodynamically stable crystalline phases: the racemic compound RI (T_m = 160 °C) and the stable form EI (T_m = 166 °C). Moreover, these analyses highlighted that DPL shows a mass loss only when heated above 265 °C (Figure 3).

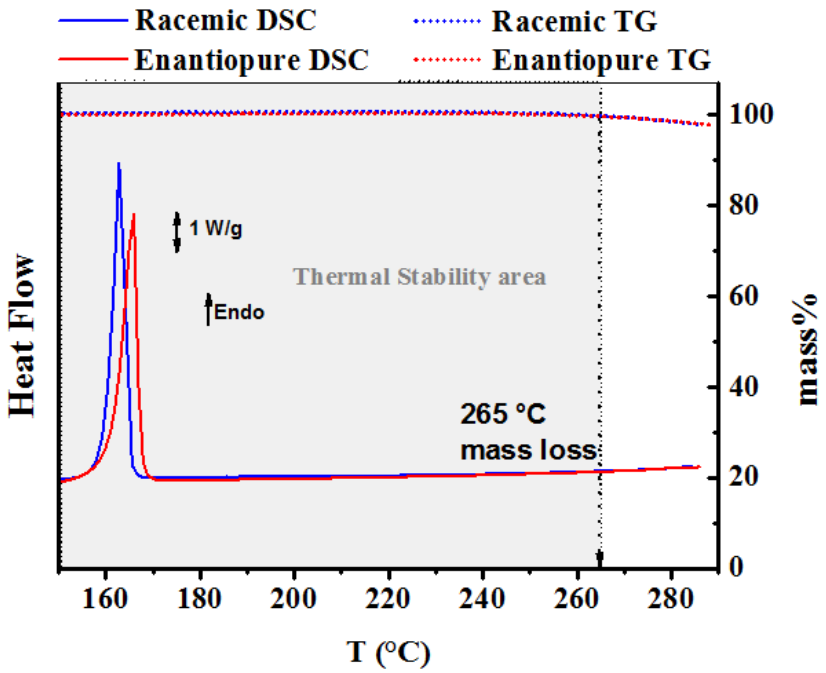

Figure 3. TG-DSC analysis of stable form EI (T_m = 166 °C) from enantiopure samples and RI (T_m = 160 °C) from racemic samples (endo up). The beginning of the mass loss was recorded around 265 °C for both compound.

The previous results of Griesser and coworkers were thus confirmed for racemic DPL: commercial batches consist of the form RI, melting at *ca.* 159 °C without detectable degradation or sublimation [5]. To prepare amorphous samples, molten solids were rapidly cooled (≥ 20 K/min) down to room temperature (confirmed by X-ray analyses, see Figure 4 (a)).

II-1-3. Stability of glassy racemic and enantiopure forms

A kinetic stability study shows that the amorphous samples of racemic and enantiopure compositions of diprophylline, prepared by quench-cooling of the melt from crystalline forms are unstable and recrystallize at temperatures below the temperature of glass transition T_g (during storage of the glass in isothermal conditions, T_{room} = 20 °C, room humidity condition 30% RH). The previous results of Griesser and coworkers have demonstrated that the amorphous form of racemic composition slowly crystallizes to its metastable form RII at room temperature [5].

As illustrated in Figure 4 (a), the XRPD patterns recorded immediately after melt-quenching (see Appendix AI-4) are defined by very similar broad halos (for both racemic and enantiopure compositions). Two amorphous contributions are presumably related to distinct short range orders in the amorphous "organization" of glassy DPL samples. The disordered signatures after vitrification confirm that DPL samples (*i.e.* at the racemic and enantiopure

compositions) prepared by melt quenching are indeed amorphous. In both cases, only one hour is sufficient to induce the presence of sharp peaks, indicating that the crystallization of the initial fully amorphous forms occured (Figure 4 (b) and (c)). Crystalline samples exhibit well-defined sharp Bragg peaks (top blue for racemic in Figure 4 (b), and top red for enantiopure compositions in Figure 4 (c), after only 13h of storage). The resulting crystalline forms obtained for the racemic composition correspond to the RII metastable form (in accordance with results of Griesser *et al*), and the stable phase EI for the enantiopure composition [8].

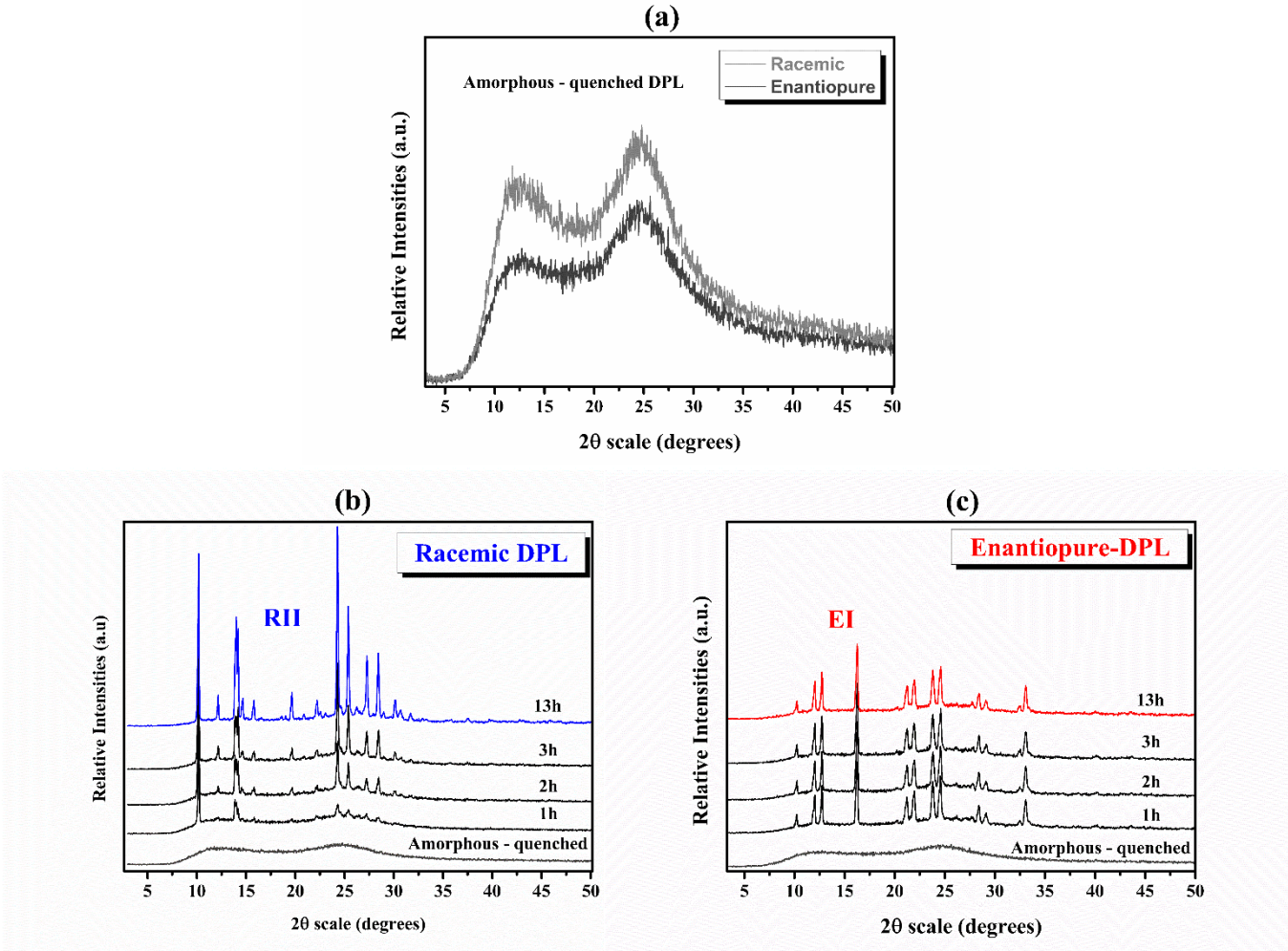

Figure 4. Comparison between X-ray diffraction patterns (XRD) of (a) racemic and enantiopure of quenched DPL samples. XRD for (b) racemic and (c) enantiopure compositions of Diprophylline samples performed under given room temperature/humidity conditions (T_{RT} = 20 °C, T_g -17 °C, atmospheric pressure, 30%RH).

Although XRPD amorphous patterns of both samples are similar, the resulting crystals are different. It is quite interesting to further characterize the molecular mobility of DPL samples with other techniques (*i.e.* TM-DSC, BDS) in order to increase our knowledge about glass-to-crystal pathways as a function of the enantiomeric composition.

II-2. Devitrification process: temperature of glass transition for 0, 50, 100% ee

In an attempt to detect a hypothetical impact of the enantiomeric composition on the properties of the amorphous state, temperature-modulated DSC (TM-DSC) analyses were performed (see Appendix AI-7), and the resulting curves were carefully compared for DPL samples at enantiomeric excess *ee* = 0% (racemic), 100% (pure enantiomer), and 50%. The amorphous materials were prepared by rapid cooling at ≥ 20 K/min from the molten state ($T_{onset\ melt}$ for RI = 159.9 °C, for EI = 164.4 °C). In TM-DSC, the complex heat capacity signal (C^*_p) can be deconvoluted into two components: the in-phase (C'_p) that describes molecular motions and the out-of-phase (C''_p) that is linked to dissipation (entropy production) [10]. It can be seen in Figure 5 (a) that no significant difference can be detected for the "in phase" contribution of the thermal signals associated with the glass transition found at 37.0 ± 0.4 °C. Simultaneously, the "out of phase" contributions have been found to be similar (Figure 5 (b)). Consistent with a previous report [11], it is confirmed that no mixing rule needs to be applied in binary systems of enantiomers for T_g [12].

The molecular dynamics analyzed by means of the determination of dynamic heterogeneity magnitudes could be characterized by the average size of cooperative rearranging regions (CRR) as defined by Donth's formula [13]:

$$N_\alpha = \frac{\rho N_A \xi^3 T_\alpha}{M_0} \ (Eq\ \mathrm{I})$$

$$\xi_\alpha = \sqrt[3]{V_\alpha} \ (Eq\ \mathrm{II})$$

$$V_\alpha = \frac{\Delta(\frac{1}{C_p})}{\rho(\delta T)^2} k_B T_\alpha{}^2 \ (Eq\ \mathrm{III})$$

With N_A the Avogadro number, ρ the density, ξ_α the characteristic length of dynamic glass transition, M_0 the molar mass for a whole molecule, $(\delta T)^2$ the mean temperature fluctuation related to the dynamic glass transition of one cooperative rearrangement region (CRR), N_α the number of structural units in one average CRR with volume V_α, $\Delta(1/C_p)$ the step of reciprocal specific heat capacity at constant pressure (obtained via the approximation $(1/C_p)_{glass} - (1/C_p)_{liquid}$) and k_B the Boltzmann constant.

Figure 5 (b) depicts the Gaussian fit of the out-of-phase C_p'' for the three samples of distinct enantiomeric compositions. The average temperature fluctuation in a cooperative rearranging regions (CRR) δT is related to the standard deviation of the Gaussian peak function (δT = FWMH/2.35) used to fit the imaginary parts where the maximum of the peak corresponds to the dynamic glass transition temperature T_α (all fits were superimposed for a more accurate interpretation; non-fitted and non-shifted data are displayed in Appendix AII-1).

The average CRR volumes were calculated assuming a similar apparent density of the amorphous phase as a function of ee (experimentally obtained, see Appendix AII-2) in this case of $\rho_{app\ amorphous\ rac} = 1.2$ g/cm^{-3} = $\rho_{app\ amorphous\ enantiopure}$ and $M_{0\ DPL}$ = 254.24 g/mol, by using the method proposed by Donth [13]. The results are reported in Table 1. Several studies from the literature report typical length scales (ξ_α) of cooperativity (obtained via TM-DSC) ranging from 1 to 3.5 nm at the glass transition temperature for different glass formers [14]. A value of 2.6 nm was obtained for H-Bonding Glasses (*i.e.* Glycerol) [15], while it is situated in the range of 2.3-3.1 nm for polymers [15]–[18] and 1.2-2.6 nm for inorganic glasses [19]. For our samples, we have found values in the range of 2.5 ± 0.2 nm. This indicates that whatever the enantiomeric composition, the average size of CRR remains constant (according to the standard deviation related to the number of measurements performed). Therefore, the use of Donth's model in these conditions does not allow discrimination between the amorphous DPL samples at various ee. Thus, it suggests that the molecular dynamics at T_g is not a function of the enantiomeric composition, or, that thermal analysis is not able to detect eventual differences in molecular arrangements of amorphous solids at various enantiomeric compositions [20].

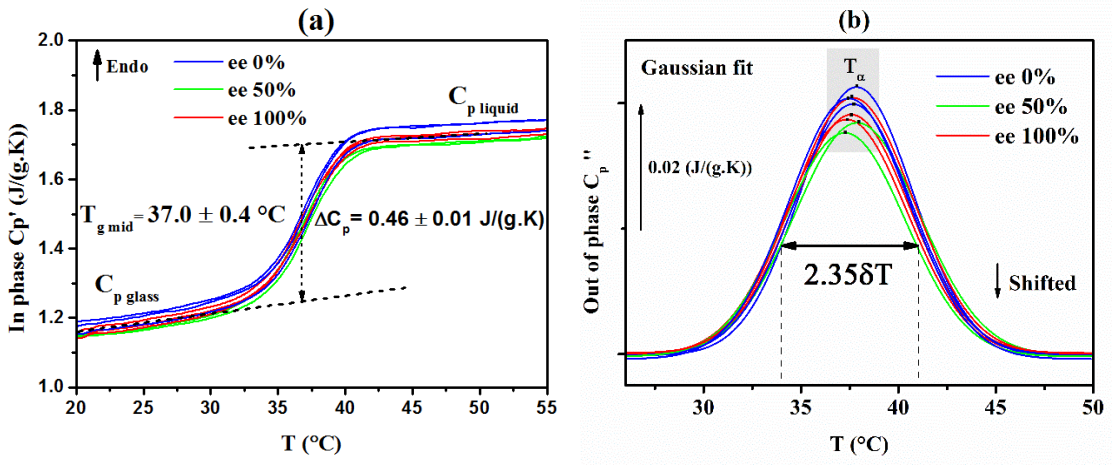

Figure 5. MT-DSC curves of (a) in-phase C_p' and (b) Gaussian fit of out-of-phase C_p'' shifted obtained for samples from compositions 0, 50, 100% ee (2 K/min, amp= 0. 318 K, p= 60 s, endo up).

Table 1. Number N_α of structural units, the cooperativity length ξ_α , volume V_α of one CRR at the glass transition temperature of DPL according to Donth's model, as a function of the enantiomeric composition (0% ee, 50% ee, 100% ee).

	0% ee	50% ee	100% ee	
N_α	50	43	56	± 9
ξ_α (nm)	2.5	2.4	2.6	± 0.2
V_α (nm^3)	15.5	13.3	16.7	± 3.0

II-3. The Relaxation Behavior of DPL

II-3-1. Identification of the experimental conditions for DPL quenching

From our best knowledge, this is the first time that molecular mobility of DPL has been investigated by means of broadband dielectric spectroscopy (BDS) technique. Thus, preliminary investigations consisted in identifying the most adequate conditions for reliable observations and characterization of either primary or secondary relaxations in the glassy and supercooled liquid states. The complex dielectric function $\varepsilon^*(f) = \varepsilon'(f) - i\,\varepsilon''(f)$ (f, frequency; ε', real part; ε'', imaginary part) associated with orientational motions of dipoles was measured by an Alpha-N impedance analyzer from Novocontrol Technologies, covering a frequency range from 10^{-1} Hz to 10^6 Hz (see Appendix AI-1). Approximately 250-300 mg of crystalline DPL powder was slightly compressed between two stainless steel plated electrodes (upper electrode 30 mm diameter) of a parallel plate capacitor, with a Teflon ring of 500 μm thickness. The Teflon ring was used in order to avoid contact between the disposable electrodes when the crystalline sample melts and to ensure, on the forthcoming measurements, a constant distance between the two electrodes. Particular precautions were taken to ensure that the capacitor was completely filled, although the existence of a few small bubbles cannot be ruled out completely. In order to investigate the molecular mobility in the glassy state, the sample was kept 5 min at 185 °C, above melting temperatures of RI (T_m = 160 °C) and EI (T_m = 166 °C) to reach complete melting. The molten sample was cooled down to a very low temperature (*i.e.* far below $T_g \approx 37$ °C) by carefully depositing the sandwiched sample electrodes on a metallic plate immersed in liquid nitrogen bath. Immediately after, the electrode assembly was inserted into the cryostat of the apparatus. The dielectric spectra were collected isothermally from -140 °C to 80 °C, increasing the temperature in different steps: in the range -140 °C to 0 °C in steps of 5 °C; from

0 to 80 °C in steps of 1 °C. The maximum deviation of temperature regulation was found to be ± 0.2 °C.

II-3-2. Comparison dielectric studies for commercial racemic and synthesized enantiopure compositions.

II-3-2-1. Primary relaxations of commercial racemic and synthesized enantiopure forms of DPL

In order to have an overlook on the role of enantiomeric composition on the dynamic properties, it is very important to consider orientational motions in the supercooled liquid state of our compounds. In the dielectric loss spectra existing in the accessible frequency domain, molecular movements in the viscous fluid are manifested by relaxation processes of different time scales. The α-relaxation process is related to the dynamic glass transition, whereas the faster and less intense secondary relaxations reflect more local dynamics. Figure 6 (a) and (b) displays real parts of the complex dielectric permittivity spectra for racemic and enantiopure compositions of DPL in the supercooled liquid state (at temperatures $T > T_{g\ DPL}$, with an increment of 1 °C). First, at low frequencies, an increase of ε' due to electrode polarization is observed for both enantiomeric compositions, which is usually occurring for moderately to highly conducting material samples [21].

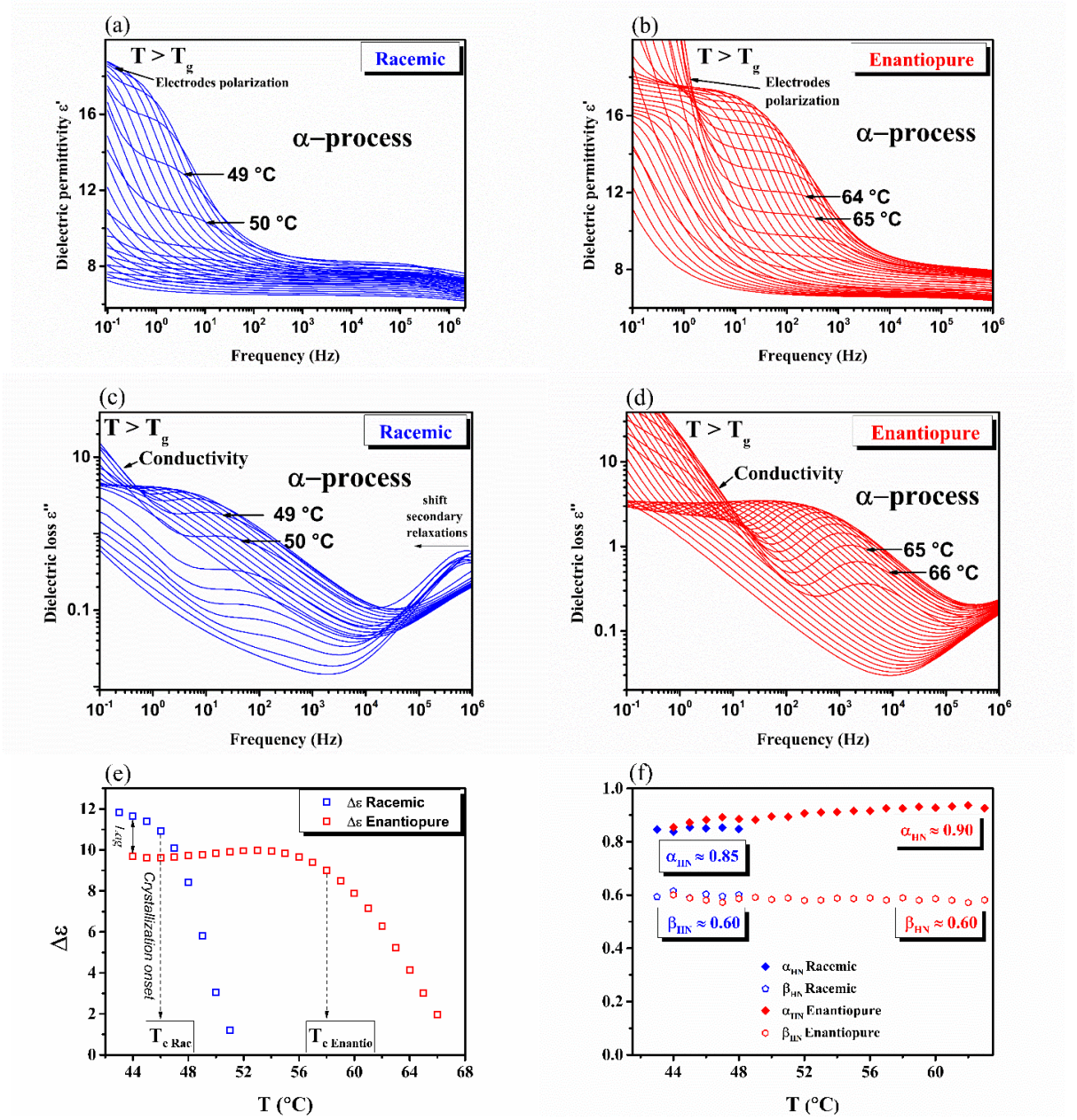

Figure 6. Real and imaginary parts (ε', ε'') of the complex dielectric permittivity vs frequency in the supercooled liquid state at temperatures $T > T_g$ for the (a, c) racemic and (b, d) enantiopure compositions (T_g = 37 °C) of DPL. Dielectric strength Δε parameter of the Havriliak-Negami relaxation function as a function of temperature in the range of analysis for racemic and enantiopure compositions (e). Respective symmetric αHN (filled diamonds) and asymmetric βHN (open diamonds) broadening parameters of the Havriliak-Negami relaxation function as a function of temperature (f).

Notwithstanding, a visible decrease of ε' in nearly one step with increasing frequency is characteristic of the primary structural relaxation process (α relaxation) from 38 °C to 57 °C for the rac-DPL, and from 38 °C to 69 °C for the enantiopure-DPL. From the dielectric loss ε" data of both compositions (Figure 6 (c) and (d)), conductivity is present at low frequency, while α relaxations are characterized by its non-Debye character with increasing frequency. One can note that a shift of secondary relaxations at high frequency is observed for the racemic sample

(Figure 6 (c)) while this situation is not observed for the enantiopure sample (Figure 6 (d)) when temperature increases. Moreover, from Figure 6 (e), it has been noticed that the dielectric strength of racemic-DPL ($\Delta\varepsilon_{rac}$) is slightly higher than dielectric strength of enantiopure-DPL ($\Delta\varepsilon_{enantio}$) at 44 °C ($T_g$ + 7 °C). Besides, $\Delta\varepsilon_{rac}$ decreases at lower temperature than $\Delta\varepsilon_{enantio}$ ($T_{c\ rac}$ - $T_{c\ enantio} \approx$ 12 °C). As crystallization proceeds, the number of relaxing DPL molecules decreases, causing a progressive weakening in the dielectric strength Δε of the α-process. This was defined from the generalized form of the Debye theory by Onsager, Fröhlich and Kirkwood as:

$$\Delta\varepsilon = \frac{1}{3\varepsilon_0} g_K F \frac{\mu^2}{K_B T} \frac{N}{V} (Eq\ \text{IV})$$

with ε_0 the dielectric permittivity of vacuum, μ the mean dipole moment of moving units in vacuum, g_K the Kirkwood correlation factor and F the Onsager factor (equal to 1). The N/V ratio represents the density of dipoles involved in the relaxation process. Therefore, dielectric strengths Δε decrease in the same way as the factor N/V due to the emergence of the cold crystallization of DPL samples. Figure 6 (e) indicates that the distinct evolution of Δε as function of temperatures for both enantiomeric composition samples is related to a distinct kinetics of crystallization. Because $\Delta\varepsilon_{rac} < \Delta\varepsilon_{enantio}$ at 44 °C, it can be suggested that the density of dipoles involved in the relaxation process for racemic and enantiopure DPL is not strictly similar. To determine relaxation times of the structural relaxation process at various temperatures, the Havriliak-Negami (HN) formula was used. Temperature dependence of the fit parameters α_{HN} and β_{HN} exponents keep a nearly constant value of 0.85 and 0.60 for racemic and 0.90 and 0.60 for enantiopure samples of DPL.

In the supercooled liquid state, the nonlinear increase of $\tau_{\alpha,}$ with lowering the temperature was described by Vogel-Fulcher-Tammann equation:

$$\tau = \tau_0 \exp\left[\frac{A}{T - T_0}\right] (Eq\ \text{V})$$

where $\tau_{0,}$ A and T_0 are fitting parameters [22]–[24]. It should be noticed that the VFT expression is sometimes adjusted by substituting the A parameter by the expression DT_0, where D is the strength parameter (related to fragility). Relaxation times of DPL samples show curved

temperature dependence when plotted as a function of 1000/T (Figure 7). The τ_α(T) dependence was measured only over 5 decades for enantiopure-DPL and 3 decades for racemic DPL (Figure 7). This distinction was due to crystallization at lower temperature for the racemic DPL sample compared to the enantiopure one. Then, extrapolation of the τ_α(T) dependence to 100 seconds is a common way of defining the glass transition temperature T_g from dielectric measurements. From the estimated parameters of the VTF fit (Table 2), a same value of T_g for both compositions was found to be of 30 °C, determined at τ_α = 100 s. Besides, by comparing the T_g value for τ_α = 10 s, closely related to the equivalent frequency of the TM-DSC analysis (period of T = 60 s, thus $\tau_{\alpha\ \text{TM-DSC}} = 1/(2\pi(1/60)) \approx 9.55$ s), a value of 34 °C was found for racemic-DPL and enantiopure- DPL, while values of 37 °C were obtained for T_α via TM-DSC.

On the basis of VFT parameters, one can also calculate the dynamic "fragility" *m* according to Böhmer *et al.* [25]:

$$m \equiv \frac{\mathrm{d}\,(\log \tau_\alpha)}{\mathrm{d}\,(T_g/T)^{T=T_g}} = \frac{D(T_0/T_g)}{(1-(T_0/T_g))^2 \ln(10)} \quad (Eq\ \mathrm{VI})$$

Since the values of $m_{\ \text{DPL}}$ is 87 ± 5, DPL (whatever its enantiomeric composition) can be classified as an intermediate glass former (30 < *m* < 100, [26]). This is a typical value for a "small molecule" compound [20].

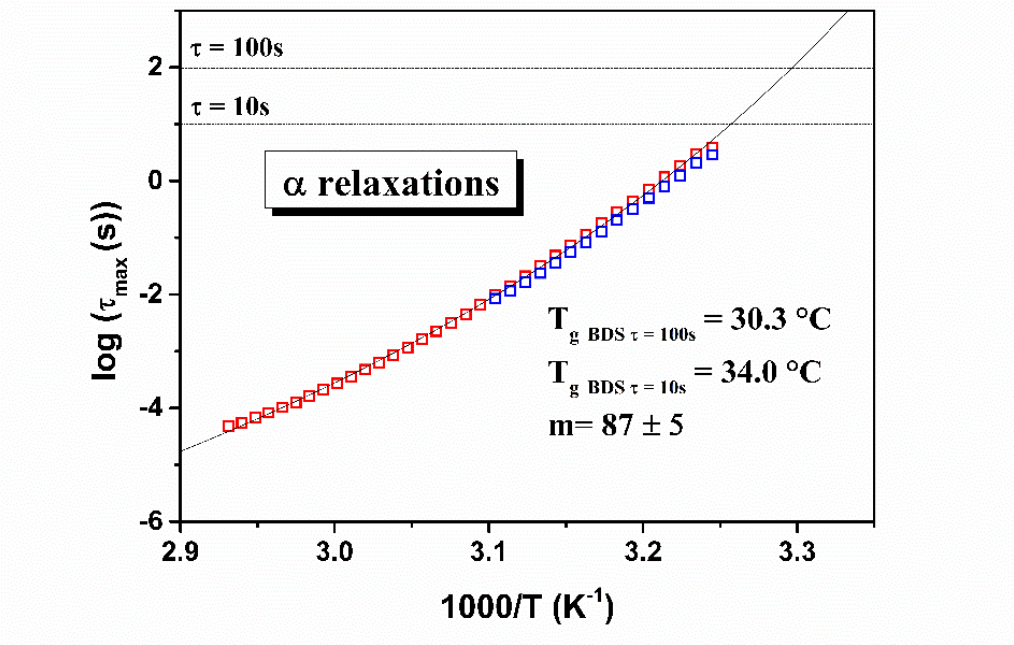

Figure 7. Temperature dependence of structural α-relaxation times in the region of high temperature of commercial racemic (blue) and synthesized enantiopure (red) DPL. Solid line is the VTF fit to the experimental data.

Table 2. Estimated parameters of the VTF fit obtained for amorphous DPL

	α process					
	T_g (τ = 100 s) (°C)	T_g (τ = 10 s) (°C)	*m*	*D*	log (τ_0)	T_0 (°C)
DPL	30 ± 1	34 ± 1	87 ± 5	8.0	-13.6	-24.3

II-3-2-2. Secondary relaxations of commercial racemic and synthesized enantiopure compositions of DPL

Figure 8 (a) and (b) presents the frequency evolution of dielectric loss ε" at various temperatures for respectively the racemic and enantiopure compositions of DPL heated from the glassy state. As it can be seen, the glassy state of DPL (whatever its enantiomeric composition) is characterized by a large molecular mobility reflected in two secondary relaxations: the slowest γ process and the fastest δ process (both described by Cole-Cole (CC) equation [27]). These secondary relaxations in amorphous DPL were found to shift toward higher frequencies upon heating, reflecting a presumed increase in molecular mobility.

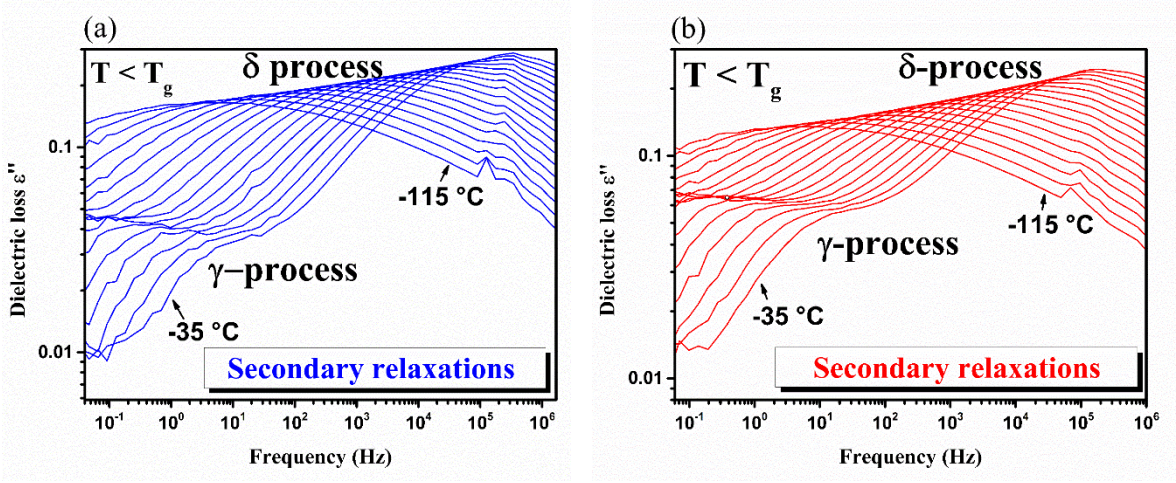

Figure 8. Dielectric loss spectra taken below T_g from -115 °C to – 35 °C, with a 5 °C step size, exhibiting the γ -relaxation and δ-relaxation occurring in the glassy state of (a) racemic and (b) enantiopure DPL.

II-3-2-3. Relaxation map of commercial racemic and synthesized enantiopure DPL

From the best fits of entire dielectric spectra obtained in both the glassy and liquid states of DPL (racemic and enantiopure) the temperature dependence for all dielectric processes were determined (see Figure 9).

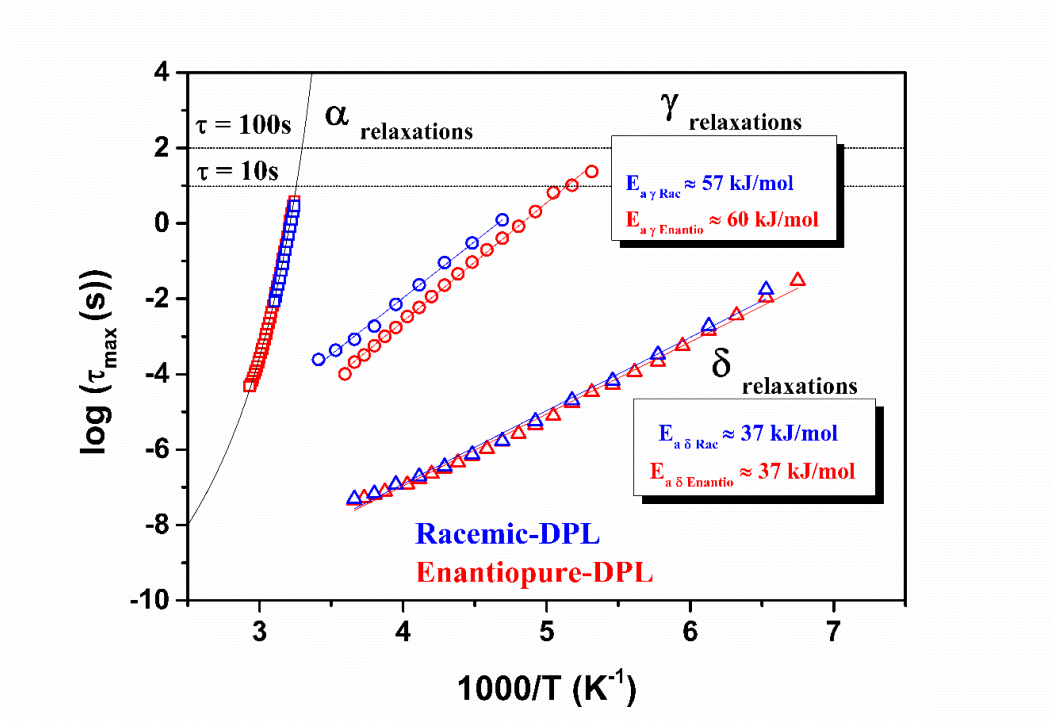

Figure 9. The experimental relaxation map of melt-quenched racemic (in blue) and enantiopure (in red) samples of DPL. Temperature dependence of the secondary γ- and δ-process are illustrated by respectively open circles and open triangles.

In the glassy state, the activation energies for the δ secondary processes were found to be Ea δ racemic ≈ Ea δ enantiopure ≈ 37 kJ/mol while for the γ processes, it was found to be Ea γ racemic ≈ 57 kJ/mol and Ea γ enantiopure ≈ 60 kJ/mol. According to recent research on amorphous pharmaceuticals, there has been a growing recognition that high activation energy barriers (typically, Ea > 50 kJ/mol) for secondary relaxation processes may be related to motions involving the whole molecule or internal conformational motions whereas low values (Ea < 50 kJ/mol) could be linked to intramolecular motions [28], [29]. Based on this classification, γ secondary processes of DPL may be related to intermolecular motions, whereas δ secondary processes are presumably from intramolecular origin. Though, it is quite surprisingly that δ processes of both enantiomeric composition samples are strictly similar in terms of activation energies as well as their evolutions of τ_α as function of 1000/T in the relaxation map, while it is not the case for γ – processes.

Besides, in order to describe such differences in a more qualitative way, both temperature dependencies were plotted versus each other, as presented in Figure 10 (a). A straight line with a slope s = 0.97 indicates that the temperature evolution of the α-relaxation time for a single enantiomer and for the racemic mixture of DPL does not follow each other perfectly, but behave in a similar ways. By comparison, Adrjanowicz *et al.* have found a slope

s = 0.95 between a single enantiomer and the racemic mixture of Ketoprofen [30]. In addition, the dispersion of the structural α-relaxation is not essentially the same for studied molecular liquids. This is illustrated in Figure 10 (b) where the normalized modulus M" (see Appendix AI-1) spectra maximum along with the minima in the region of the high-frequency side of the α-process are not superimposable.

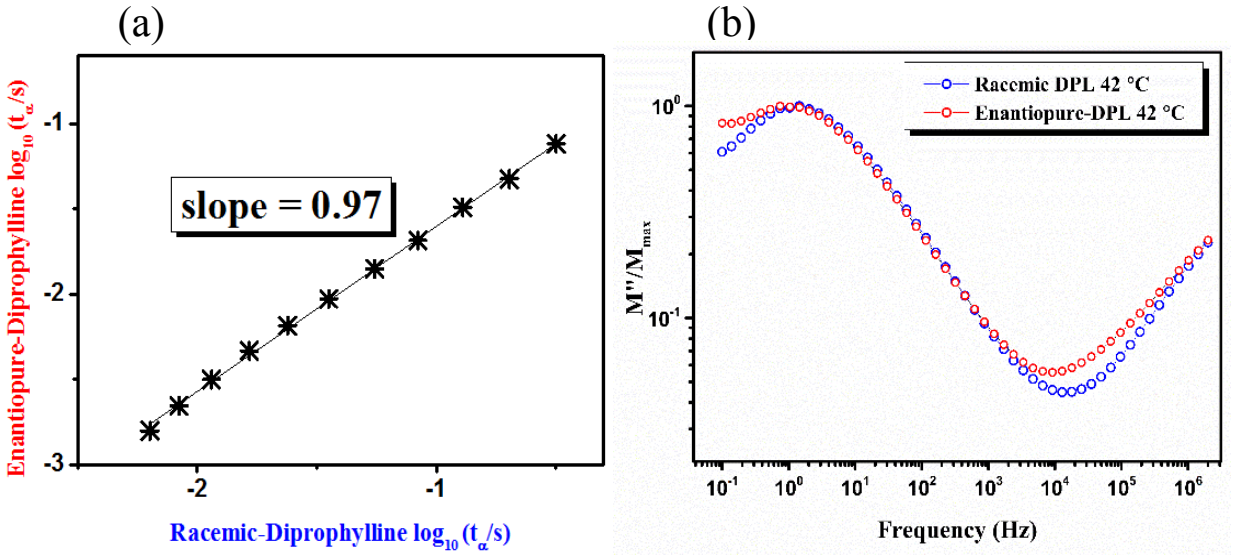

Figure 10. (a) Temperature dependence of τ_α for racemic-DPL and enantiopure-DPL plotted versus each other (b) Comparison of the normalized modulus M" for racemic-DPL and the enantiopure-DPL taken at 42 °C (T_g + 5 °C).

From these data, it is evidenced that the relaxation behaviors of racemic and enantiopure DPL samples are similar in both the glassy and the supercooled liquid melt; but some slight distinctions exist: in the glassy state, the dielectric strengths of secondary γ processes are not similar for both samples. In the supercooled liquid state, dielectric strengths of α-relaxation varies with enantiomeric composition. As demonstrated in previous studies, the crystal structure of the metastable form RII for the racemic composition of DPL consists of bimolecular layers formed by centrosymmetric dimeric associations [8]. One can suggest that the hypothetical presence of dimers in the glassy state may be responsible for distinct densities of dipoles involved in the relaxation process. This could presumably explain the lag between $\Delta\varepsilon_{rac}$ and $\Delta\varepsilon_{enantio}$ in Figure 6 (e). Oppositely, because of the very low stability of the metastable form EII of enantiopure DPL, no information regarding its crystal structure has been evidenced.

The intriguing relaxation behaviors of our samples led us to reconsider the incidence of chemical purity in the commercial batch of racemic DPL samples and in the synthesized enantiopure DPL in order to clarify our previous results.

II-3-3. Purification process

Purification procedures were applied on racemic and enantiopure of DPL sample: by means of recrystallization from ethanol/water (95/5, *v/v*) and slurry at room temperature (Appendix AII-3). The corresponding chromatograms obtained for the products and the purified samples (*e.g. (S)*-DPL) are depicted in Figure 11. Among all the impurities remaining in the sample (See Data Pharmacopeia, Appendix III), Theophylline (TPH) was identified as the most prominent impurity for all our samples. In the adapted chromatographic experimental conditions, TPH and DPL retention times were found to be 17.4 and 22.3 min, respectively. The quantity of TPH was determined as 0.52% *wt* for synthesized enantiopure DPL and less than 0.03% *wt* after purification.

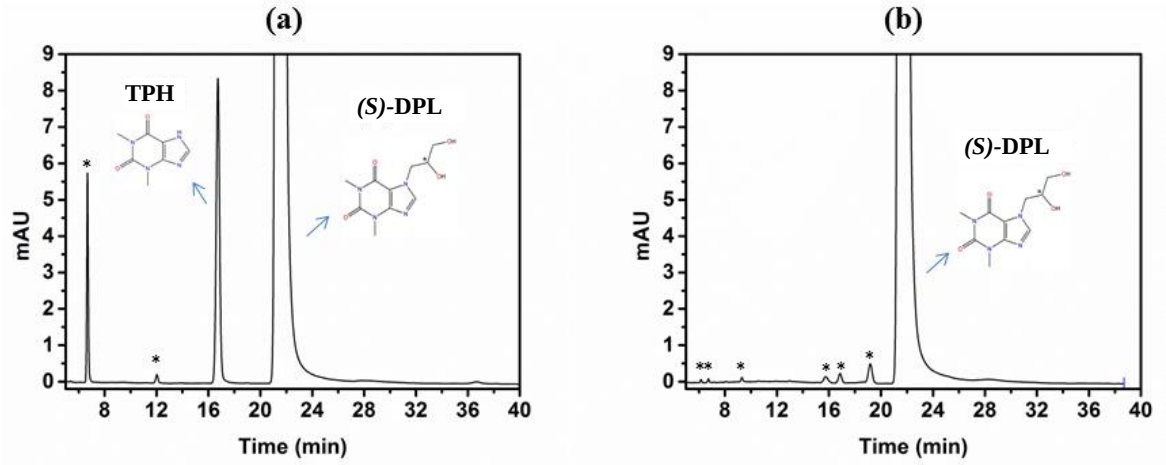

Figure 11. HPLC chromatograms of (S)-DPL samples (a) after synthesis and (b) after purification by recrystallization. Stars represent other unidentified impurities in DPL samples.

The chromatograms obtained with the commercial batch and the purified samples (*i.e.* RAC-DPL) are depicted in Figure 12. In this case, the quantity of TPH was determined as 0.14 % *wt* for commercial racemic DPL and less than 0.03 % *wt* after purification.

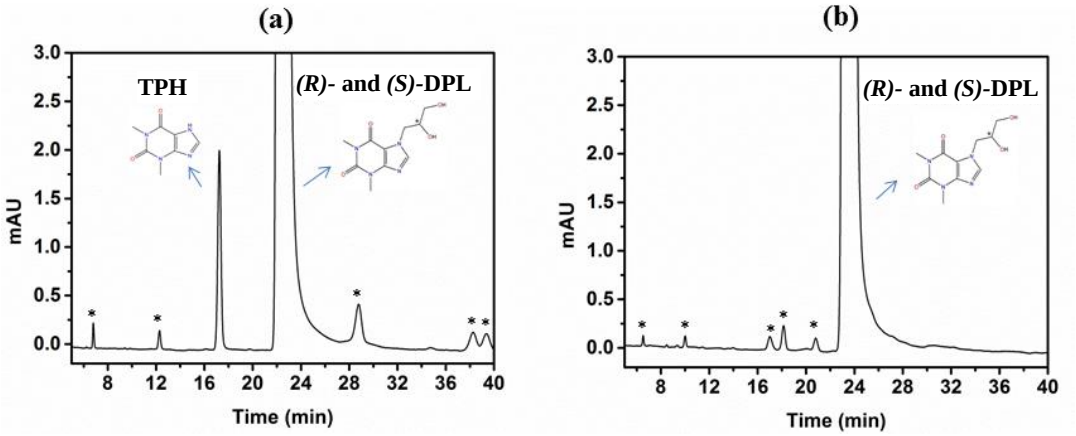

Figure 12. HPLC chromatograms of Rac-DPL samples from (a) commercial batch and (b) after purification by recrystallization. Stars represent other unidentified impurities in DPL samples.

II-3-4. Chirality: same relaxations between purified racemic and purified enantiopure compositions

Figure 13 (a) and (b) display real parts of the complex dielectric permittivity spectra of purified racemic and purified enantiopure compositions of DPL in the supercooled liquid state ($T_{g\ rac\ purified\ DPL}$ = 36.9 °C and $T_{g\ enantio\ purified\ DPL}$ = 37.3 °C, values obtained by TM-DSC, data not shown). A visible decrease of ε' in nearly one step with increasing frequency is characteristic of the presence of a primary structural relaxation process for both enantiomeric compositions. One can see that the electrode polarization effect is less pronounced for the purified racemic sample while it is moderately present for purified enantiopure DPL, compared to their impure homologous (Figure 6 (a) and (b)). Besides, at low frequencies, the dielectric loss obtained for purified racemic DPL is less affected by conductivity leading to a well-distinguishable α-relaxation (Figure 13 (c)). In contrast, the dielectric loss obtained for purified enantiopure DPL (Figure 13 (d)) is still impacted by conductivity. This result suggests that the presence of impurities in samples cannot be the principal cause of the conductivity effect. The general experimental conditions and electrodes assembly are also involved [31]. Moreover, from Figure 13 (e), no lag between dielectric strengths of both purified DPL samples have been evidenced, suggesting that the impurities present in our samples could affect the density of dipoles of DPL in the relaxation process. Nonetheless, $\Delta\varepsilon_{rac}$ decreases at lower temperatures than $\Delta\varepsilon_{enantio}$ ($T_{c\ enantio} - T_{c\ rac} \approx 2$). By comparing these values with the non-purified samples ($T_{c\ enantio} - T_{c\ rac} \approx 12$), it confirms that kinetics of crystallization of DPL is impacted by the chemical purity. Though, temperature dependence of the fit parameters α_{HN} and β_{HN} exponents keep

nearly constant values of 0.92 and 0.54 for purified racemic and 0.87 and 0.59 for purified enantiopure samples of DPL (Figure 13 (f)).

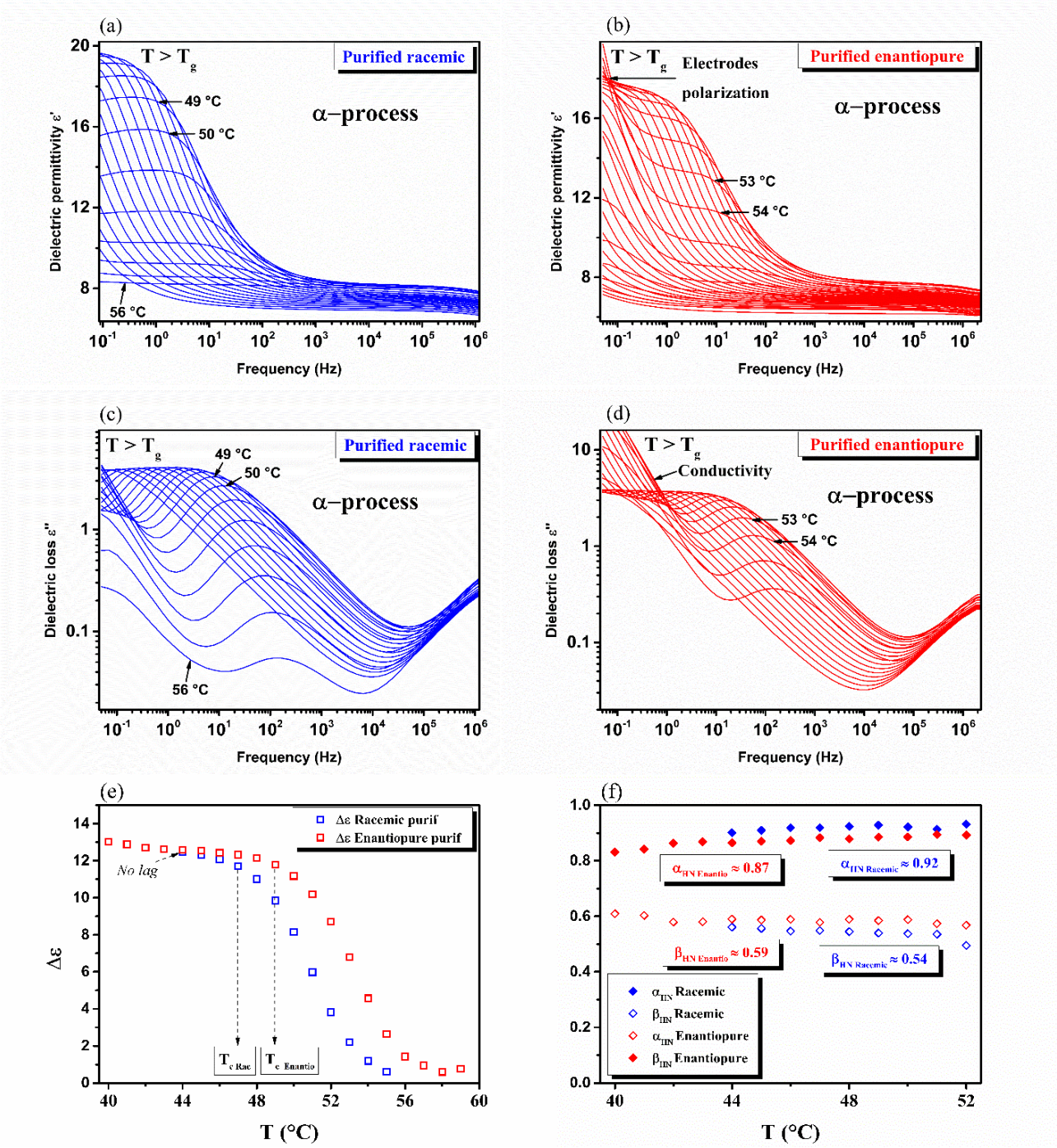

Figure 13. Real and imaginary parts (ε', ε'') of the complex dielectric permittivity vs frequency in the supercooled liquid state at temperatures $T > T_g$ for the (a, c) purified racemic and (b, d) purified enantiopure compositions (T_g = 37 °C) of DPL. Dielectric strength Δε parameter of the Havriliak-Negami relaxation function as a function of temperature in the range of analysis for purified racemic and enantiopure DPL (e). Their respective symmetric αHN (filled diamonds) and asymmetric βHN (open diamonds) broadening parameters of the Havriliak-Negami relaxation function as a function of temperature (f).

Relaxation times of purified DPL samples show curved temperature dependence when plotted as a function of 1000/T (Figure 14). The τ_α (T) dependence was measured only over 3 decades for both samples. From the estimated parameters of VTF fit (Table 3), the value of $T_{g\ \tau = 100\ s\ ,\ purified\ DPL}$ = 29 ± 1 °C is nearby the $T_{g\ \tau = 100\ s,\ impure\ DPL}$ = 30 ± 1 °C ; as well as the value of $T_{g\ \tau = 10\ s\ ,\ purified\ DPL}$ = 33 ± 1 °C is similar to $T_{g\ \tau = 10\ s\ ,\ impure\ DPL}$ = 34 ± 1 °C.

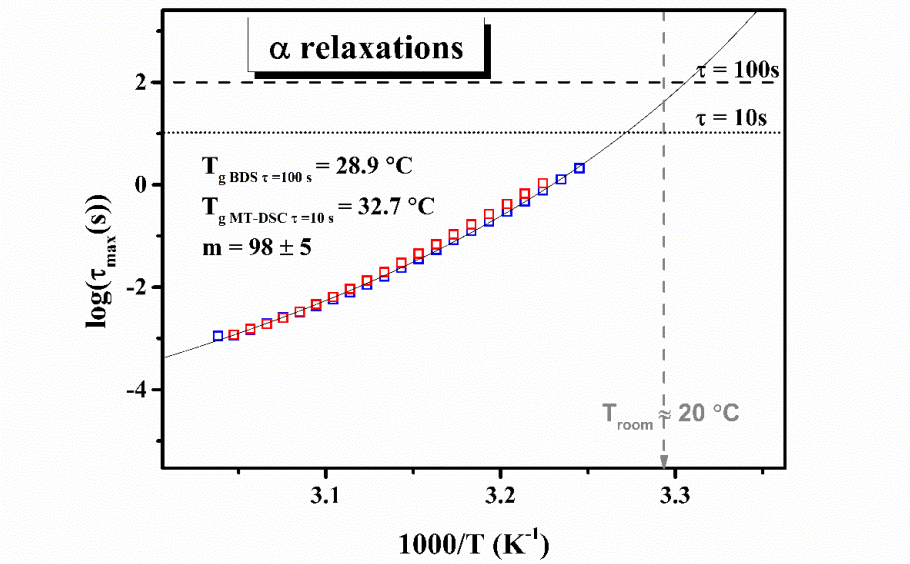

Figure 14. Temperature dependence of structural α-relaxation times in the region of high temperatures for purified racemic (blue) and enantiopure (red) DPL samples. Solid line is VTF fit to the experimental data.

Table 3. Estimated parameters of the VTF fit obtained for purified amorphous racemic- and enantiopure-DPL

	α process					
	T_g (τ = 100 s) (°C)	T_g (τ = 10 s) (°C)	*m*	*D*	log (τ_0)	T_0 (°C)
Purified DPL	29 ± 1	33 ± 1	98 ± 5	3.4	-9.4	-4.6

The glassy states (at very low temperature, -115 °C to -35 °C) of both compositions are only characterized by the fastest δ processes, while the slowest γ processes, observed for the non-purified samples (Figure 6 (e) and (f)), are not occurring in these dielectric data (Figure 15 (a) and (b)). It has been evidenced in the literature (for polymeric or composite systems essentially) that the humidity/moisture content may cause the occurrence of secondary relaxations [32], [33]. Since all measurements were performed in the same experimental conditions and since no γ-process is occurring for pure samples, it can be postulated that the emergence of this new relaxation process could be hardly attributed to the presence of

water/humidity remaining in DPL samples. The activation energies for the δ secondary processes of purified samples are similar to that of non-purified samples ($E_{a\ \delta\ purified\ racemic} \approx 39$ kJ/mol $\approx E_{a\ \delta\ purified\ enantiopure}$). Data are summarized in Table 4. These results suggest that:

(i) δ process is conceivably from intramolecular origin in DPL enantiomers.

(ii) γ process could presumably be related to the presence of impurities.

A perspective of this work would consist in conducting theoretical density functional theory (DFT) calculations, in order to gain insights into the origin of these secondary relaxations [34].

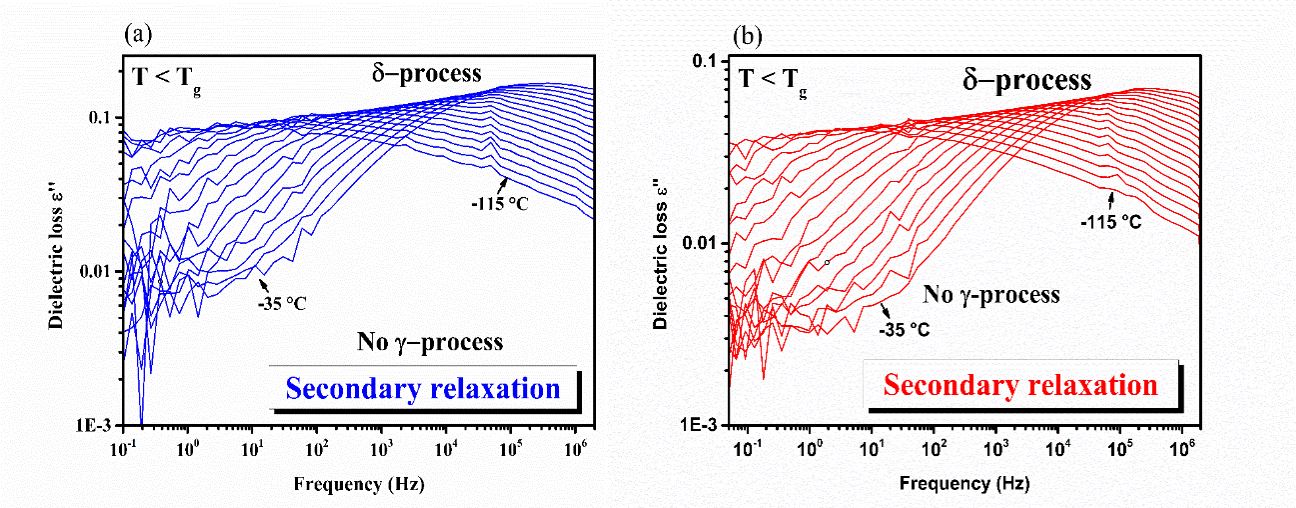

Figure 15. Dielectric loss spectra of purified DPL taken below T_g from -115 °C to – 35 °C, with a 5 °C step size, exhibiting only δ-relaxation occurring in the glassy state of DPL racemic (a) and enantiopure (b).

Table 4. Summary of the activation energies E_a of secondary processes of DPL before and after purification.

	Secondary processes of DPL	
	$E_{a\ \gamma}$ (kJ/mol)	$E_{a\ \delta}$ (kJ/mol)
Rac- DPL	57	37
Enant- DPL	60	37
Purif Rac- DPL	/	39
Purif Enant- DPL	/	39

From the best fits of entire dielectric spectra obtained both in the liquid and glassy states for purified racemic and enantiopure DPL samples, the temperature dependence for all dielectric processes were determined and are presented in Figure 16.

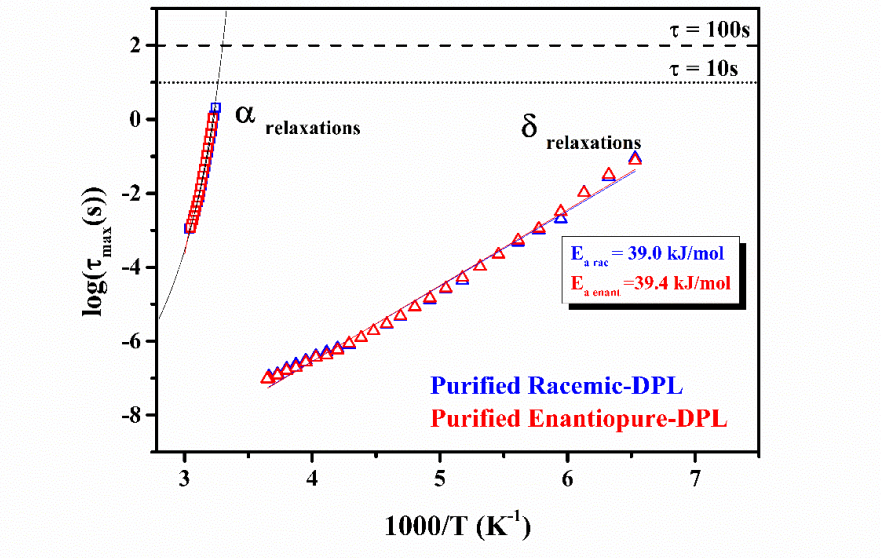

Figure 16. The experimental relaxation map of melt-quenched purified racemic (in blue) and purified enantiopure (in red) DPL. Temperature dependence of the secondary δ-processes is illustrated by open up triangles.

By comparing both purified enantiomeric compositions, their $\tau_\alpha(T)$ dependence are superimposable with a similar estimated value of fragility ($m_{\text{purified DPL}} = 98 \pm 10$). Moreover, a straight line with the slope s = 1 indicates that their temperature evolution of the α-relaxation times follow each other perfectly (Figure 17 (a)). This is also confirmed by their superimposition of normalized modulus M" spectra in Figure 17 (b).

To summarize this comparative dielectric study of racemic and enantiopure DPL before and after purification, it was shown that the presence of chemical (and/or structural[3]) impurities could have an influence on the relaxation behavior of DPL. First, a γ process is occurring in the glassy state of impure samples of DPL, but it disappears for purified samples. Secondly, the characterization of the primary structural relaxation in all our samples showed slight distinctions on the dielectric data before and after the purification (*i.e.* the non-superimposition of $\tau_\alpha(T)$, and the slight lag between normalized modulus M" spectra and the slight shift between fragility values). Besides, once the samples were purified, no clear distinction has been observed between the racemic mixture and the pure enantiomer of DPL, which suggests that the molecular dynamics in the glassy and the supercooled liquid states of DPL is not a function of the enantiomeric composition. To gain insights into the role of impurities in the molecular

[3] *According to Coquerel, "in addition to the pre-requisite chemical purity, a solid is 'structurally pure' when it exhibits the same 3D molecular arrangement for every particle"* [35]. *In other word, a sample containing a single polymorphic form is "structurally pure" whereas a mixture of polymorphs or a mixture of crystals and amorphous form is not.*

mobility of DPL, dielectric measurements were conducted on purified DPL enriched with known amounts of TPH, the most prominent impurity in our DPL samples.

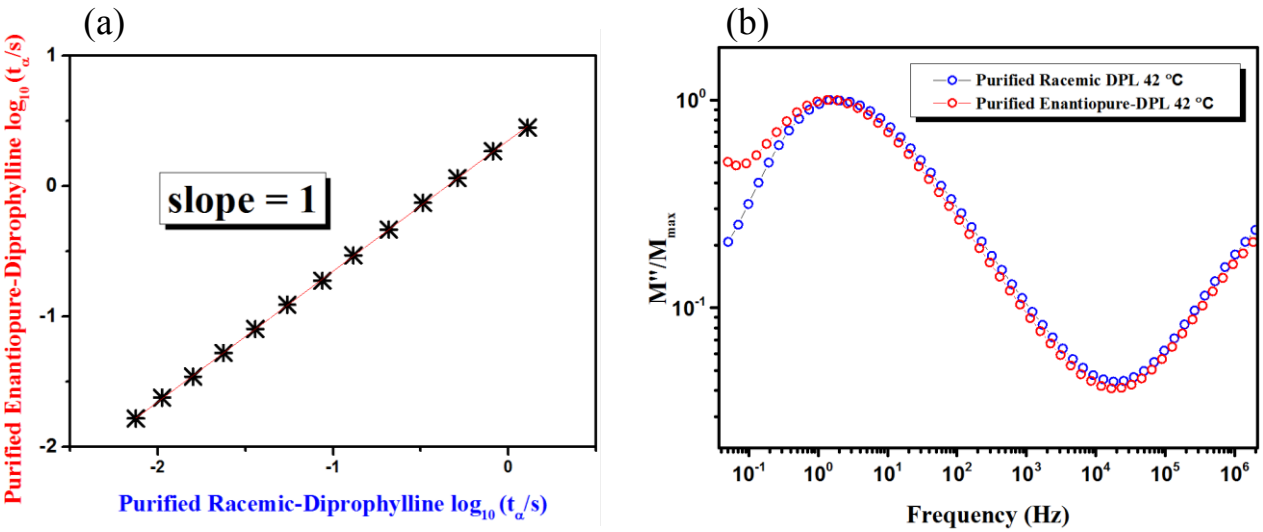

Figure 17. (a) Temperature dependence of structural α-relaxation times in the region of high temperatures. Solid blue and red lines are respectively the VTF fits to the experimental data for the purified racemic and the purified enantiopure compositions. (b) Temperature dependence of τ_α for purified racemic-DPL and purified enantiopure-DPL plotted versus each other (c) Comparison of the normalized modulus M'' for purified racemic-DPL and purified enantiopure-DPL taken at 42 °C (T_g + 5 °C).

II-3-5. Influence of TPH on the relaxation behavior of DPL

II-3-5-1. Preparation of samples enriched with TPH

As previously discussed, impurities may slightly affect the molecular dynamics of DPL, justifying the need for purification before further rationalization of the experimental phenomena. The next part is dedicated to the precise determination of these impurities, and especially for TPH that was found to be the most prominent one. Because of the very slight differences observed for the relaxation processes (*i.e.* primary and secondary) at both enantiomeric compositions of DPL before and after purification, it was decided to substantially increase the impurity content (% *wt* TPH) in our purified samples in order to observe how it affects relaxation behaviors. The amounts of 2.5 % *wt* TPH and 5 % *wt* TPH were chosen. After an accurate calibration of *% wt* TPH achieved using HPLC (see Appendix AI-3), the quantification of the *% wt* TPH in our samples has been carried out (see data in Table 5).

Table 5. Estimated % wt Theophylline (TPH) remaining in enriched samples of racemic – and -enantiopure-DPL via HPLC analysis.

Samples	% *wt* Theophylline (TPH) estimated by HPLC		
	Purified	+ 2.5 % TPH	+ 5 % TPH
Racemic-DPL	< 0.03 %	2.6 %	5.1%
Enantiopure-DPL	< 0.03 %	2.2 %	4.5%

II-3-5-2. Study of the secondary relaxations with enriched samples

Figure 18 presents the frequency evolution of dielectric loss ε" at various temperatures for purified racemic DPL with (a) < 0.03 % *wt* (b) 2.6 % *wt* and (c) 5.1 % *wt* TPH, and for purified enantiopure-DPL with (d) < 0.03 % *wt* (e) 2.2 % *wt* and (f) 4.5 % *wt* TPH. As can be seen, the glassy state (at very low temperatures, -115 °C to -35 °C) of all samples is characterized by the fastest δ processes (Figure 18 (a-f)). Then, regarding the γ process, it is clear that it is not present for the purified samples. However, for racemic DPL enriched with 2.6 % *wt* TPH and enantiopure DPL enriched with 2.2 % *wt* TPH, both dielectric loss spectra lead us to suppose a slight relaxation in the region of the γ process. By considering now the racemic-DPL enriched with 5.1 % *wt* TPH, a well-shaped γ process is observed while another slight contribution in the region of the γ process is observed for enantio-DPL enriched with 4.5 % *wt* TPH. The corresponding activation energies for the secondary processes of all samples are summarized in Table 6. These results suggest that a δ secondary process is from intramolecular origin of the DPL enantiomers, while a γ process is presumably closely related to the presence of impurities. Finally, regarding the nature of the γ process, two scenarios can be envisaged:

(i) Since TPH is a rigid molecule, the only visible motions in dielectric spectroscopy could be their motions as a whole (which could therefore justify the value of activation energy of $E_{a\gamma}$ > 50 kJ/mol).

(ii) Since the γ relaxations were also well observed for commercial racemic samples and synthesized enantiopure samples with respectively a relatively low amount of % *wt* TPH determined at 0.14 and 0.56, the other potential impurities (not identified) may play an important role in the emergence of the γ process.

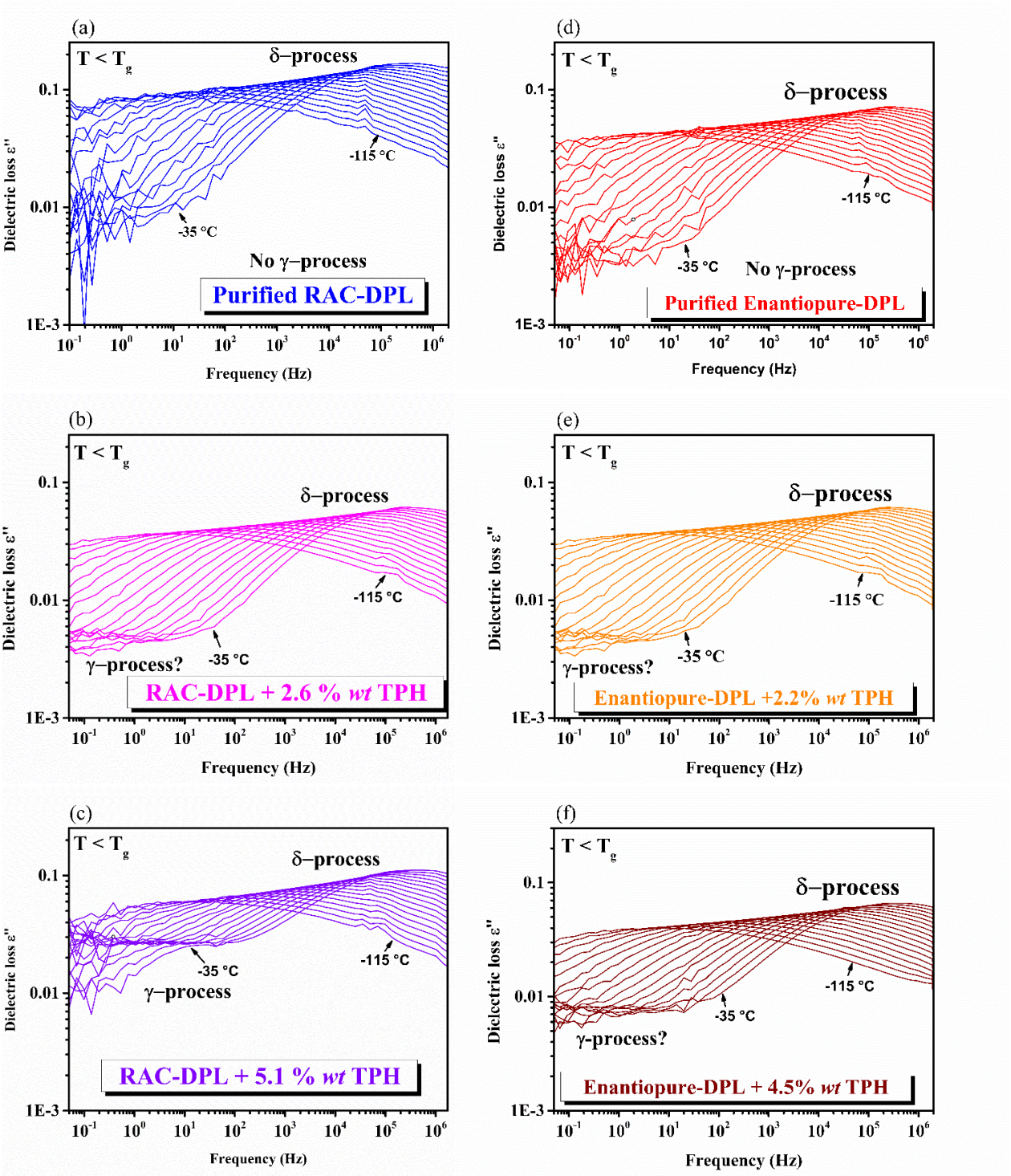

Figure 18. Dielectric loss spectra of DPL taken below T_g from -115 °C to – 35 °C, with a 5 °C step size, in the glassy state of (a) purified racemic-DPL (b) enriched racemic-DPL + 2.6 % wt TPH and (c) enriched racemic-DPL + 5.1 % wt TPH, (d) purified enantiopure-DPL (e) enriched enantiopure-DPL + 2.2 % wt TPH and (f) enriched enantiopure-DPL + 4.5 % wt TPH.

Table 6. Summary of the activation energies E_a of secondary processes for enriched DPL samples.

	Secondary processes of enriched samples of DPL			
	$E_{a\,\gamma}$ (kJ/mol)	$E_{a\,\delta}$ (kJ/mol)	*m*	T_g (τ = 10 s) (°C)
Purif. Rac- DPL	/	39	98	33
Com. Rac- DPL (0.14 %TPH)	57	37	87	34
Rac-DPL + 2.6 %TPH	/	39	98	33
Rac-DPL + 5.1 %TPH	57	38	98	33
Purif Enant- DPL	/	39	99	33
Synth. Enant-DPL (0.56 % TPH)	60	36	87	34
Enant-DPL + 2.2 %TPH	/	37	99	33
Enant-DPL + 4.5 %TPH	52	42	99	33

II-3-5-3. Study of the primary relaxations with enriched samples

In order to investigate the influence of chemical purity on the primary structural relaxation, direct comparison of the normalized modulus M" for racemic-DPL and enantiopure-DPL with various amounts of % *wt* TPH at 42 °C are shown in Figure 19 (a) and Figure 19 (b).

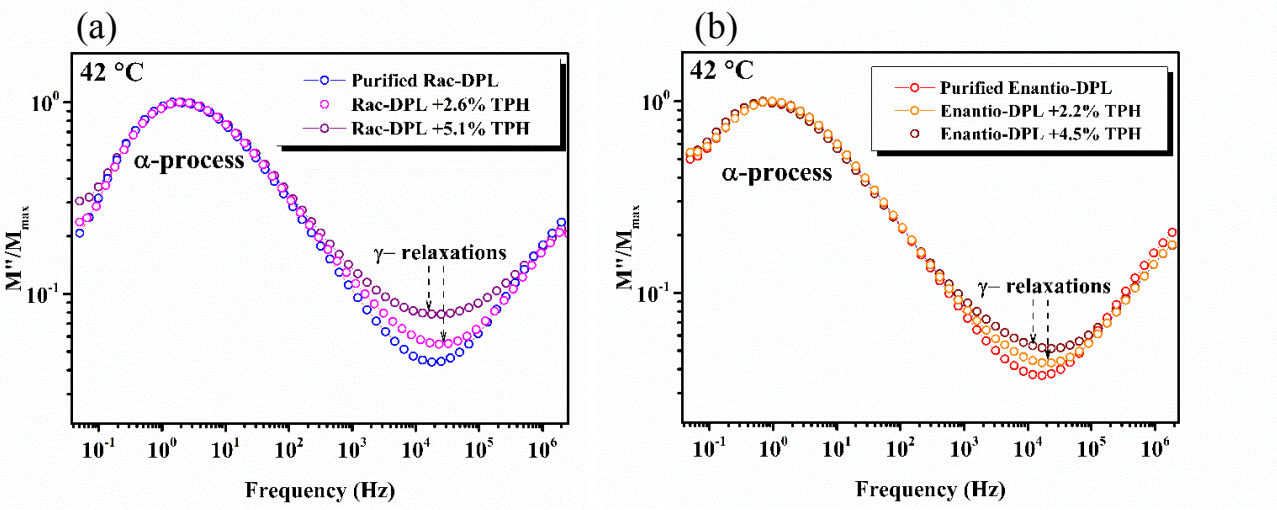

Figure 19. Comparison of the normalized modulus M" for (a) purified Rac-DPL; Rac-DPL +2.6 % wt TPH and Rac-DPL +5.1 % wt TPH. (b) Purified Enantio-DPL, Enantio-DPL + 2.2 % wt TPH, Enantio-DPL + 4.5 % wt TPH taken at 42 °C.

Once more, for both enantiomeric compositions, the higher the impurity content in our sample, the higher the position of the M''/M_{max} at the high-frequency α-peak. This result suggests that this increase is simply the high-frequency flank of γ and/or δ-peaks, submerged

under the dominating α –peak, as it has been already interpreted in the literature for other samples [36], [37].

In the supercooled liquid state, the nonlinear increase of $\tau_{\alpha,}$ with lowering the temperature was described by VFT equation for both enriched racemic and enantiopure compositions. Table 6 summarizes the VFT fit parameters obtained for all samples. One can note that the glass transitions (at τ = 10 s) and the fragility obtained for all samples whatever the enantiomeric composition or the chemical purity do not change substantially.

II-3-6. Discussion

To summarize the collected results, the molecular mobility of the racemic mixture and the single enantiomer of amorphous DPL has been investigated by BDS for the first time, covering a temperature range of more than 200 °C. Whatever the enantiomeric composition, numerous variations in the relaxation maps were observed before and after chemical purification of samples (via recrystallization in ethanol/water). Additionally, three distinct relaxation processes were detected for non-purified DPL samples, labeled as:

(i) α associated to the primary structural relaxation process of DPL

(ii) γ representing the secondary relaxations that are observed for samples containing impurities (*i.e.* TPH and others)

(iii) δ that presumably consist of secondary relaxations due to motions of the flexible part of DPL molecules [8]

while only α and δ relaxations were observed for purified samples. Thus, it is deduced that impurities in our samples may have an impact on the dielectric data either in the supercooled liquid state or in the glassy state. Indeed, by comparing the evolution of dielectric strength of their primary relaxations as a function of temperature, it was confirmed that the kinetics of crystallization for pure DPL samples is different than for non-purified ones. In the glassy state, as stated above, the γ-process is occurring for the non-purified materials (*i.e.* commercial racemic 0.14 % *wt* TPH, synthesized enantiopure 0.56 % *wt* TPH) as well as for enriched samples (Rac + 5.1 % *wt* TPH and Enantio + 4.1 % *wt* TPH). It has been found in the literature that for Celecoxib (CEL), the addition of 10 % *wt* of excipients in the binary mixtures with CEL causes the freezing of motions of the molecular group Ph-SO_2NH2 in CEL, reflected in the γ-process [38]. In our case, TPH (and/or other impurities) could presumably play an important role in the mobility of DPL, resulting in the γ-process. The presence of the others potential impurities, such as etophylline, proxyphylline, and caffeine should not be underestimated, and

will need to be considered in future experiments. A perspective of this work would consist in conducting theoretical density functional theory (DFT) calculations, in order to gain insights into the origin of these secondary relaxations [34]. After the purification processes applied to our samples, the value of fragility of purified DPL samples has been found to be rather similar than for non-purified samples. Moreover, the comparative dielectric study between the purified samples has led to the conclusion that the dynamic behaviors of a single enantiomer and of the racemic mixture of DPL in the glassy and supercooled liquid state are very much alike, even quasi-identical (depending to the specific thermal treatments). In the course of the comparative study for single enantiomer and racemic mixture of Ketoprofen [30], the authors conclude in an analogous way about the similar dynamic behaviors between both enantiomeric compositions. Nevertheless, a study of τ_α(T) dependencies measured in the vicinity of the glass transition with elevated pressure showed promising results in terms of improving knowledge of glassy dynamics of chiral molecules [30]. This could represent an interesting perspective for DPL.

In this second chapter, it has been shown that decreases of dielectric strengths of the α-relaxation (*i.e.* relative to the crystallization processes of samples) depend on the enantiomeric composition of DPL as well as chemical purity of samples. Therefore, for the next chapter, the crystallization behavior of DPL from the amorphous state with special emphasis of enantiomeric excess (ee %) and chemical purity was addressed.

References:

[1] Bruchhausen, P. D. F. von; Ebel, P. D. S.; Hackenthal, P. D. E.; Dannhardt, P. D. G.; Frahm, P. D. A. W.; Holzgrabe, P. D. U.; Keller, K.; Nürnberg, E.; Rimpler, H.; Schneider, G. Econazol. In *Hagers Handbuch der Pharmazeutischen Praxis*; B Eds.; Springer Berlin Heidelberg, **1993**, 1–163.

[2] Seton, L.; Khamar, D.; Bradshaw, I. J.; Hutcheon, G. A. Solid State Forms of Theophylline: Presenting a New Anhydrous Polymorph. *Cryst. Growth Des.* **2010**, *10* (9), 3879–3886.

[3] Griesser, U. J.; Burger, A. The Polymorphic Drug Substances of the Europ. Pharmacopoeia, Part 8: Thermal Analytical & FTIR-Microscopic Investigations of Etofylline Crystal Forms. **1993**, *61* (2), 133–143.

[4] Griesser, U. J.; Auer, M. E.; Burger, A. Micro-Thermal Analysis, FTIR- and Raman-Microscopy of (R,S)-Proxyphylline Crystal Forms. *Microchem. J.* **2000**, *65* (3), 283–292.

[5] Griesser, U. J.; Auer, M. E.; Burger, A. The Polymorphic Drug Substances of the European Pharmacopoeia, Part 10: Diprophylline. **1999**, *67* (4), 319–330.

[6] Brandstätter, M.; Grimm, H. Beitrag zur Polymorphie organischer Verbindungen. *Microchim. Acta*, **1956**, *44* (7–8), 1175–1182.

[7] Kuhnert-Brandstätter, M. *Thermomicroscopy in the Analysis of Pharmaceuticals*; Pergamon Press, **1971**.

[8] Brandel, C.; Amharar, Y.; Rollinger, J. M.; Griesser, U. J.; Cartigny, Y.; Petit, S.; Coquerel, G. Impact of Molecular Flexibility on Double Polymorphism, Solid Solutions and Chiral Discrimination during Crystallization of Diprophylline Enantiomers. *Mol. Pharm.* **2013**, *10* (10), 3850–3861.

[9] Fukuoka, E.; Makita, M.; Nakamura, Y. Glassy State of Pharmaceuticals. V. Relaxation during Cooling and Heating of Glass by Differential Scanning Calorimetry. *Chem. Pharm. Bull.* **1991**, *39* (8), 2087–2090.

[10] Schawe, J. E. K. Principles for the Interpretation of Modulated Temperature DSC Measurements. Part 1. Glass Transition. *Thermochim. Acta* **1995**, *261*, 183–194.

[11] Gallis, H. E.; Cees van Miltenburg, J.; Oonk, H. A. J. Polymorphism of Mixtures of Enantiomers: A Thermodynamic Study of Mixtures of d- and l-Limonene. *Phys. Chem. Chem. Phys.* **2000**, *2* (24), 5619–5623.

[12] Gordon, J. M.; Rouse, G. B.; Gibbs, J. H.; Jr, W. M. R. The Composition Dependence of Glass Transition Properties. *J. Chem. Phys.* **1977**, *66* (11), 4971–4976.

[13] Donth, E. Characteristic Length of the Glass Transition. *J. Polym. Sci. Part B Polym. Phys.* **1996**, *34* (17), 2881–2892.

[14] Rijal, B.; Delbreilh, L.; Saiter, A. Dynamic Heterogeneity and Cooperative Length Scale at Dynamic Glass Transition in Glass Forming Liquids. *Macromolecules* **2015**, *48* (22), 8219–8231.

[15] Hempel, E.; Hempel, G.; Hensel, A.; Schick, C.; Donth, E. Characteristic Length of Dynamic Glass Transition near T_g for a Wide Assortment of Glass-Forming Substances. *J. Phys. Chem. B* **2000**, *104* (11), 2460–2466.

[16] Puente, J. A. .; Rijal, B.; Delbreilh, L.; Fatyeyeva, K.; Saiter, A.; Dargent, E. Segmental Mobility and Glass Transition of Poly(ethylene-Vinyl Acetate) Copolymers : Is There a Continuum in the Dynamic Glass Transitions from PVAc to PE? *Polymer* **2015**, *76*, 213–219.

[17] Delpouve, N.; Delbreilh, L.; Stoclet, G.; Saiter, A.; Dargent, E. Structural Dependence of the Molecular Mobility in the Amorphous Fractions of Polylactide. *Macromolecules* **2014**, *47* (15), 5186–5197.
[18] Saiter, A.; Delbreilh, L.; Couderc, H.; Arabeche, K.; Schönhals, A.; Saiter, J.-M. Temperature Dependence of the Characteristic Length Scale for Glassy Dynamics: Combination of Dielectric and Specific Heat Spectroscopy. *Phys. Rev. E* **2010**, *81* (4), 041805-1–041805-8.
[19] Saiter, A.; Saiter, J.-M.; Golovchak, R.; Shpotyuk, M.; Shpotyuk, O. Cooperative Rearranging Region Size and Free Volume in As–Se Glasses. *J. Phys. Condens. Matter* **2009**, *21* (7), 075105-1–075105-7.
[20] Descamps, M. *Disordered Pharmaceutical Materials*; Wiley-VCH Verlag GmbH & Co.: Weinheim, Germany, **2016**.
[21] *Broadband Dielectric Spectroscopy*; Kremer, F., Schönhals, A., Eds.; Springer Berlin Heidelberg: Berlin, Heidelberg, **2003**.
[22] Vogel, H. The Law of the Relation between the Viscosity of Liquids and the Temperature. *Phys. Z.* **1921**, *22*, 645.
[23] Fulcher, G. S. Analysis of Recent Measurements of the Viscosity of Glasses. *J. Am. Ceram. Soc.* **1925**, *8* (6), 339–355.
[24] Tammann, G.; Hesse, W. Die Abhängigkeit Der Viscosität von Der Temperatur Bie Unterkühlten Flüssigkeiten. *Z. Für Anorg. Allg. Chem.* **1926**, *156* (1), 245–257.
[25] Böhmer, R.; Ngai, K. L.; Angell, C. A.; Plazek, D. J. Nonexponential Relaxations in Strong and Fragile Glass Formers. *J. Chem. Phys.* **1993**, *99* (5), 4201–4209.
[26] Angell, C. A. Proceedings of the International Discussion Meeting on Relaxations in Complex Systems Relaxation in Liquids, Polymers and Plastic Crystals — Strong/Fragile Patterns and Problems. *J. Non-Cryst. Solids* **1991**, *131*, 13–31.
[27] Cole, K. S.; Cole, R. H. Dispersion and Absorption in Dielectrics I. Alternating Current Characteristics. *J. Chem. Phys.* **1941**, *9* (4), 341–351.
[28] Wojnarowska, Z.; Adrjanowicz, K.; Wlodarczyk, P.; Kaminska, E.; Kaminski, K.; Grzybowska, K.; Wrzalik, R.; Paluch, M.; Ngai, K. L. Broadband Dielectric Relaxation Study at Ambient and Elevated Pressure of Molecular Dynamics of Pharmaceutical: Indomethacin. *J. Phys. Chem. B* **2009**, *113* (37), 12536–12545.
[29] Wlodarczyk, P.; Kaminski, K.; Adrjanowicz, K.; Wojnarowska, Z.; Czarnota, B.; Paluch, M.; Ziolo, J.; Pilch, J. Identification of the Slower Secondary Relaxation's Nature in Maltose by Means of Theoretical and Dielectric Studies. *J. Chem. Phys.* **2009**, *131* (12), 125103-1–125103-7.
[30] Adrjanowicz, K.; Kaminski, K.; Tarnacka, M.; Szutkowski, K.; Popenda, L.; Bartkowiak, G.; Paluch, M. The Effect of Hydrogen Bonding Propensity and Enantiomeric Composition on the Dynamics of Supercooled Ketoprofen – Dielectric, Rheological and NMR Studies. *Phys. Chem. Chem. Phys.* **2016**, *18* (15), 10585–10593.
[31] Mantheni, D. R.; Maheswaram, M. P. K.; Munigeti, R.; Perera, I.; Riga, A.; Alexander, K. S. Solid- and Liquid-State Studies of a Wide Range of Chemicals by Isothermal and Scanning Dielectric Thermal Analysis. *J. Therm. Anal. Calorim.* **2013**, *115* (3), 2253–2260.
[32] Zhao, H.; Li, R. K. Y. Effect of Water Absorption on the Mechanical and Dielectric Properties of Nano-Alumina Filled Epoxy Nanocomposites. *Compos. Part Appl. Sci. Manuf.* **2008**, *39* (4), 602–611.
[33] Hakme, C.; Stevenson, I.; David, L.; Boiteux, G.; Seytre, G.; Schönhals, A. Uniaxially Stretched Poly(ethylene Naphthalene 2,6-Dicarboxylate) Films Studied by Broadband Dielectric Spectroscopy. *J. Non-Cryst. Solids* **2005**, *351* (33–36), 2742–2752.

[34] Schammé, B.; Mignot, M.; Couvrat, N.; Tognetti, V.; Joubert, L.; Dupray, V.; Delbreilh, L.; Dargent, E.; Coquerel, G. Molecular Relaxations in Supercooled Liquid and Glassy States of Amorphous Quinidine: Dielectric Spectroscopy and Density Functional Theory Approaches. *J. Phys. Chem. B* **2016**, *120* (30), 7579–7592.
[35] Coquerel, G. The "structural Purity" of Molecular solids—An Elusive Concept? *Chem. Eng. Process. Process Intensif.* **2006**, *45* (10), 857–862.
[36] Schneider, U.; Brand, R.; Lunkenheimer, P.; Loidl, A. Excess Wing in the Dielectric Loss of Glass Formers: A Johari-Goldstein β-Relaxation? *Phys. Rev. Lett.* **2000**, *84* (24), 5560.
[37] Ngai, K. L.; Lunkenheimer, P.; León, C.; Schneider, U.; Brand, R.; Loidl, A. Nature and Properties of the Johari–Goldstein β-Relaxation in the Equilibrium Liquid State of a Class of Glass-Formers. *J. Chem. Phys.* **2001**, *115* (3), 1405–1413.
[38] Grzybowska, K.; Chmiel, K.; Knapik-Kowalczuk, J.; Grzybowski, A.; Jurkiewicz, K.; Paluch, M. Molecular Factors Governing the Liquid and Glassy States Recrystallization of Celecoxib in Binary Mixtures with Excipients of Different Molecular Weights. *Mol. Pharm.* **2017**, *14*(4), 1154–1168.

Chapter III

The Crystallization Behavior of a Chiral Compound: Case of Diprophylline (DPL)

Foreword

In the previous chapter, the characterization of DPL in the glassy state was carried out. Two parameters were considered: the chemical purity and the enantiomeric composition. By investigating the molecular mobility in our samples, it has been evidenced that chemical purity plays a role in terms of secondary relaxations, *i.e.* a new γ process is occurring in samples containing TPH. Nevertheless, regarding primary relaxations, it has been highlighted that molecular mobility in the amorphous state is not (or barely) impacted by either the addition of a small quantity of TPH (≈ < 5 % *wt* TPH) or changes of the enantiomeric composition in a wide temperature range.

With the aim of improving the knowledge about the behavior of pharmaceutical drugs in the amorphous state, we focused our attention in this section on the crystallization behavior of DPL from the amorphous state. The various equilibria between enantiomers have been deeply investigated (see Foreword Chapter II, page 55). The binary phase diagram reveals an interesting situation: annealing DPL supercooled melts at various enantiomeric compositions can induce either the crystallization of stable or metastable enantiomeric and racemic compounds but also metastable solid solutions. This rich and complex polymorphic behavior of DPL was shown to be related to its conformational flexibility [1]. Herein, preliminary studies consisted in reconsidering the polymorphic behaviors explicitly of both racemic and enantiopure of DPL. The ultimate objective of this investigation is focused on the exact role of enantiomeric composition on the nucleation and growth mechanisms, but also on the impact of other parameters such as chemical purity and specific thermal treatments on the nature, kinetics, and morphological features of produced crystalline particles.

III-1. Review about Preparation and Characterization of Crystalline Phases of DPL

III-1-1. Solid state characterization of RI, RII (from racemic composition)

Racemic DPL was purchased from Sigma-Aldrich (USA, purity 99%) and consisted of a white crystalline powder. In accordance with the previous results of Griesser and co-workers [2], the commercial batch consisted of the stable RI form (Figure 1, black diffractogram), with a melting temperature of *ca.* 159 °C without detectable degradation or sublimation.

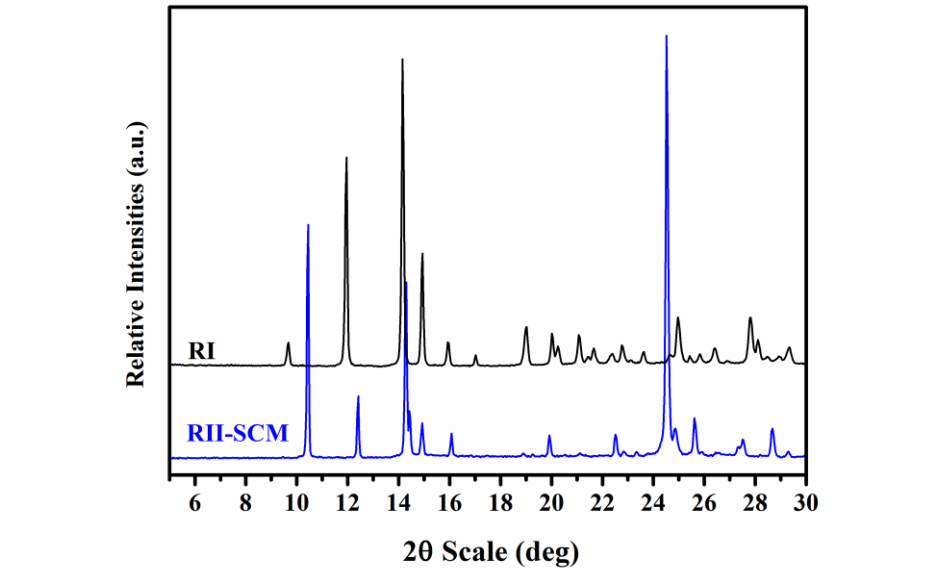

Figure 1. XRPD diffractograms of RI and RII crystallized from the SCM.

The recrystallization from the SCM at 100 °C (heating rate at 2 °C/min) results in a second polymorph of the racemic compound, RII ($T_{melt\ onset}$ = 148.4 °C). Since this lower melting polymorph has a lower melting enthalpy than RI (Figure 2), the Burger-Ramberger law (Chapter I section I-4-1-2) predicts that RII is thermodynamically less stable than RI with a monotropic character. However, RII exhibits a rather high kinetic stability at the solid state allowing its handling and storage for many months.

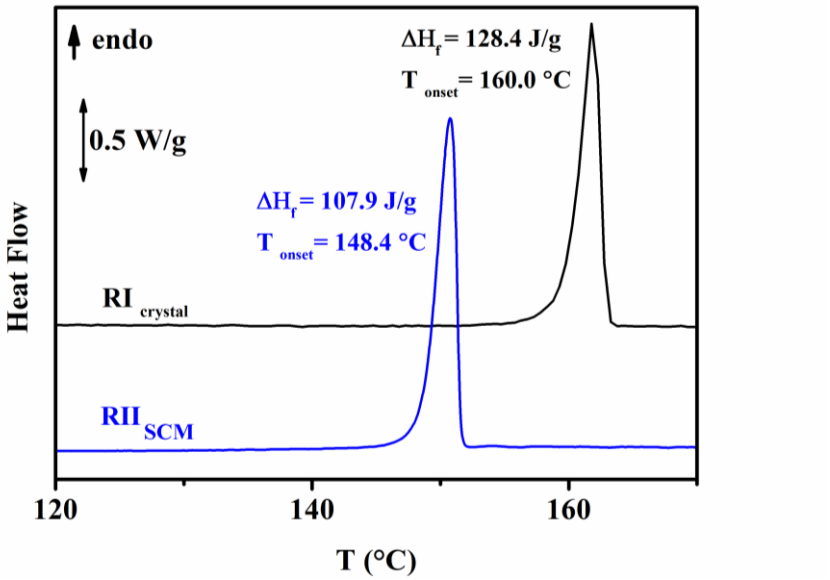

Figure 2. DSC thermograms of RI (black) and RII (blue) obtained by supercooled melt crystallization. Heating rate at 2 K/min.

Single crystals of sufficient quality for Single Crystal X-Ray Diffraction (SC-XRD) were obtained by Brandel and co-workers [1] for RI and RII (RII single crystals can be seen in Figure 3).

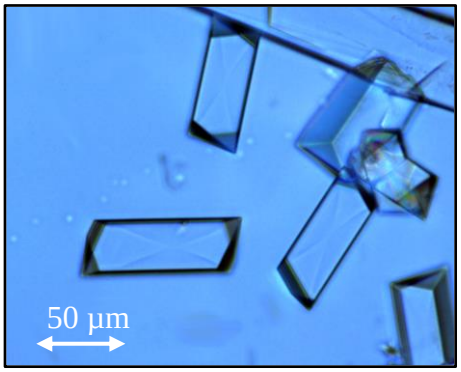

Figure 3. Optical microscopy image of RII single crystals obtained from an IPA solution. This figure was taken from [3].

This was achieved by rapid cooling of a quiescent highly supersaturated (β>3) isopropyl alcohol (IPA) solution of racemic DPL from 70 °C to room temperature. Table 1 summarizes the main results and relevant parameters of the SC-XRD experiments.

Table 1. Crystallographic data at 298 K for RI and RII. Adapted from [1].

	RI	**RII**
Crystal system	monoclinic	monoclinic
Space group (Z)	$P2_1/c$ (4)	$P2_1/c$ (4)
***a* (Å)**	4.5605(8)	7.4520(9)
***b* (Å)**	12.8524(22)	12.2227(15)
***c* (Å)**	19.1195(3)	12.8962(16)
***β* (deg)**	92.029(3)	98.015(2)
vol (Å^3)	1119.96	1163.16

Then, the stable crystal form RI consist of stackings of monolayers made of H-bonded DPL molecule. The theophylline fragments in the RI structure are roughly oriented parallel to the slices, allowing the occurrence of π stacking between corrugated (100) molecular layers (Figure 4).

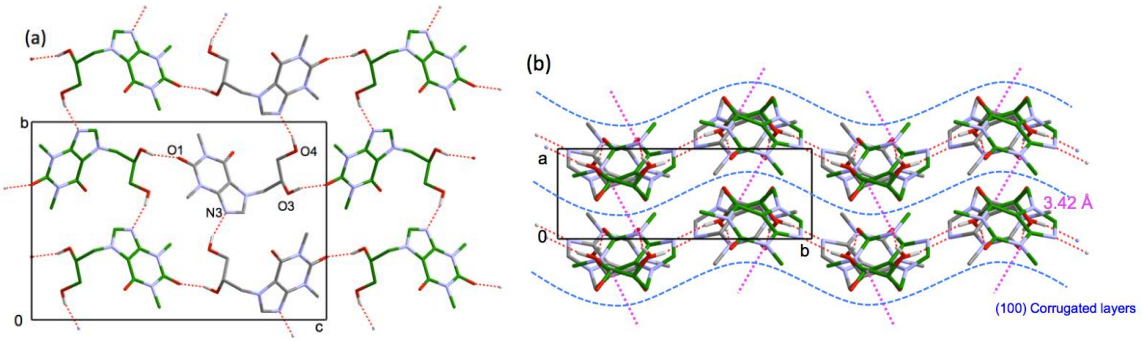

Figure 4. Projections of the RI crystal packing along the a axis (a) showing the heterochiral and corrugated (100) molecular slices and (b) projection along the c axis showing the stacking of these slices along a. Taken from [4].

Besides, the crystal structure of RII consists of bimolecular layers by centrosymmetric dimeric associations (Figure 5 (a)). Considering only the major enantiomer of each molecular site, the two heterochiral DPL molecules are H-bonded in a head-to-tail fashion. Each dimer is connected by means of (O4-H···N3) H-bonds to four neighboring dimers of the same (100) slice (Figure 5 (b)). The packing of these slices is stabilized by weak H-bonds as well as by π-stacking between theophylline fragments (Figure 5 (c)).

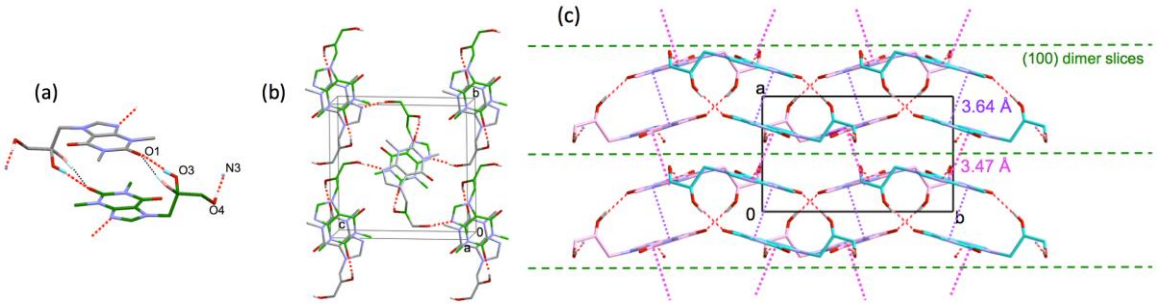

Figure 5. Unit cell of RII crystal structure showing the heterochiral dimers (a) and their stacking (b), projection along c axis (c). Molecules from a same dimer are drawn with the same color. Taken from [4].

III-1-2. Crystal structures of EI, EII (from enantiopure composition)

The description of the synthesis method of the pure enantiomers *(S)*- and *(R)*- DPL was reported earlier in Chapter II section II-1-1. Similarly to the racemic mixture, a metastable form of DPL pure enantiomer (labeled EII) could be produced by annealing the enantiopure SCM for about 90 min at T = 90 °C. The diffractogram of this form is well distinguishable from the stable form EI (Figure 6). It is worth noting that a previous study proved that EII undergoes a progressive and irreversible solid-solid transition to EI within 20 minutes after its preparation [1]. Single crystals of the stable phase EI were also obtained by slow evaporation of *(S)*- DPL saturated solutions at room temperature in a 95:5 (*v:v*) acetone: water mixture and seeded with EI (crystallographic data in Table 2). The stable crystal form EI consists of stackings of monolayers made of H-bonded DPL molecules. The slices are held together by means of van der Waals and CH···O contacts. The theophylline fragments are almost perpendicular to the (001) planes allowing π stacking that stabilizes the molecular slices (Figure 7). Nevertheless, production of suitable single crystals of EII failed in solution or from SCM.

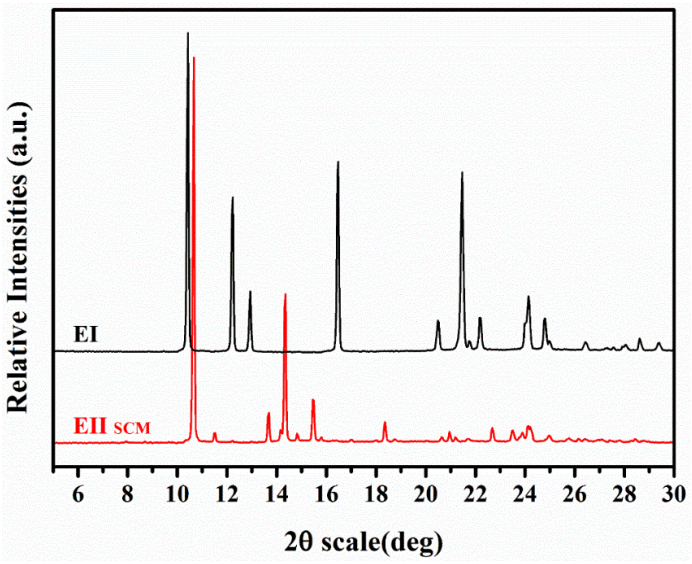

Figure 6. XRPD diffractograms of EI and EII crystallized from the SCM.

Table 2. Crystallographic Data at 298 K for EI. Adapted from [1].

	EI *(S)*
Crystal system	monoclinic
Space group (Z)	$P2_1$ (2)
***a* (Å)**	4.5191(6)
***b* (Å)**	14.1612(19)
***c* (Å)**	8.9530(12)
***β* (deg)**	99.129(2)
vol (Å ^{3})	565.70

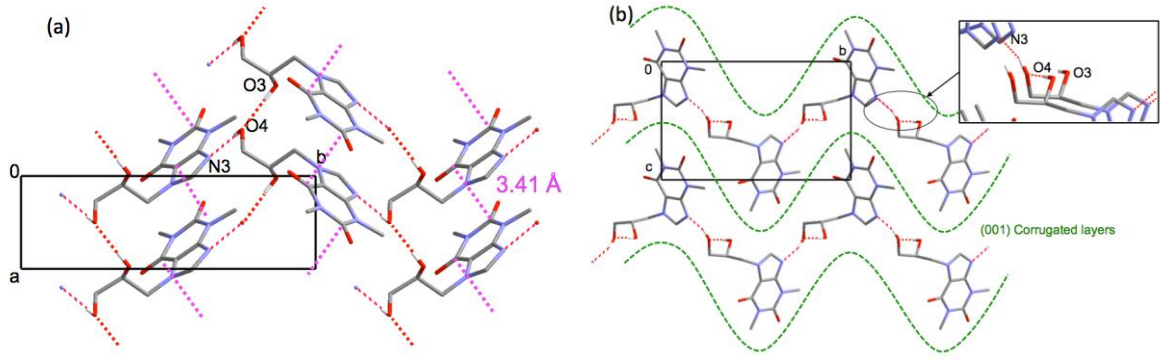

Figure 7. Projections of the EI crystal structure along the c axis (a) and along the a axis (b) showing the stacking along c of (001) slices. Taken from [4].

Hence, recrystallization from the SCM at 100 °C (heating rate at 2 °C/min) results in the polymorph EII of the enantiopure composition (T_{melt} *ca.* 119.4 °C - Figure 8). Given the large

difference between ΔH_f of both polymorphs ($\Delta H_{f\ EII} << \Delta H_{f\ EI}$), the SCM substance is presumably not fully converted into EII during crystallization. Nevertheless, it has been established previously that EII is monotropically related to EI according to the Burger-Ramberger law [1]. More information about this topic is discussed later in this chapter. Table 3 reports thermochemical data for the four crystalline forms identified for DPL.

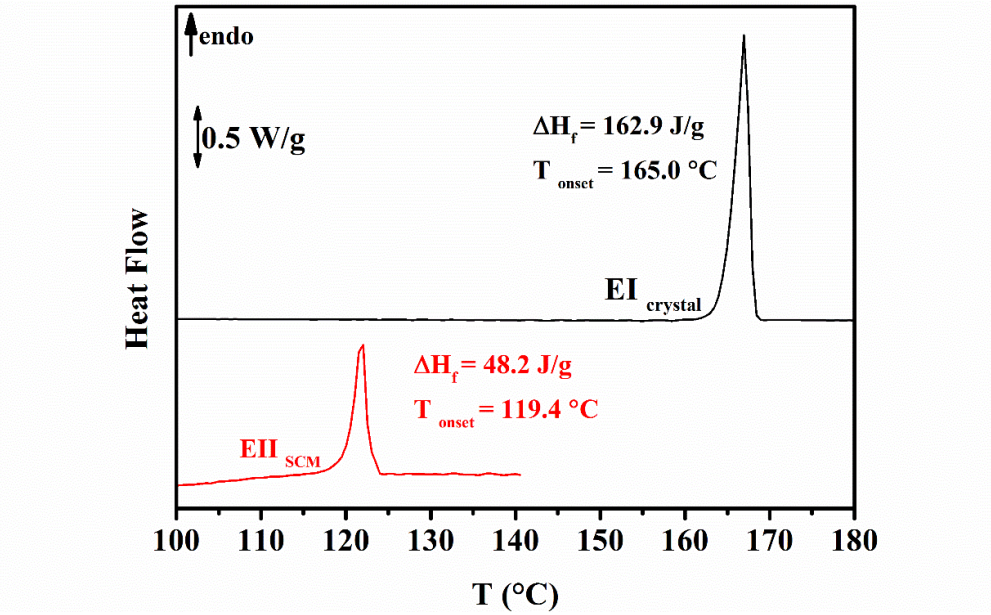

Figure 8. DSC thermograms of EI (black) and EII obtained from the SCM (red). Heating at 2 °C/min.

Table 3. Thermochemical Data Obtained for the different DPL forms.

	Racemic DPL (ee 0%)		**Enantiopure DPL (ee 100%)**	
Form	RI (stable)	RII (metastable)	EI (stable)	EII (metastable)
T_{melt}^{onset} (°C)	160.0	148.4	165.0	119.4
ΔH_f (J/g)	128.4	107.9	162.9	48.2
Crystallization	Solvent	Melt or Solvent	Melt or Solvent	Melt
Calcd density ($g.cm^{-3}$)	1.493	1.508	1.452	

III-1-3. Global binary phase diagram between DPL enantiomers

The binary phase diagram between DPL enantiomers studied by Brandel *et al.* [1] revealed a complex behavior originating from the presence of stable and metastable solid forms for the pure enantiomer and the racemic composition. From physical mixtures of the two thermodynamically stable phases RI and EI, DSC analyses have evidenced the existence of an invariant temperature at 152 ± 0.75 °C, giving proof of the presence of an eutectic reaction whose composition is close to ee 50% (Figure 9).

Combined XRPD, DSC and HSM analyses were used in order to characterize the crystallization from the melt (see Appendix AI-8 for HSM). Concerning the metastable equilibrium between pure enantiomer EI *(R)* and *(S)*, the existence of a metastable conglomerate was confirmed at T_{onset} = 137.0 °C. Moreover, melting of crystalline samples involving metastable crystalline phases RII and EII confirmed the existence of two metastable solid solutions labeled respectively ssRII and ssEII [1], as illustrated in Figure 9. The balance between either metastable equilibria is driven by kinetics conditions of crystallization, as well as selected enantiomeric excess. Indeed, with an annealing (above T_g) of DPL glasses samples, the crystallization of ssRII is kinetically favored for ee ranging from 0 to 70 %, while ssEII crystallizes when ee is in the range 70 to 100 ee%.

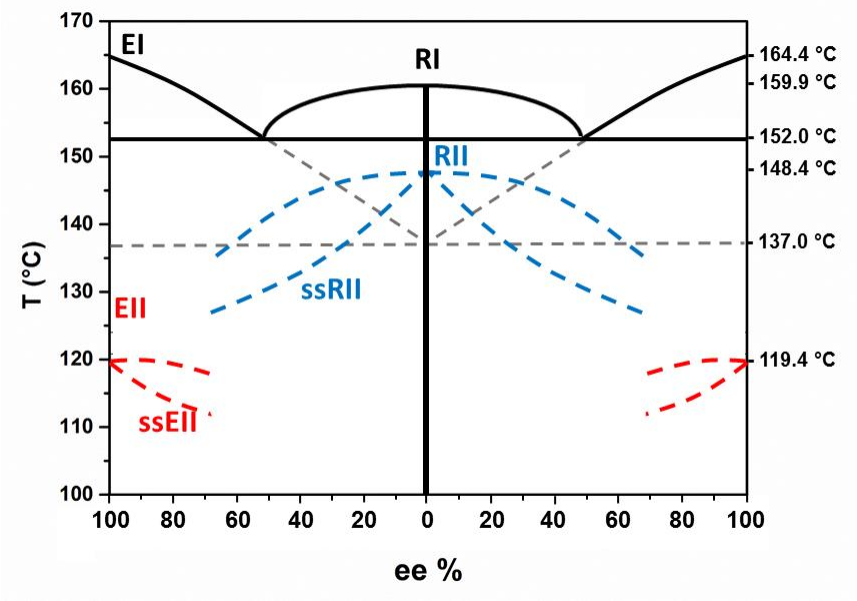

Figure 9. Experimental phase diagram: eutectic equilibria between RI and EI (in black) and accessible part of solid solutions ssEII (red) and ssRII (blue) of crystalline phases EII and RII. Metastable conglomerate between EI(R) and EI(S) (gray). Stable equilibria are shown by solid lines whereas dashed lines indicate metastable equilibria (adapted from Clément Brandel, PhD, Thesis [1]).

III-2. Crystallization study of DPL from the amorphous state – Characterization of a new metastable polymorphic form: Primary Crystals (PC)

III-2-1. Identification of the experimental conditions for DPL recrystallization

Understanding the crystallization behavior of organic materials is of utmost importance in order to develop amorphous pharmaceutical solids [5], [6]. The objective of the present section is to provide a clear picture of the successive events occurring during temperature-induced recrystallization from amorphous DPL samples. First, preliminary investigations consisted of identifying the most adequate conditions for reliable observations and characterization of the amorphous state through its glass transition ($T_{g\,DPL} \approx 37$ °C). Starting materials consisted of the known stable forms [1], namely, EI for the pure enantiomer and RI for the racemic composition. The absence of weight loss by sublimation or chemical degradation up to 265 °C was checked by TG-DSC (see-Figure 3 in Chapter II-1-3), and it confirmed the possibility of producing amorphous DPL by fast cooling (*ca.* 20 °C/min) from the molten state. On the basis of trial and error experiments, two protocols were found suitable for detailed comparative observations, illustrated in Figure 10. Protocol A denotes conventional linear heating at 2 °C/min from room temperature to 185 °C, whereas Protocol B includes isothermal steps at 85 °C ± 5 °C and/or 125 °C ± 5 °C with durations (hereafter denoted as t_1 and t_2) adjusted to reach complete physical transformations. These two thermal profiles were applied to all enantiomeric compositions so as to observe recrystallization behaviors (*i.e.* polymorph selection, nucleation mode, growth rate, and morphologies).

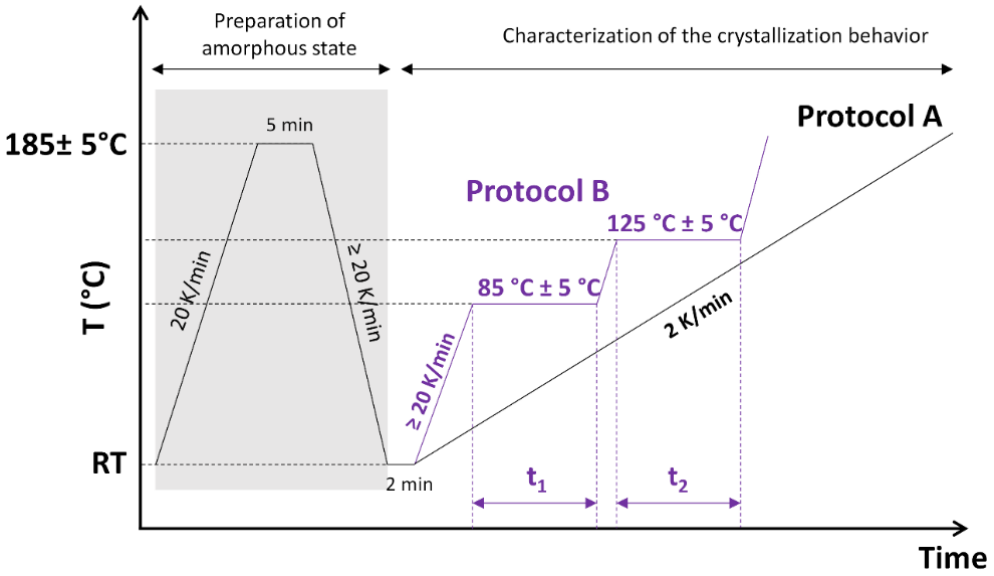

Figure 10. Applied thermal treatments for preparation of glassy DPL samples from the molten state and observation of DPL recrystallization from the supercooled melt.

III-2-2. Characterization of the recrystallization behavior of DPL at racemic composition

III-2-2-1. Melting of the stable crystalline phases

Prior to study of DPL recrystallization from the racemic SCM, protocol A was implemented in DSC, using both commercial racemic DPL with 0.14 % *wt* of TPH and samples purified by recrystallization with a reduced quantity of TPH (below the limit of detection of HPLC, *i.e.* < 0.03 % *wt* of TPH) as starting materials. Figure 11 shows the thermal signal recorded during a first heating step of commercial crystalline racemic DPL (Figure 11 (a)) and highlights the melting of the stable phase RI at $T_{melt\ onset}$ = 160.0 °C, ΔH_m = 128.4 J/g whereas the melting of RI was recorded at $T_{melt\ onset}$ = 162.0 °C, ΔH_m = 170.6 J/g for the purified sample. An increase of melting point and a larger heat of melting are reliable arguments of a successful purification process [7].

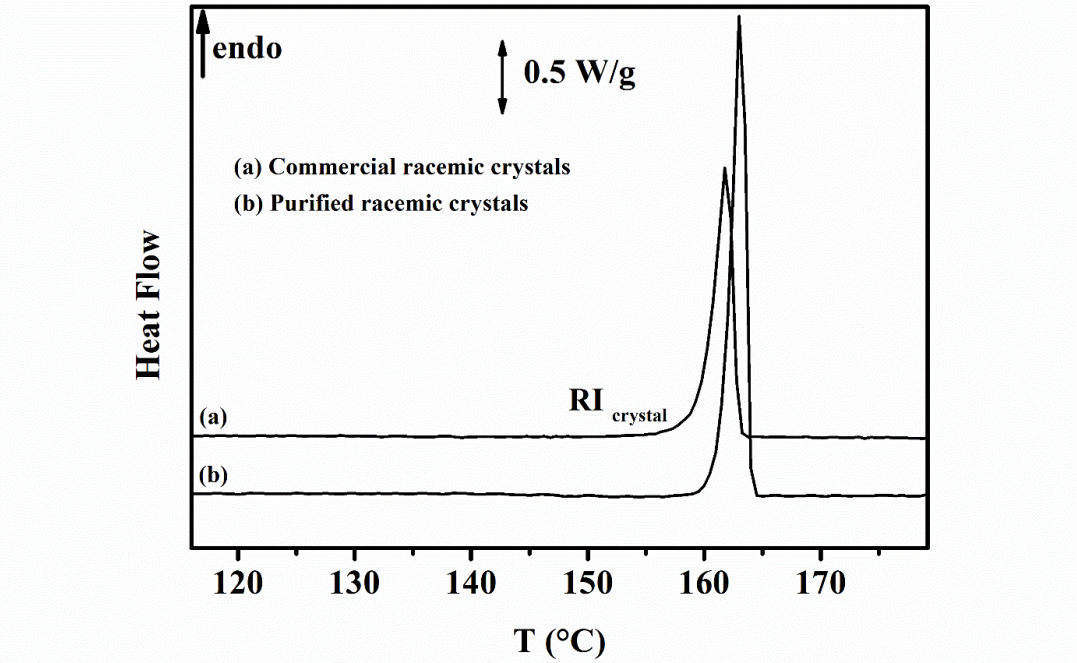

Figure 11. DSC thermograms of commercial RI (a), of purified RI (b). The heating rate was 2 °C/min.

III-2-2-2. Characterization of the new metastable phase (PC, at ee 0%)

a. A double exothermic phenomenon

It was reported earlier that progressive heating of SCM racemic DPL produces the metastable polymorph RII (T_m = 148 °C, Figure 9) [1]. From the DSC analysis of the SCM (*i.e.* second heating) of commercial and purified samples shown in Figure 12, two successive exothermic peaks are however detected in the temperature range 65 – 110 °C, indicating a two-step crystallization behavior from the SCM. As expected, the purified sample gives rise to a higher melting point for the RII crystal form (onset at 149.6 °C with ΔH_m = 137.7 J/g) than for the commercial sample (onset at 148.7 °C with ΔH_m = 125.7 J/g). Interestingly, the change in chemical purity also affects the crystallization behavior through a shift in temperature by *ca.* 10 °C and an inversion in magnitude of the associated enthalpies of exothermic peaks. From these data, it can be suggested that TPH (and possibly other impurities) might hinder or delay the nucleation and growth of DPL. This observation was also reported for amorphous D-Mannitol which recrystallizes at higher temperature when doped with the structurally very alike molecule Sorbitol [8]. Besides, the occurrence of two successive events might be interpreted either as the two-step (or bimodal) crystallization of the same crystal form [9]–[11] or as the formation of two different crystal forms with distinct nucleation and growth rates and/or

mechanisms [12]–[14]. This second hypothesis implies a solid – solid (or solid – liquid – solid) transition from one phase to the other since only the melting peak of RII is detected at *ca.* 150 °C.

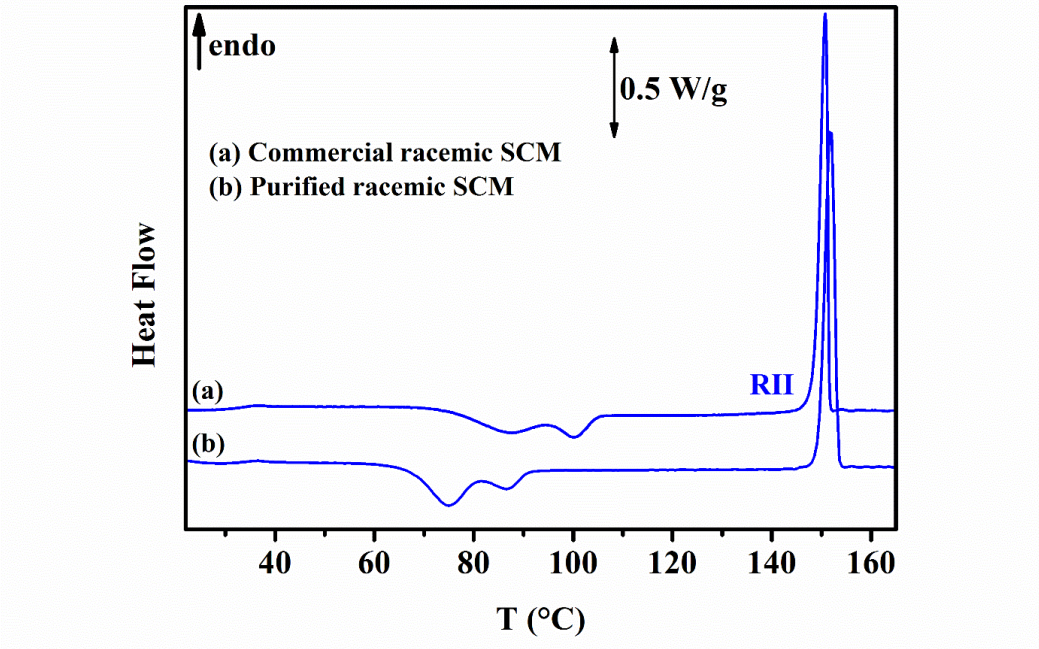

Figure 12. DSC curves of the SCM at the racemic composition of DPL; Heating rate: 2 °C/min.

b. A multi-step crystallization

Hot stage optical microscopy experiments were carried out to get further information about this complex behavior. Applying protocol A to purified racemic DPL at a constant heating rate of 2 °C/min, three distinct phenomena, illustrated in Figure 13, could be identified. The first one consists of the nucleation and growth of well-shaped lozenges with a mean size in the range of 30 – 50 µm along their main axis (Figure 13 (a)). By increasing the temperature, two other events take place and spread progressively in the SCM material up to 130 °C. They consist of the heterogeneous nucleation of a second crystal form that develops as large domains with the typical shape of form RII [1]. Concomitantly, one can observe marked alterations of the initial particles, probably indicative of a solid-solid transition toward the same crystal form RII (Figure 13 (b, c)). This interpretation implies that the initial well-shaped particles (labeled hereafter PC for Primary Crystals) might constitute a new crystalline form of DPL, which was further investigated by implementing different thermal profiles.

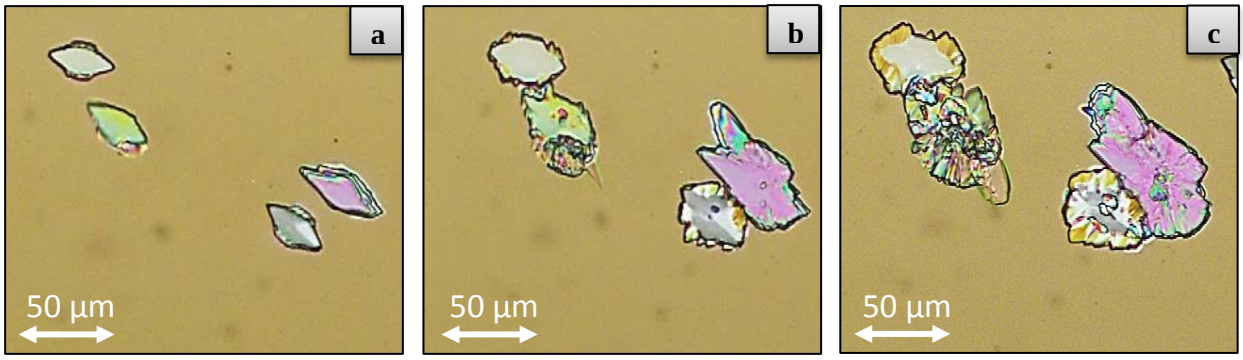

Figure 13. HSM images of racemic DPL for the evolution of the hexagonal-shaped morphology crystals at (a) 75 °C (b) 82 °C (c) 88 °C during a heating ramp of 2 °C/min of Protocol A.

c. Morphology of PC crystals (ee 0%)

Protocol B was therefore applied with t_1 = 35 min at 90 °C and t_2 = 1 min at 125 °C. In these optimized conditions, the crystal shape of form PC could be carefully analyzed, revealing that this new form often develops as twinned polycrystalline particles composed of lozenge-shaped single crystals (Figure 14 (a)) giving rise to unusual pseudo-hexagonal assemblies shown in (Figure 14 (b)). By maintaining the sample at 90 °C for more than 30 min before heating to 125 °C, the three-step process described above was confirmed, as shown in Figure 14 (c, d).

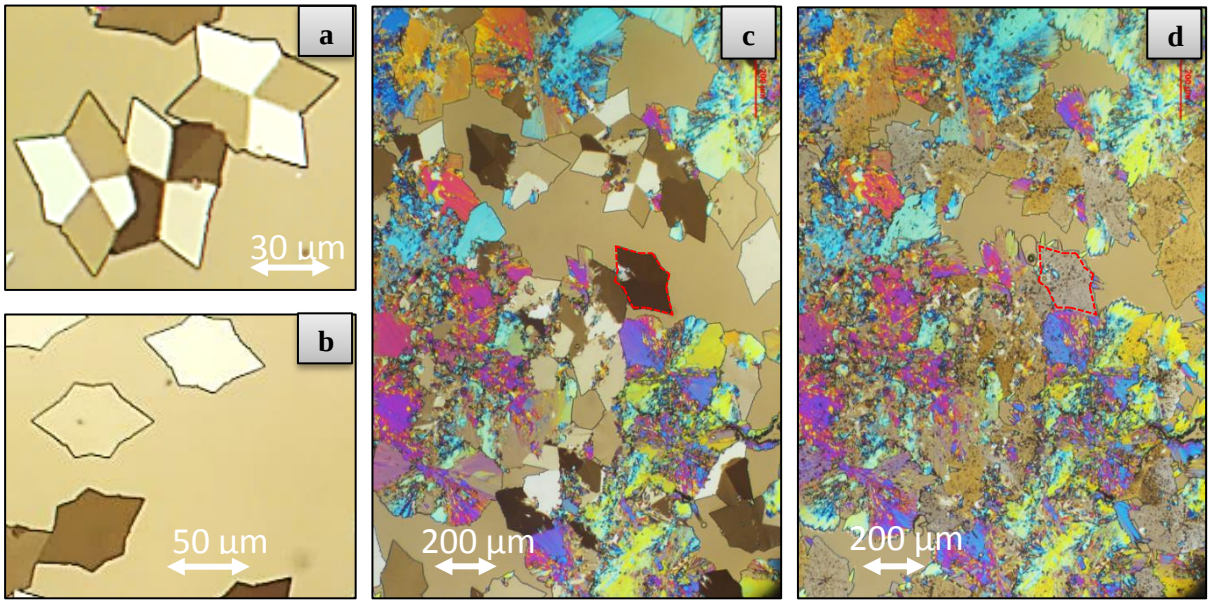

Figure 14. HSM observations of a recrystallizing racemic SCM using Protocol B to racemic DPL and showing PC obtained at 90 °C (a,b), the mixture of PC and RII crystals at 90 °C (c), and the complete transition toward RII at 125 °C (d).

d. Solid-solid transition of metastable PC into ssRII

The existence of the previously unreported PC form was unambiguously demonstrated by annealing at 80 °C during 20 min, inducing the formation of a mixture of crystal forms that could be analyzed by XRPD. In Figure 15, one can compare the diffraction patterns of form RII obtained by solvent crystallization (for comparison purpose) or produced by heating the SCM up to 125 °C with that collected after annealing of the amorphous sample at 80 °C. It appears that the annealed samples contain several specific diffraction peaks (marked by stars in Figure 15 (c)) that do not match with the XRPD signature of form RII or any other known form of DPL. Despite a limited number of Bragg peaks for PC, probably caused by weak crystallinity and/or preferred orientation, this sample is shown to consist of a physical mixture of RII and PC crystal forms.

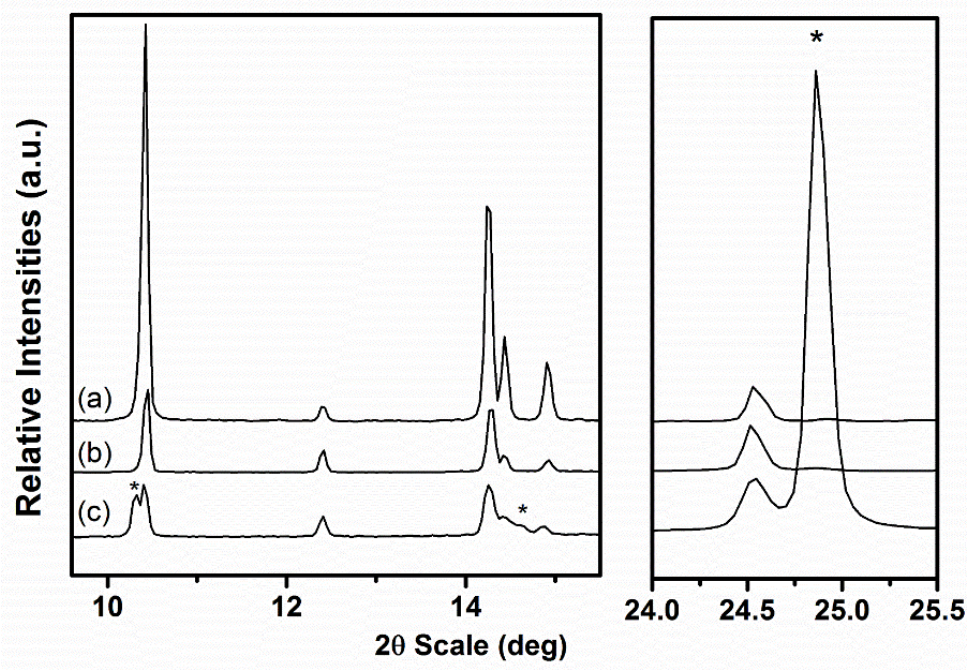

Figure 15. Selected 2θ ranges of XRPD patterns collected for racemic DPL: Form RII produced by solvent crystallization (a), from the SCM with protocol A up to 125 °C (b) and PC + RII obtained with protocol B up to 80 °C during 20 min (c). The diffraction peaks specific to PC are marked with stars.

Additionally, Figure 16 compares selected ranges of Raman shifts (lattice vibrations at low wavenumbers and carbonyl or C=C double bond *stg* vibrations [3], [15]) (see Appendix AI-9 for Raman spectroscopy) for the same PC particle obtained at 90 °C and subsequently heated up to 125 °C with reference to spectra recorded for RII and for amorphous DPL.

It is evidenced from these data that the Raman signature of PC resembles that of the amorphous material and that heating up to 125 °C induces a transition from PC to RII. Furthermore, PC can be unambiguously identified by its large peak at *ca.* 1650 cm^{-1}, whereas its Raman shifts at low wavenumbers can hardly be differentiated from that of the amorphous state. Such similarities between Raman spectra of PC and amorphous DPL might actually be related to analogous molecular arrangements of these solid forms, which would at least partially explain the fast development of PC from the undercooled liquid, presumably facilitated by the absence of a significant energy barrier [14].

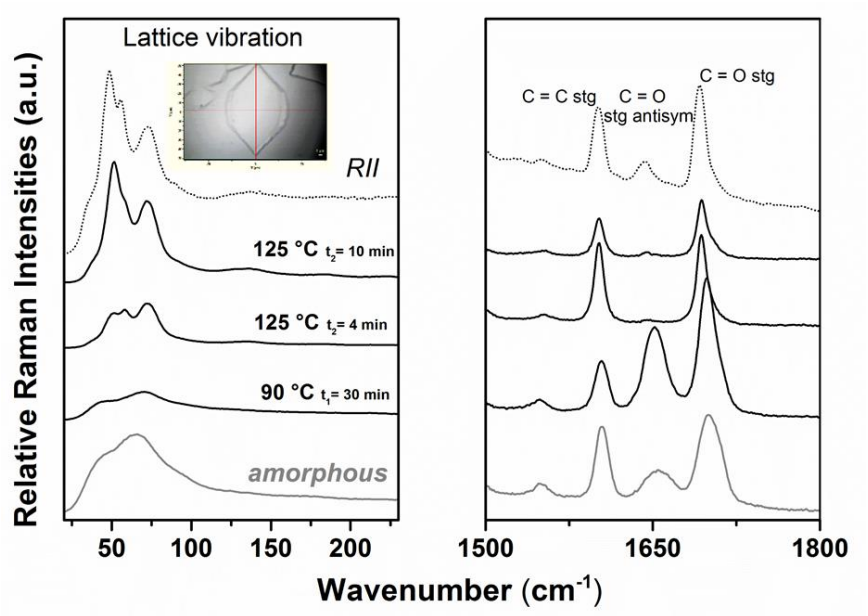

Figure 16. Selected wavenumber regions of Raman spectra for racemic DPL. The gray spectra depict reference materials (amorphous and form RII) whereas black spectra were obtained from the particle shown in the insert at different temperatures.

III-2-2-3. Impact of TPH on racemic DPL PC crystallization

Since chemical purity was shown to have an impact on the crystallization behavior of DPL from the SCM (Figure 12), a complementary investigation was performed to analyze the influence of TPH (shown to constitute the major component in the impurity profile of the starting material) on the proportion of PC produced when applying protocol B with t_1 = 40 min at 80 °C. In these conditions, it appeared (Figure 17) that increasing the mass fraction of TPH favors the formation of PC, with some of the major diffraction peaks of RII becoming almost undetectable at TPH fractions higher than 2.3 % *wt*. For instance, the addition of 3.7 % *wt* of

TPH leads to a mixture of RII and PC, with a probable strong preferred orientation since only a few peaks of RII are detected at 14.3° and 14.9° (2θ), whereas major reference peaks are missing (10.5°, 13.0°) or very weak (24.55°). This point highlights, in consistency with DSC analysis and microscopy observations, that particles of the RII form develop from pre-existing PC that act as favorable surfaces for the secondary nucleation of RII.

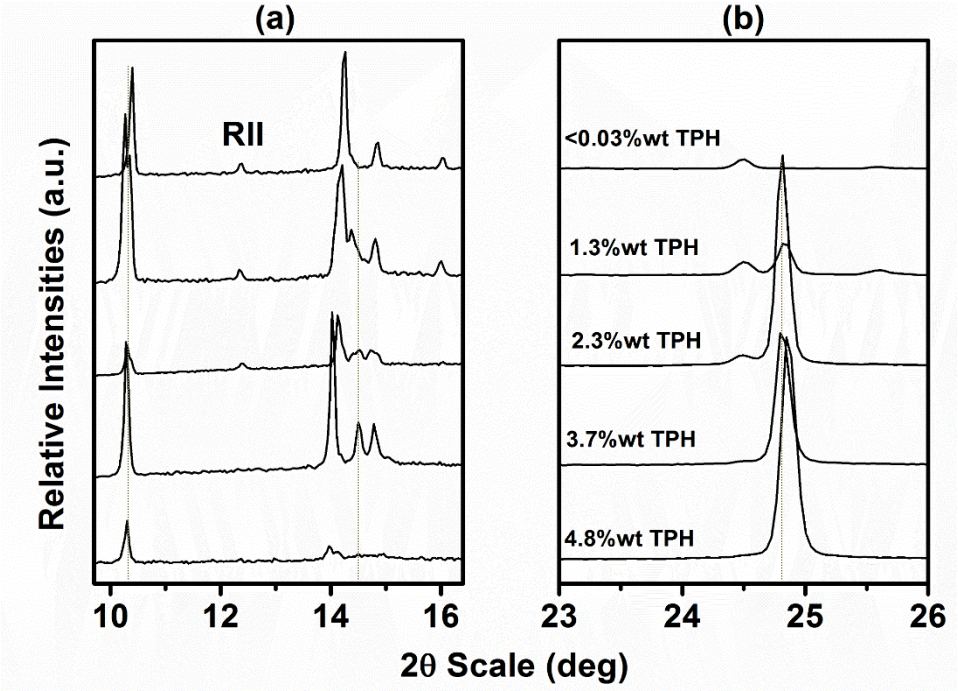

Figure 17. XRPD diffractograms of racemic samples doped by TPH obtained with protocol B: 90 °C 30 min for each samples. Diffraction peaks of PC are marked with vertical dotted bars.

In relation to the similarity between Raman spectra of PC and amorphous DPL, one may suggest that PC constitutes a "kinetic form" that nucleates easily from the SCM, whereas spontaneous nucleation of RII is more difficult or kinetically hindered in the SCM. However, once PC are present in the sample, heterogeneous nucleation of RII occurs readily, and the faster growth of this form, together with its higher thermodynamic stability, induces a progressive transition from PC to RII upon heating above 100 °C.

Regarding the two exothermic phenomena detected in the temperature range 65-110 °C (depending on the chemical purity of DPL samples, Figure 12), it seems reasonable to suggest that they might be induced by the two successive crystallization events, the first one being associated with the nucleation and growth of PC, and the second one, about 10 °C higher, is due to the secondary nucleation and fast growth of RII particles, as consistently observed by optical microscopy.

Hence, the crystallization of racemic DPL from the SCM appears as a complex multistep process determined by the relative nucleation difficulty of two crystal forms, by the associated kinetic competition and by the chemical purity of samples. From DSC results, it appeared that a small proportion of TPH is sufficient to hinder or delay the spontaneous nucleation of PC particles. The control of chemical purity and suitable annealing steps are however able to favor the formation and development of large and well-shaped PC particles. These initial crystals (and presumably other physical impurities or available surfaces) are required for the subsequent development of the more stable form RII.

III-2-3. Characterization of the recrystallization behavior of DPL at enantiopure composition

III-2-3-1. Characterization of the recrystallization from the SCM

Figure 18 presents a set of selected DSC curves obtained during successive heatings of a purified DPL sample with ee = 100%, according to protocol A. The first curve is consistent with the presence of the stable form EI (T_m = 165 °C, ΔH_m = 168.3 J/g) recovered after synthesis and purification. The other curves (b - d) depict the crystallization and subsequent melting behaviors from the SCM and exhibit, in contrast with the racemic composition, a single exothermic peak in the temperature range 80 – 100 °C. As deduced from melting events, this crystallization step leads to one or several crystal forms, with a poorly predictable character indicative of a diverse behavior. Figure 18 (b) illustrates the formation of form EI only, whereas Figure 18 (c) indicates a partial crystallization of form EII that melts at 121.5 °C before recrystallization/melting of EI [1]. In a few occurrences, a third partial melting is observed at 156.0 °C, revealing the probable existence of a transient polymorph labeled EIII. When the molten sample in the DSC pan is carefully covered with a Kapton film (Figure 18 (e)), the exothermic event extends over a temperature range larger than 20 °C, and only the melting of EII is observed.

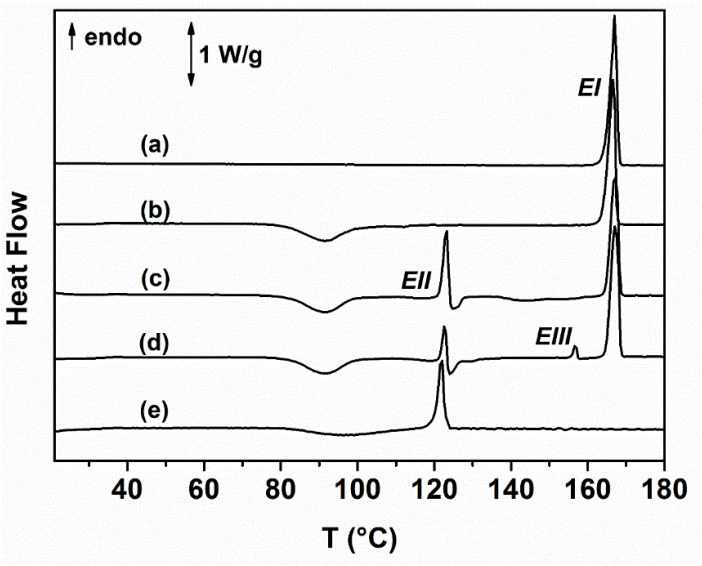

Figure 18. DSC curves obtained with enantiopure DPL: (a) freshly purified sample of form EI; (b-d) illustration of various melting behaviors after crystallization from the SCM in a closed pan; (e) same conditions with an open pan and DPL sample covered with a Kapton film.

Hot stage optical microscopy was used to further investigate the crystallization behavior of enantiopure amorphous DPL, using either protocol A or B. Consistent with previous observations [1], particles of form EI could be recognized as well-shaped elongated crystals with a length usually larger than 500 µm along the direction of fast growth (Figure 19 (a)), whereas EII particles obtained by annealing at 90 °C give rise to quasi-circular spherulitic aggregates initiated from a single nucleation point (Figure 19 (b)). The new form EIII was produced by a long annealing (2 days) at 125 °C and can only be described as a dense cross-linked agglomerate of very thin and elongated particles, as illustrated in Figure 19 (c). However, the three polymorphs could also be unambiguously identified and differentiated by XRPD, with a surprisingly good crystallinity shown in Figure 20.

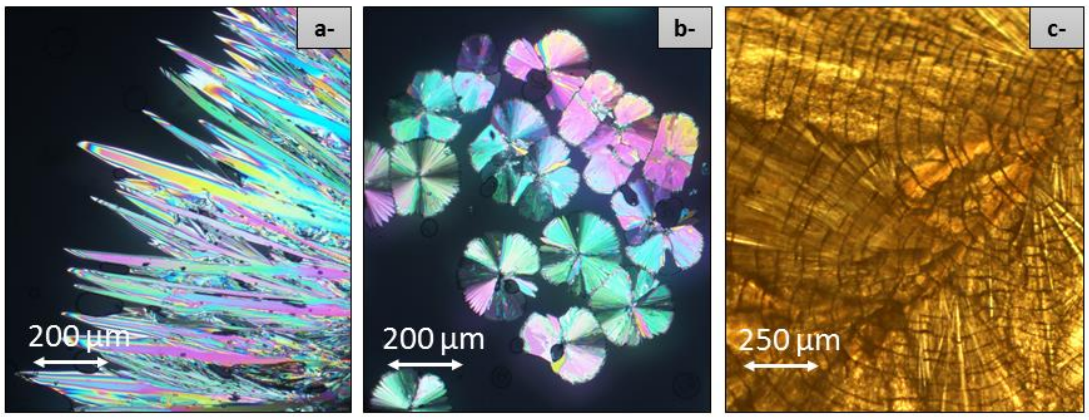

Figure 19. Optical microscopy pictures depicting the typical crystal shapes of enantiopure DPL recrystallized from the SCM. EI produced by heating to 145 °C (a) ; EII obtained at 90 °C after 90 min (b) and EIII obtained by long annealing at 125 °C (c).

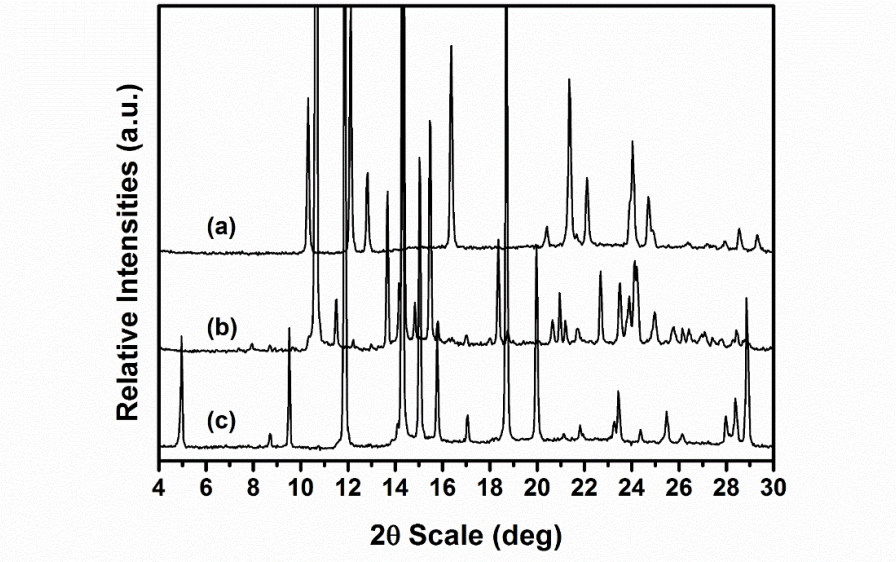

Figure 20. XRPD patterns for the three identified crystalline forms of enantiopure DPL: EI (a), EII (b), and EIII (c).

III-2-3-2. Heterogeneous crystallization of ssEII on the edges of PC crystals

As in the case of racemic DPL, the early stages of crystallization from the SCM were more carefully explored by optical microscopy, applying various temperature programs and high magnification (×100). The implementation of an annealing step of *ca.* 15 min at 85 °C (protocol B) revealed the formation of a first set of well-shaped crystalline particles with a lozenge or roughly hexagonal morphology and a mean size of 20-40 μm along the main axis (Figure 21). Some of these primary crystals (presenting similarities with PC particles described above) develop as twinned particles and give rise to "star-shaped" aggregates that look like those observed at the racemic composition (see Figure 14 (a)). Furthermore, most of these initial crystals serve as support surfaces for the rapid heterogeneous secondary nucleation of spherulites that could be readily recognized as EII crystals.

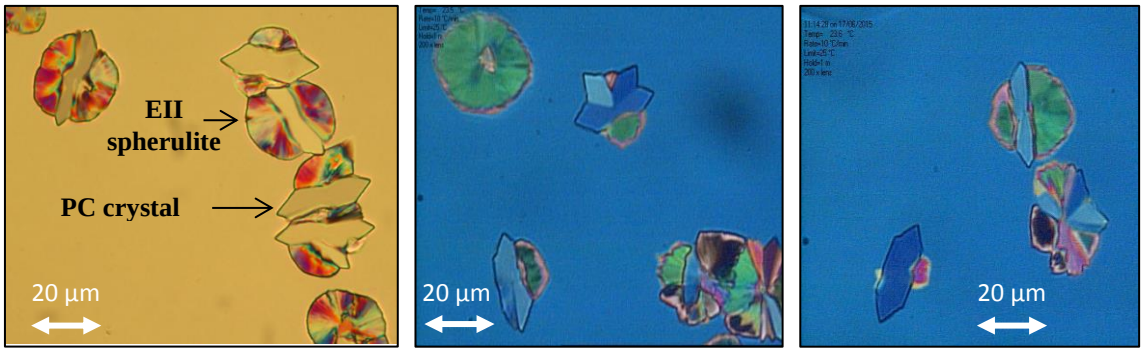

Figure 21. Optical microscopy images showing the early stages of spontaneous crystallization of enantiopure DPL from the SCM at 85 °C: PC crystals nucleate first and spherulites of form EII appear on lateral faces of pseudo-hexagonal PC particles.

III-2-3-3. Comparison between PC crystals from racemic composition and the pure enantiomer

From our numerous observations, it is noteworthy that only the two lateral faces of pseudo-hexagonal PC act as nucleation areas for EII, whereas other faces keep developing in the SCM growth medium. Attempts to identify PC grown at enantiopure composition by XRPD were unsuccessful, but comparisons of Raman spectra (Figure 22 (d-e)) confirmed that PC produced at racemic and enantiopure compositions corresponds to the same crystal forms. Moreover, specific Raman shifts can be associated with each solid form, despite similarities between the spectra of PC and form EII (Figure 22 (c-e)).

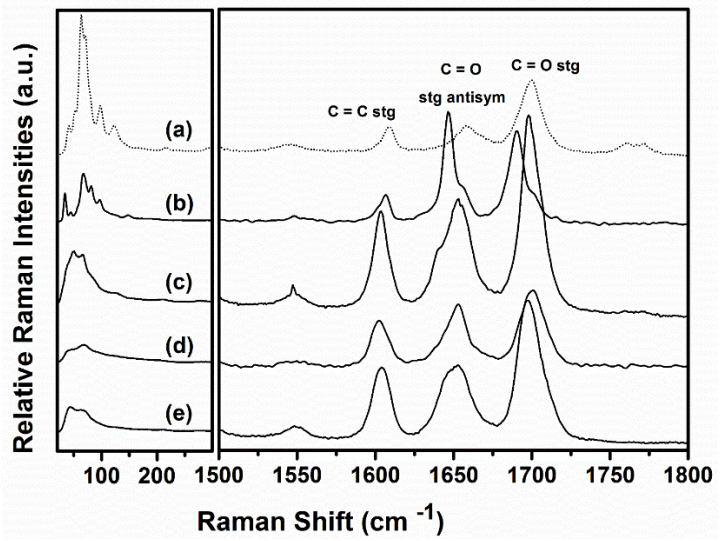

Figure 22. Selected wavenumber regions of Raman spectra for enantiopure DPL. The gray spectrum depicts reference materials (a: form EI) whereas black spectra were obtained for EIII (b), EII (c), PC crystal for the enantiopure composition (d) and PC crystal for the racemic composition (e)

Consistent with optical microscopy observations, it can therefore be assumed that crystallization from the SCM in the temperature range of 60 – 100 °C occurs according to similar mechanisms whatever the enantiomeric composition: a first crystalline population (PC) is initially formed by spontaneous nucleation and growth in the undercooled liquid. Specific faces of these well-shaped particles serve as support areas for the heterogeneous nucleation of a second crystalline population that develops faster than PC, and further heating induces either a melting or a solid-solid transition toward one of the two metastable phases, EII or RII.

III-2-3-4. Characteristics of PC

Although the enantiomeric composition of PC is not known, it is likely that its fast growth from the SCM is favored by a poor enantioselectivity thus suggesting that this form might consist, as forms EII and RII, of a solid solution of DPL enantiomers. Hence, it can be deduced from our results that:

(i) the new crystal form PC most probably constitutes a third solid solution in the binary system between DPL enantiomers (although it cannot be excluded that PC might correspond to a conglomerate).

(ii) this complex multistep crystallization behavior is a consequence of the difficult spontaneous nucleation of EII or RII crystal forms from the SCM, whereas formation of PC is likely to be favored by conformational/structural analogies existing between the SCM and PC crystals.

From a morphological point of view, crystalline form PC develops as twinned polycrystalline particles composed of lozenge-shaped single crystals. Figure 23 (a) depicts the unusual pseudo-hexagonal assemblies of PC particles obtained by using a suitable thermal treatments (*i.e.* Protocol B) at the racemic composition. Besides, for a racemic-DPL sample with 2.5 % *wt* TPH, the morphology of PC crystals appears as almost perfect shaped-star assemblies (Figure 23 (b)). This implies that the unusual pseudo-hexagonal assemblies (Figure 23 (a)) are variants of the star-like shape crystals (Figure 23 (c)).

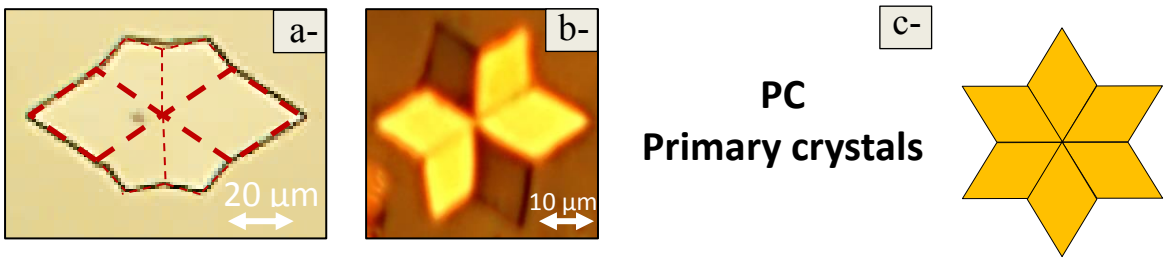

Figure 23. PC crystals observed by optical microscopy with a Protocol B at (a) 90 °C 32 min from racemic DPL with 0.14 % wt TPH and (b) 85 °C 30 min from racemic DPL + 2.5 % wt TPH. (c) Schematic view of PC assemblies with a star-like shape.

III-2-4. Incidence of the enantiomeric composition of the supercooled melt on the recrystallization behavior of DPL

From the above statements, it can be anticipated that particles of the new PC form might be formed during the crystallization from the amorphous state whatever the enantiomeric composition of DPL. Using purified samples, this was confirmed by performing DSC analyses and optical microscopy observations. The DSC curves shown in Figure 24 present the evolution of exothermic crystallization events as a function of the enantiomeric composition and reveal a continuous evolution of the onset temperature for the first exothermic phenomenon, with the lowest crystallization temperature detected at 20% ee ($T_{onset} \approx 65$ °C). When departing further from the racemic composition, the crystallization event is observed at increasing temperatures and reaches more than 80 °C for enantiopure samples (ee = 100%). More interestingly, the second event previously identified as the formation of RII progressively merges with the first exothermic event and consistently disappears at 100% ee.

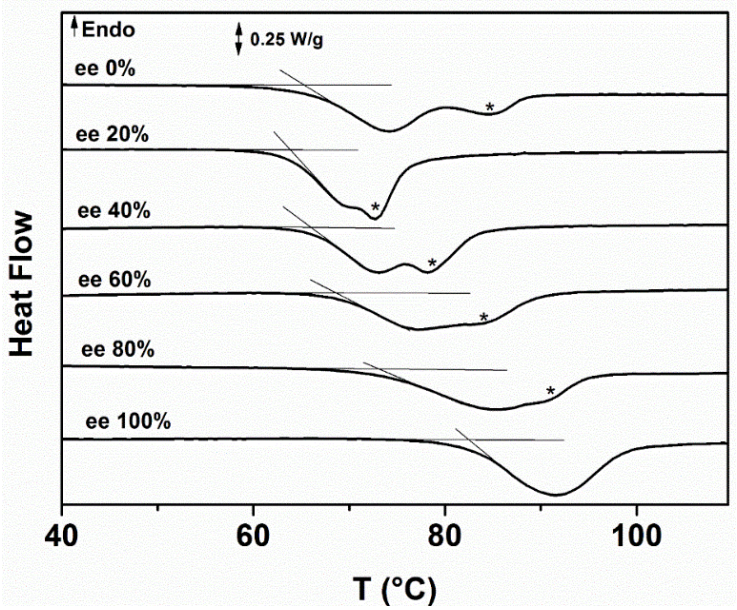

Figure 24. Exothermic part of the DSC curves obtained from the SCM of DPL at different enantiomeric compositions. The star symbols (*) depict RII exothermic signatures.

The optical microscopy images presented in Figure 25 confirm the systematic occurrence of large PC that constitute favorable areas for the subsequent nucleation of EII (at high ee) or RII (at lower ee), usually observed after 10 – 15 min at 90 °C when using protocol B. Our observations also confirm the effects of the kinetic competition between these metastable solid solutions, with EII exhibiting a faster development of its easily recognizable spherulites

compared to the larger domains of RII particles. From careful observations performed at 60% ee, it appeared however feasible to visualize the concomitant formation of EII and RII (Figure 25 (c)) consistent with previous DSC and XRPD results [1].

HSM observations were performed using protocol B (90 °C, $t_{annealing}$= 10 - 15 min) on DPL glasses exhibiting various enantiomeric compositions (*i.e.* 20, 40, 60 %*ee*). After a few minutes of annealing, the typical hexagonal-shaped PC crystals crystallized systematically whatever the enantiomeric excess. One can see from Figure 25 that the enantiomeric composition of the SCM has no detectable incidence on the morphology of the PC particles.

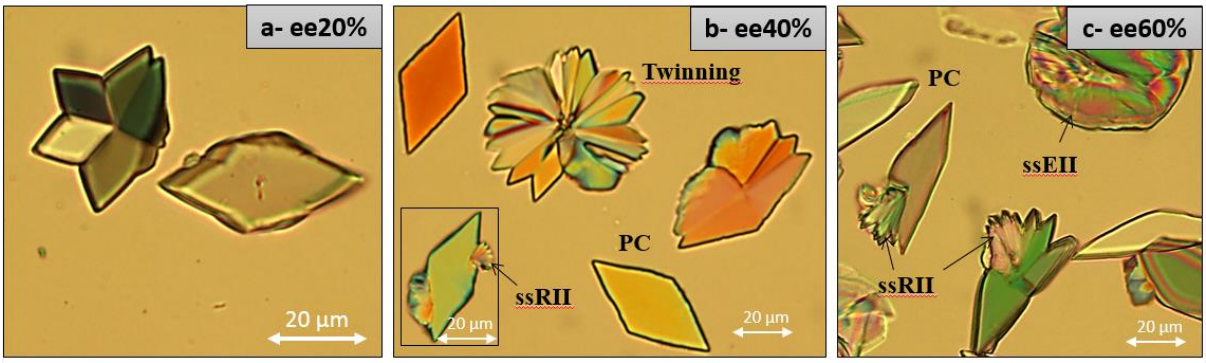

Figure 25. Optical microscopy images of DPL crystals obtained from the SCM at 90 °C for various enantiomeric compositions.

III-2-5. Recrystallization behavior from the SCM with covered samples

Several studies postulated that apparently minor changes in the experimental conditions frequently lead to different crystallization pathways [16]. Recent works have identified key parameters for the characterization of crystallization from glassy systems. In the literature, current explanations differ regarding "surface enhanced crystal growth"[17]. Among them, the role of covering glass-forming materials during recrystallization has been suggested. In the case of Paracetamol, two crystallization pathways from an amorphous state have been reported; results suggest that surface crystallization predominates in the uncovered samples, leading to forms I and II, whereas in the covered samples, bulk crystallization dominates, and leads to form III (stability order: amorphous < Form III < Form II < Form I) [18]. In the case of the two amorphous drugs Indomethacin and Nifedipine, it was observed that crystal growth at the free surface was much faster than through the bulk (below the glass transition T_g) due to the surface diffusion which is from 2 to 6 orders of magnitude larger than in the bulk [19]–[21]. Furthermore, several studies have shown that molecules on the free surface of an organic glass

can be much more mobile than those in the bulk. Thus, one of the conclusions is that surface mobility is directly responsible for fast crystal growth on free surfaces, and may be involved in bulk crystal growth through the creation of voids and free surfaces [16]. A second argument is that diffusion can be significantly faster on the free surface of a molecular glass than inside [21], [22]. The high mobility of surface molecules is quantitatively understood from their special environment: a surface molecule has fewer neighbors than a bulk molecule and a larger freedom of movement. Additionally, this behavior may reflect a relatively low energy barrier to nucleation at the surface [20], [23], which explains why nucleation usually occurs at the surface, followed by crystal growth along the surface and into the bulk [24] [25].

The next section investigates in more details one of them namely the influence of sample covering (using a glass cover slide) on the polymorphic behavior of DPL enantiomers [26]. Thereby, an internship (SMS lab, level: undergraduate third year, supervised by Clément Brandel and co-supervised by myself) has been focused on this topic. Two parameters have been considered: (i) the covered/uncovered situations and (ii) the influence of thickness of the amorphous films sandwiched between the cover and the glass slides. For this purpose, a sample of racemic DPL with 2.3 % *wt* TPH was selected so as to observe recrystallization behaviors. At this percentage of impurity content, an annealing at 90 °C during 30 min of glassy racemic DPL leads to a mixture of RII + PC crystals, as proved by the XRPD shown in Figure 17, which is the ideal case to examine carefully the influence of thickness on the occurrence of one phase or the other. For this purpose, protocol B was slightly adapted (*i.e.* 70 °C 45 min) so as to slow down the phenomenon of crystallization for a careful HSM study.

III-1-1-1. **Case of the racemic mixture with 2.3% *wt* TPH**

Preliminary experiments consisted in observing the behavior of uncovered samples with a homogeneous film of thickness 10 μm by means of HSM with a specific thermal treatment (*i.e.* Protocol B with annealing at 70 °C). After t_{anneal} = 45 min, typical PC crystals crystallized and transformed into a population of poorly defined morphology attributed to RII crystals. However, some birefringent PC crystals still remained. In the covered situation, a large population of PC crystals has been kinetically favored with respect to RII (Figure 26 (b)).

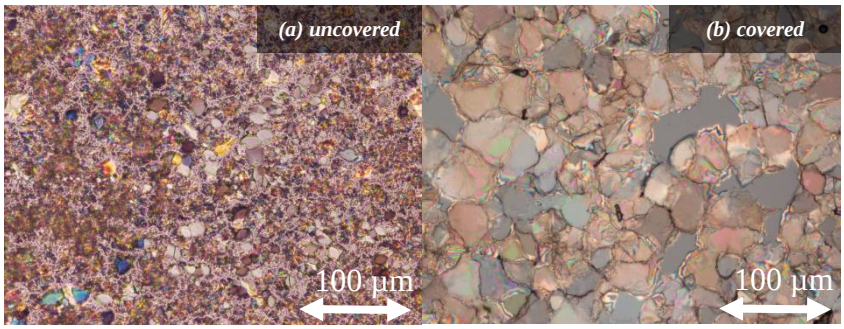

Figure 26. Photographs of racemic DPL with 2.3 % wt TPH depicting crystals obtained from the SCM at 70 °C, annealing duration = 45 min for (a) an uncovered sample and (b) a covered sample. Thickness: 10 µm

In previous sections of this chapter HSM observations were performed by creating a film sandwiched between the cover and the glass slide without controlling specifically the thickness of the films (estimated < 5 μm). In order to rationalize the effect of this parameter, the observation of the recrystallization behaviors (*i.e.* with Protocol B and annealing at 70 °C during 45 min) was carefully performed for controlled and covered films of thicknesses set at 10, 20 and 30 µm. After t_{anneal} = 2 min, the number of nucleation sites was found to increase with the thicknesses of the film (Figure 27 (a-d)), and after t_{anneal} = 45 min, it appeared that the size of the grown PC particles (with very few occurrence of ssRII) was smaller (Figure 27 (e-h)), as confirmed by the lower dimensions of PC crystals reported in Table 4. From these results, a hypothesis is that a larger quantity of SCM matter (for the greater thicknesses) induces a higher probability of nucleation processes, thus resulting in numerous crystals of smaller sizes. Besides, it confirms that PC constitutes a "kinetic form" that nucleates easily from the SCM, whereas spontaneous nucleation of RII is more difficult or kinetically hindered in the SCM whatever the thickness of the covered amorphous film.

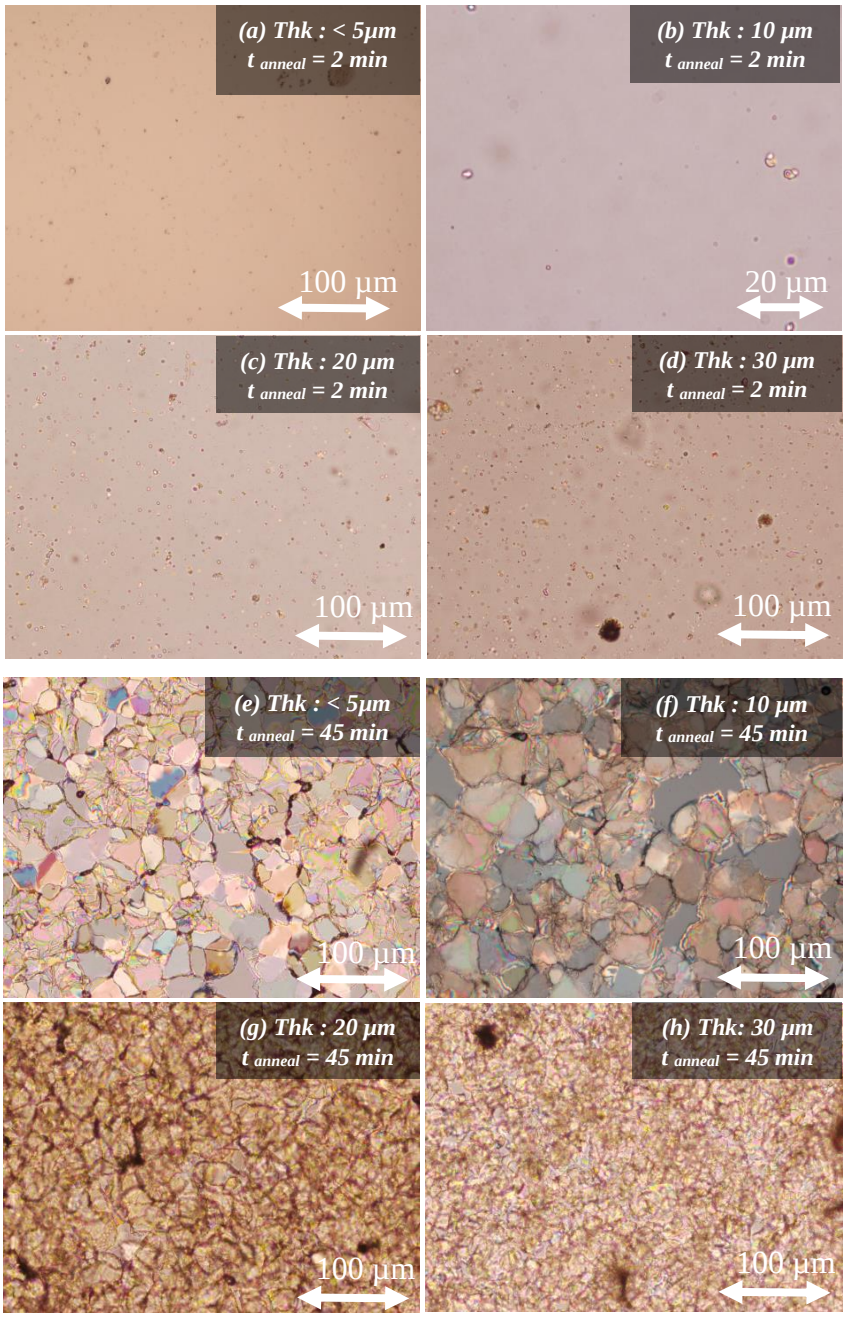

Figure 27. Optical microscopy images of racemic DPL with 2.3 % wt TPH showing the influence of the thickness (Thk) of amorphous films on the PC crystals obtained from the SCM at 70 °C $t_{annealing}$ = 45 min for each films.

Table 4: Evolution of the dimensions of the PC crystals as a function of annealing time (t_{anneal}) versus the thickness (thk) of the films.

t_{anneal}/thk	< 5µm	10 µm	20 µm	30 µm		< 5µm	10 µm	20 µm	30 µm
0 min	*Not measurable*	*Not measurable*	*Not measurable*	*Not measurable*	**25 min**	*25 µm*	*28 µm*	*26 µm*	*20 µm*
5 min	*8 µm*	*6 µm*	*7 µm*	*8 µm*	**30 min**	*31 µm*	*32 µm*	*30 µm*	*20 µm*
10 min	*12 µm*	*12 µm*	*10 µm*	*11 µm*	**35 min**	*36 µm*	*36 µm*	*30 µm*	*20 µm*
15 min	*16 µm*	*17 µm*	*18 µm*	*17 µm*	**40 min**	*43 µm*	*41 µm*	*30 µm*	*20 µm*
20 min	*22 µm*	*21 µm*	*22 µm*	*20 µm*	**45 min**	*50 µm*	*42 µm*	*30 µm*	*20 µm*

III-1-1-2. **Case of pure enantiomer *(S)*-DPL**

Since recrystallization of the pure enantiomer *(S)*-DPL from amorphous state can lead to one or several crystal forms (see DSC curves in Figure 18), a different approach was applied for the racemic composition. Only preliminary experiments have been carried out in order to characterize "surface crystallization". For this purpose, the evolution at room temperature of a drop of amorphous solid obtained by means of quenching from the melt was monitored by HSM. Within a few hours (at RT), some crystals appeared; by morphological identification, one can suggest that the metastable PC + EII are present in the bulk of the drop whereas the stable phase EI is detected only at surfaces (Figure 28 (a) and (b) respectively). However, with a similar thermal treatment, the monitoring of recrystallization by means of XRPD analyzes of an amorphous drop of pure enantiomer (*(S)*-DPL) resulted in the diffraction pattern of the stable phase EI (see Figure 4 (c) in Chapter II-II-1-3). By contrast, when the molten sample in the DSC pan is carefully covered with a Kapton film (Figure 18 (e)), only the melting of EII is observed. Analogously to the case of racemic DPL, these observations promote the hypothesis that amorphous solid-vapor interfaces may play an important role in the crystallization behavior of an enantiopure sample. Further experiments are required to characterize accurately the surface crystallization of amorphous DPL enantiomers (*e.g.* spin-coating could be used for obtaining thinner films (≈ nm to μm) and studying the DPL recrystallization).

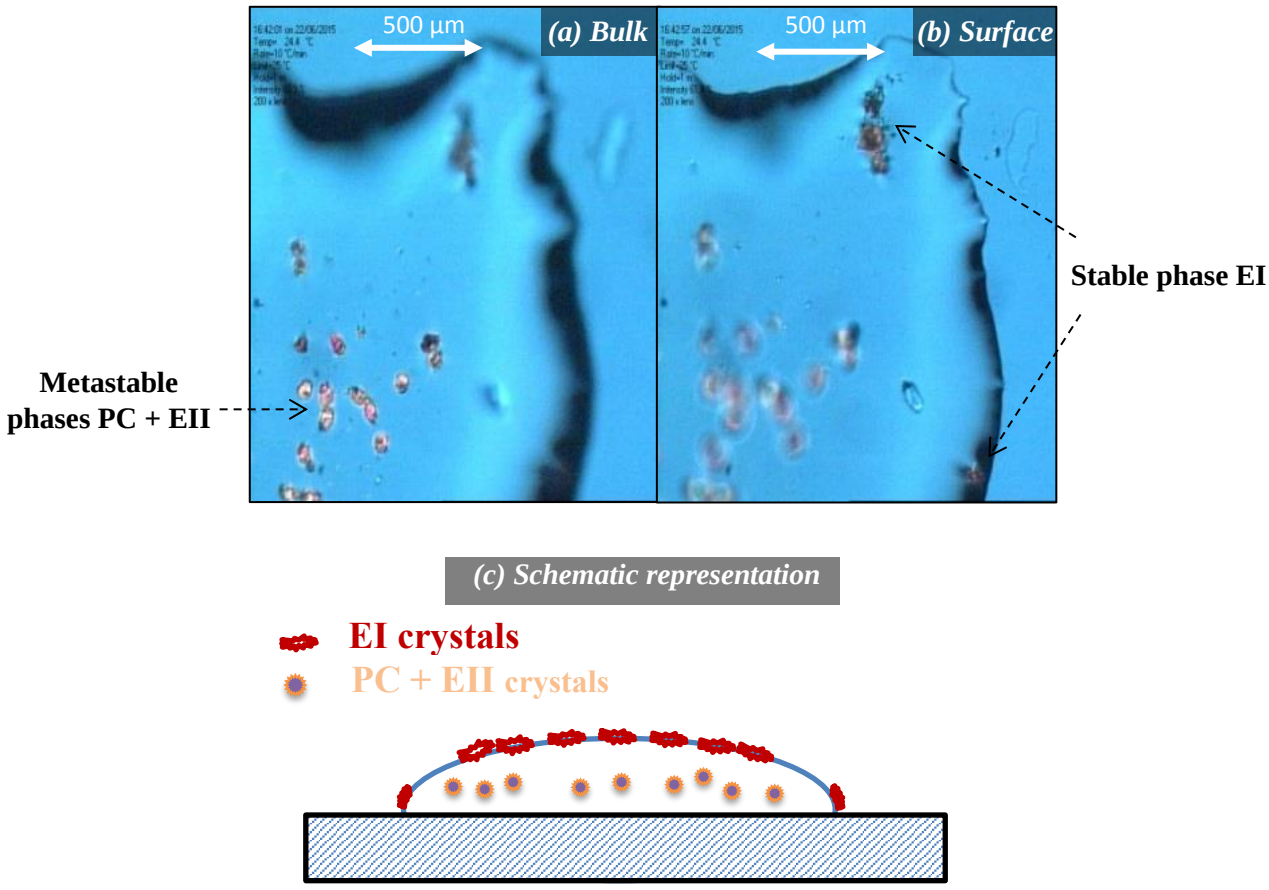

Figure 28. Crystallization of a glassy drop of enantiopure DPL at room temperature. Microscopic images are focused on the bulk (a), and on the surface (b). Schematic representation of the putative crystallization behavior in the bulk of enantiopure DPL (c).

III-2-6. Discussion

The binary system formed by DPL enantiomers constitutes an illustration of the rich and diverse crystallization behavior that can be encountered among chiral pharmaceutical compounds. In the continuity of previous investigations that revealed the occurrence of three possible situations (racemic compound, conglomerate and solid solution) in this system, the present study demonstrated that crystallization from the supercooled melt occurs as a complex multistep process involving the homogeneous nucleation and growth of a first population (PC: primary crystals) that acts as support for the development of secondary populations constituted of metastable solid solutions with higher growth rates. Although specific impurities (TPH) favor the formation of PC, these initial particles are of poor stability and convert into a more stable form. The systematic occurrence of PC at any enantiomeric composition indicates a poor chiral selectivity (*i.e.*, a probable third solid solution in this system) and suggests a fixed scheme

in the crystallization mechanisms, from which it can be deduced that preventing or delaying the crystallization from the SCM should primarily focus on hindering the formation of this transient crystal form. More generally, this case study illustrates the necessity to obtain sufficient knowledge on the exact nature and nucleation conditions of the very first crystalline particles (*i.e.* polymorphs, surface effects …) developing from an amorphous state [27].

As a perspective, starting from a racemic SCM sample with a large amount of PC crystals, it could be interesting to find a process to manage ultimately the resulting crystalline phases (*e.g.* seed with one of the pure enantiomer on a DPL sample containing PC crystals: this may lead to the formation of EII).

References:

[1] Brandel, C.; Amharar, Y.; Rollinger, J. M.; Griesser, U. J.; Cartigny, Y.; Petit, S.; Coquerel, G. Impact of Molecular Flexibility on Double Polymorphism, Solid Solutions and Chiral Discrimination during Crystallization of Diprophylline Enantiomers. *Mol. Pharm.* **2013**, *10* (10), 3850–3861.

[2] Griesser, U. J.; Auer, M. E.; Burger, A. The Polymorphic Drug Substances of the European Pharmacopoeia, Part 10: Diprophylline. *ResearchGate* **1999**, *67* (4), 319–330.

[3] Brandel, C.; Cartigny, Y.; Coquerel, G.; ter Horst, J. H.; Petit, S. Prenucleation Self-Assembly and Chiral Discrimination Mechanisms during Solution Crystallisation of Racemic Diprophylline. *Chem. - Eur. J.* **2016**, *22* (45), 16103–16112.

[4] Brandel, C. Structural Purity and Solid-Solid Transitions in Molecular Crystals. PhD Thesis, University of Rouen, **2013**.

[5] Chen, J.; Sarma, B.; Evans, J. M. B.; Myerson, A. S. Pharmaceutical Crystallization. *Cryst. Growth Des.* **2011**, *11* (4), 887–895.

[6] Yu, L. Amorphous Pharmaceutical Solids: Preparation, Characterization and Stabilization. *Adv. Drug Deliv. Rev.* **2001**, *48* (1), 27–42.

[7] Plato, C.; Glasgow, A. R. Differential Scanning Calorimetry as a General Method for Determining the Purity and Heat of Fusion of High-Purity Organic Chemicals. Application to 95 Compounds. *Anal. Chem.* **1969**, *41* (2), 330–336.

[8] Yu, L.; Mishra, D. S.; Rigsbee, D. R. Determination of the Glass Properties of D-Mannitol Using Sorbitol as an Impurity. *J. Pharm. Sci.* **1998**, *87* (6), 774–777.

[9] Chattoraj, S.; Bhugra, C.; Telang, C.; Zhong, L.; Wang, Z.; Sun, C. C. Origin of Two Modes of Non-Isothermal Crystallization of Glasses Produced by Milling. *Pharm. Res.* **2012**, *29* (4), 1020–1032.

[10] Willart, J.-F.; Carpentier, L.; Danède, F.; Descamps, M. Solid-State Vitrification of Crystalline Griseofulvin by Mechanical Milling. *J. Pharm. Sci.* **2012**, *101* (4), 1570–1577.

[11] Trasi, N. S.; Boerrigter, S. X. M.; Byrn, S. R. Investigation of the Milling-Induced Thermal Behavior of Crystalline and Amorphous Griseofulvin. *Pharm. Res.* **2010**, *27* (7), 1377–1389.

[12] Andronis, V.; Zografi, G. Crystal Nucleation and Growth of Indomethacin Polymorphs from the Amorphous State. *J. Non-Cryst. Solids* **2000**, *271* (3), 236–248.

[13] Willart, J.-F.; Durand, M.; Briggner, L.-E.; Marx, A.; Danède, F.; Descamps, M. Solid-State Amorphization of Linaprazan by Mechanical Milling and Evidence of Polymorphism. *J. Pharm. Sci.* **2013**, *102* (7), 2214–2220.

[14] Kulkarni, S. A.; McGarrity, E. S.; Meekes, H.; Horst, J. H. ter. Isonicotinamide Self-Association: The Link between Solvent and Polymorph Nucleation. *Chem. Commun.* **2012**, *48* (41), 4983–4985.

[15] Gunasekaran, S.; Sankari, G.; Ponnusamy, S. Vibrational Spectral Investigation on Xanthine and Its Derivatives—theophylline, Caffeine and Theobromine. *Spectrochim. Acta. A. Mol. Biomol. Spectrosc.* **2005**, *61* (1–2), 117–127.

[16] Yu, L. Surface Mobility of Molecular Glasses and Its Importance in Physical Stability. *Adv. Drug Deliv. Rev.* **2016**, *100*, 3–9.

[17] Di Martino, P.; Conflant, P.; Drache, M.; Huvenne, J.-P.; Guyot-Hermann, A.-M. Preparation and Physical Characterization of Forms II and III of Paracetamol. *J. Therm. Anal.* **1997**, *48* (3), 447–458.

[18] Nanubolu, J. B.; Burley, J. C. Investigating the Recrystallization Behavior of Amorphous Paracetamol by Variable Temperature Raman Studies and Surface Raman Mapping. *Mol. Pharm.* **2012**, *9* (6), 1544–1558.

[19] Wu, T.; Yu, L. Surface Crystallization of Indomethacin Below T G. *Pharm. Res.* **2006**, *23* (10), 2350–2355.

[20] Zhu, L.; Wong, L.; Yu, L. Surface-Enhanced Crystallization of Amorphous Nifedipine. *Mol. Pharm.* **2008**, *5* (6), 921–926.

[21] Zhang, W.; Brian, C. W.; Yu, L. Fast Surface Diffusion of Amorphous *O* -Terphenyl and Its Competition with Viscous Flow in Surface Evolution. *J. Phys. Chem. B* **2015**, *119* (15), 5071–5078.
[22] Brian, C. W.; Yu, L. Surface Self-Diffusion of Organic Glasses. *J. Phys. Chem. A* **2013**, *117* (50), 13303–13309.
[23] Zhu, L.; Brian, C. W.; Swallen, S. F.; Straus, P. T.; Ediger, M. D.; Yu, L. Surface Self-Diffusion of an Organic Glass. *Phys. Rev. Lett.* **2011**, *106* (25), 256103-1–256103-4.
[24] Zhu, L.; Jona, J.; Nagapudi, K.; Wu, T. Fast Surface Crystallization of Amorphous Griseofulvin Below T_g. *Pharm. Res.* **2010**, *27* (8), 1558–1567.
[25] Zhang, S.; Lee, T. W. Y.; Chow, A. H. L. Crystallization of Itraconazole Polymorphs from Melt. *Cryst. Growth Des.* **2016**, *16* (7), 3791–3801.
[26] Lemercier, A.; Viel, Q.; Brandel, C.; Cartigny, Y.; Dargent, E.; Petit, S.; Coquerel, G. Optimization of Experimental Conditions for the Monitoring of Nucleation and Growth of Racemic Diprophylline from the Supercooled Melt. *J. Cryst. Growth* **2017**, in press.
[27] Viel, Q.; Brandel, C.; Cartigny, Y.; Eusébio, M. E. S.; Canotilho, J.; Dupray, V.; Dargent, E.; Coquerel, G.; Petit, S. Crystallization from the Amorphous State of a Pharmaceutical Compound: Impact of Chirality and Chemical Purity. *Cryst. Growth Des.* **2017**, 17 (1), 337–346.

Conclusions and Prospects

Conclusions and Prospects

The amorphous state constitutes one of the most intriguing state of matter. It challenges our common understanding of the physicochemical properties of pharmaceutical molecular compounds. Indeed, the "universal" relationships between dynamics and crystallization tendencies of glass formers is still uncovered. With the aim of improving the knowledge about the behavior of chiral pharmaceutical drugs in the amorphous state, this work was devoted to the study of the effect of enantiomeric excesses on the amorphous DPL behavior.

An interesting situation was revealed during the study of the binary phase diagram between DPL enantiomers. Indeed, annealing DPL supercooled melts (SCM) with various enantiomeric compositions can induce the presence of two metastable solid solutions, namely RII from racemic and EII from enantiopure compositions.

The first part of this thesis was devoted to the evaluation of the exact role of enantiomeric composition on the glass-to-crystal pathway of DPL. For this purpose, a robust protocol has been established to ensure reliable observations and characterization of the glassy state to the supercooled liquid state through its glass transition. For the first time, the molecular mobility of the racemic mixture and a single enantiomer of amorphous DPL has been investigated by Broadband Dielectric Spectoscopy (BDS) covering a temperature range of more than 200 °C. Two distinct relaxation processes were detected for DPL molecules, labeled as: (i) α associated to the primary structural relaxation process of DPL and (ii) δ that are secondary relaxations presumably due to motions of the flexible part of DPL molecules. The comparative dielectric study of the purified samples proved that the dynamic behaviors of a single enantiomer and of the racemic DPL mixture are very similar. Besides, another secondary relaxation γ was found in samples containing Theophylline (TPH), the main impurity of DPL identified by chromatographic measurements. As a matter of fact, the γ-process occurred for impure materials (*i.e.* commercial racemic with 0.14 % *wt* TPH, synthesized enantiopure with 0.56 % *wt* TPH), as well as for the enriched racemic samples (+5.1 % *wt* TPH). A DPL/impurities unknown association may explain the emergence of this new γ-process.

Secondly, the objective was to provide a clear picture of the successive events occurring upon temperature-induced recrystallization from amorphous DPL samples. Two specific thermal profiles were applied to all enantiomeric compositions to provide a global view of the recrystallization behaviors (*i.e.* crystal form or polymorph selection, nucleation mode, and

morphologies). As stated above, the binary system formed by DPL enantiomers constitutes an illustration of the rich and diverse crystallization behavior that can be encountered among chiral pharmaceutical compounds. In the continuity of the previous investigations, the present study demonstrated that the crystallization from the SCM occurs as a complex multistep process illustrated in Figure 1. It involves the homogeneous nucleation and growth of a first population (PC: primary crystals) that acts as support for the development of secondary populations constituted of metastable solid solutions with higher growth rates. Some characteristics of PC can be highlighted: these initial particles exhibit a well-defined crystal shape but are of poor stability and convert into a more stable form. It was established that PC constitutes a "kinetic form" that nucleates easily from the SCM, whereas spontaneous nucleation of RII or EII is more difficult or kinetically hindered in the SCM. Besides, the systematic occurrence of PC at any enantiomeric composition indicated a poor chiral selectivity, *i.e.* a probable third solid solution in this system, even though it cannot be excluded that those particles consist of a conglomerate. Consequently, it suggests a fixed scheme in the crystallization mechanism, from which it can be deduced that preventing or delaying the crystallization from the SCM should primarily hinder the formation of this transient crystal form. More generally, this case study illustrates the necessity to obtain sufficient knowledge about the exact nature and nucleation conditions of the very first crystalline particles developing from an amorphous state.

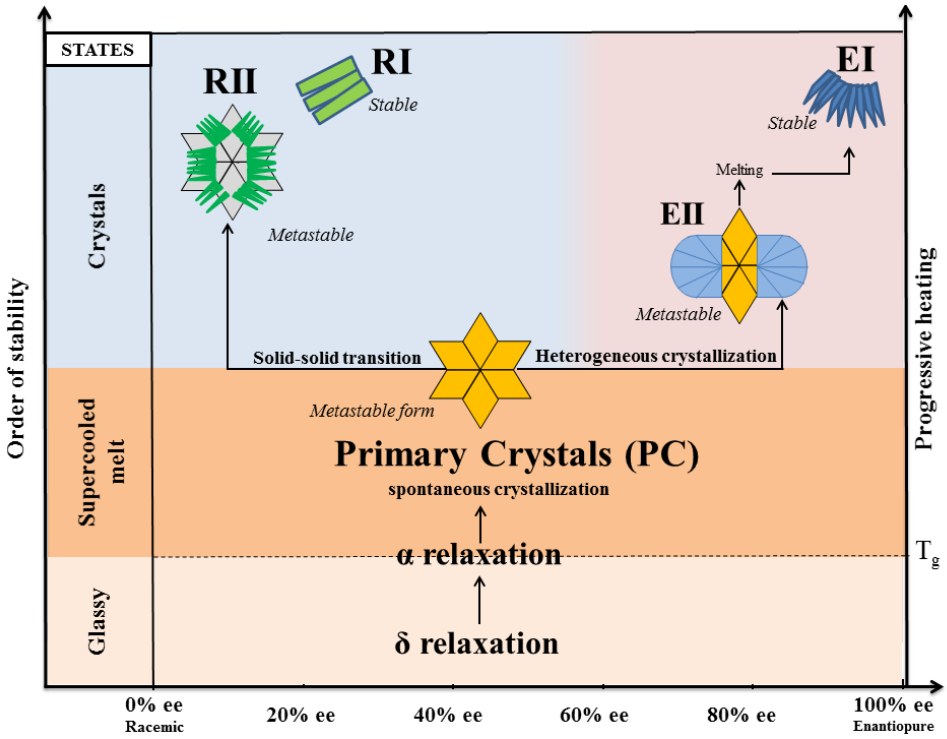

Figure 1. Scheme depicting the mechanisms of recrystallization from an initial glassy sample of DPL during a progressive heating.

Another parameter that needs to be considered is the "surface enhanced crystal growth" that could control crystallization abilities of glassy DPL. The conducted studies demonstrated that at various DPL enantiomeric compositions, the presence of interfaces (either PC/SCM and/or solid-vapor) favored the heterogeneous nucleation of a more stable form (*i.e.* EII, EI and/or RII). From our preliminary results about the surface-induced crystallization of amorphous DPL, crystallization in confined conditions (*e.g.* Spin-coating) would be interesting so as to stabilize the phases unstable in bulk states.

In order to propose an answer to the initial question, "*Considering the whole panel of enantiomeric compositions, are there preliminary signs of these distinct metastable forms in the amorphous state?"* and regarding the target sets, we can assess that:

i) Along the results obtained during this PhD thesis, it has been proved that the global molecular mobility in the glassy to the supercooled liquid state of DPL molecules is the same whatever the enantiomeric composition. Although spontaneous nucleation of the metastable primary crystals PC in the supercooled liquid state occurs whatever the enantiomeric composition, this transient crystal form has been found to be favored by a small amount of impurity content (mainly TPH). The latter has been detected in the glassy state with the emergence of a new secondary relaxation γ-process.

ii) Due to the impact of chemical purity on the molecular mobility of DPL, it could be significantly important for other borderline systems to pay peculiar attention to the chemical purity of the as-received samples prior to the study of dielectric or recrystallization behaviors from an amorphous state. The characterization of the first crystals obtained might be of major incidence, for example in order to manage adequately the physical stability of an amorphous pharmaceutical substance.

Extensions of this research are numerous, including the investigation of crystallization from the amorphous state of structurally related chiral compound such as Proxyphylline ($C_{10}H_{14}N_4O_3$), and/or other Xanthine derivatives (*e.g.* Etophylline …). Another perspective of this work would consist in conducting theoretical density functional theory (DFT) calculations, in order to gain insights into the origin of secondary relaxations in pure and enriched DPL.

Appendices

Appendix I : Experimental techniques

AI-1. Broadband Dielectric Spectroscopy (BDS)

Broadband Dielectric Spectroscopy (BDS) is a powerful technique to investigate the relaxation dynamics of various materials. It enables monitoring the molecular mobility as reflected in the relaxation processes over a wide frequency range up to 16 decades at various temperatures and pressures. The basic principle of BDS is based on investigating the motion of permanent dipoles present in material as an effect of applied alternating electric field E(ω). In the frequency range f = $\omega/2\pi$ of the electrical field E(ω), different phenomena can occur in the material: (i) the dielectric dispersion $\varepsilon'(\omega)$ and absorption $\varepsilon''(\omega)$ from dipole relaxation originating from reorientational motion of molecular dipoles that are described by the complex dielectric permittivity $\varepsilon^*(\omega) = \varepsilon'(\omega) - i\varepsilon''(\omega)$; and (ii) electrical conduction arising from the translational motions of electric charges and represented by the complex conductivity $\sigma^*(\omega) = \sigma'(\omega) + i\,\sigma''(\omega)$. The latter is related to the complex permittivity by the equation $\sigma^*(\omega) = i\,\omega\varepsilon_0\varepsilon^*$ (with ε_0 the vacuum permittivity) or the complex electric modulus $M^*(\omega) = M'(\omega) + iM''(\omega)$ related to the complex dielectric permittivity as $M^*(\omega) = 1/\varepsilon^*(\omega)$. The BDS technique measures the complex electrical impedance $Z^*(\omega)$ that is used to obtain the characteristic complex quantities ($\varepsilon^*(\omega)$, $\sigma^*(\omega)$, and $M^*(\omega)$) mentioned previously. For this purpose, a sinusoidal voltage $U^*(\omega)$ at a fixed frequency is applied to the sample:

$$U^*(\omega) = U_0 \exp(j(\omega t)) \quad (Eq\ I)$$

The current $I_S^*(\omega)$ in then measured across the sample:

$$I_S^*(\omega) = I_0 \exp(j(\omega t + \varphi)) \quad (Eq\ II)$$

Where φ is the phase shift between the applied voltage and measured current. Then, the value of the complex impedance $Z^*(\omega)$ is obtained by this expression:

$$Z^*(\omega) = \frac{U^*(\omega)}{I^*(\omega)} \quad (Eq\ III)$$

For a capacitor C* filled with a material, the complex dielectric permittivity ε^* is defined as:

$$\varepsilon^*(\omega) = \frac{C^*(\omega)}{C_0} \quad (Eq\ IV)$$

Where C_0 is the capacitance of the empty capacitor.

The capacitance of the empty capacitor can be expressed as [1]:

$$C_0 = \frac{\varepsilon_0}{d} S \ (Eq\ \mathrm{V})$$

Where ε_0 is the permittivity of vacuum, S is the surface of one electrode and d is the distance between the plates as depicted in Figure 1.

Thus, the complex permittivity (ε*) can be derived by measuring the complex impedance Z*(ω) of the sample:

$$\varepsilon^*(\omega) = \frac{1}{i\omega \mathrm{Z}^*(\omega) C_0} \ (Eq\ \mathrm{VI})$$

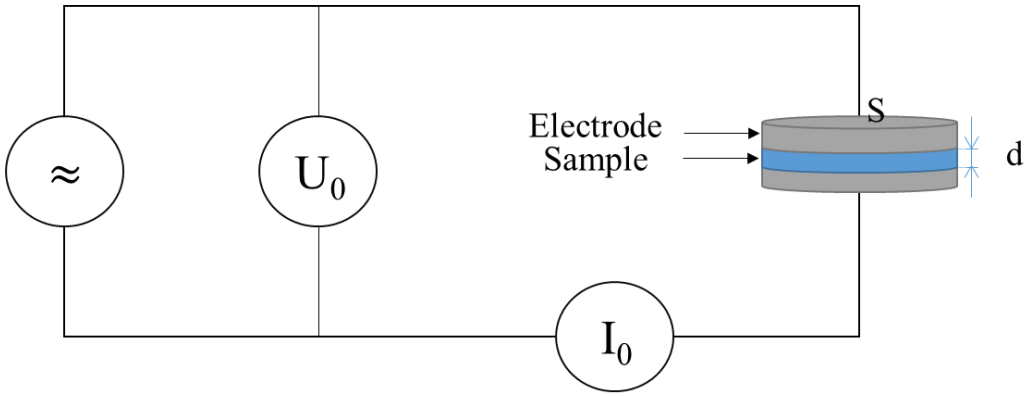

Figure 1: Schematic view of the measurement principle of dielectric spectroscopy

In this work, ambient pressure dielectric permittivity measurements were performed using 30 mm diameter stainless steel plated electrodes. The broadband dielectric converter (Alpha-A Analyzer from Novocontrol Technologies) allows the measurement of the complex dielectric permittivity (real and imaginary parts) in the frequency range 10^{-1} Hz to 10^{6} Hz. Non-isothermal dielectric spectra were collected over a wide temperature range from -140 °C to 100 °C with appropriate successive steps. The temperature control was carried out using the Quattro system (Novocontrol Technologies) to allow a temperature stability ± 0.2 °C. The sample was kept in a pure nitrogen atmosphere during the whole period of measurement. Amorphous samples were prepared *ex-situ* by the quench cooling technique. A small amount (around 250-300 mg) of powder was carefully sandwiched between the two parallel electrodes. A Teflon ring was used to align electrodes. The temperature was increased largely above the respective melting point of the compound (according to the protocol described in Chapter III 2-1). A totally amorphous compound was obtained by rapid quenching of the electrode to – 30 °C (T_g – 70 °C) before immediate analysis (in order to limit the influence of the atmospheric moisture). For each experiment, a fresh new amorphous sample was prepared and calibration was performed.

AI-2. Polarimetry and refractometry

The enantiomeric excess of a sample can be measured by refractometry and polarimetry. The optical rotation α of a sample (in general a solution), is measured by a polarimeter. The sample is placed in a measurement cell (a 10 cm long cylinder) thermostated at a temperature T and a monochromatic polarized light (wavelength λ) passes through the sample. A deviation of the plan of this polarized light occurs at an angle α_λ^T. By knowing the specific optical rotation of the pure enantiomer $[\alpha_\lambda^T]°$ (°.dm^{-1}.L.g^{-1}), the specific optical rotation of the sample $[\alpha_\lambda^T]$ can be deduced as well as the enantiomeric excess, with the following equation:

$$ee = \frac{[\alpha_\lambda^T]}{[\alpha_\lambda^T]°} = \frac{\alpha_\lambda^T}{c \times l \times [\alpha_\lambda^T]°} \ (Eq\ Ap.\text{VII})$$

where l is the length of the sample in which the polarized light passes through and c is the concentration (g.L^{-1}) of the sample (*i.e.* both enantiomers), which can be determined by refractometry using a calibration curve. In this work, we used a Mettler Toledo RE50 refractometer and Perkin-Elmer 341 polarimeter (Figure 2).

Figure 2: Photography of the polarimeter (left) and the refractometer (right) used in this work.

AI-3. High Performance Liquid Chromatography (HPLC)

Chromatographic measurements were performed with a HPLC apparatus Dionex (LPG-3400SD, Courtaboeuf, France), equipped with a P680 pump, a manual injection valve (20 µL), and a UV-vis detector (VWD-3100). The data were collected with a computer using the Chromeleon software from Dionex (Courtaboeuf, France). The column was a Luna C18 (150 x 4,6 mm x 3 µm) and the mobile phase was composed of acetonitrile-water with phosphoric acid (0.1 %), (5:95 (*v/v*), pH 3.5). The temperature was set at 22 °C, and the flow rate was 1 mL/min. The detection wavelength was 271 nm. Theophylline (TPH) was found as the major impurity for all our samples. In the above conditions, TPH and DPL retention times were found to be 17.4 and 22.3 min, respectively. The quantity of TPH was determined as 0.14 % *wt* for commercial racemic DPL batch, 0.52 % *wt* for enantiopure DPL synthesized, and less than 0.03 % *wt* for both after purification.

I) Motivations for accurate determination of TPH in DPL

As previously discussed, impurities may affect the molecular mobility of the molecule studied, justifying the need of purification before further rationalizing the experimental phenomena. Some impurities have been listed in the pharmacopoeia such as TPH, Etophylline and Proxyphylline. The following part is dedicated to the precise determination of those impurities, and especially for TPH that was found to be the major one.

The most straightforward way to assign peaks within the chromatogram is to inject standard solutions under identical analytical conditions and compare the retention factor (k)(Figure 3).

$$k_A = \frac{t_{R_A} - t_0}{t_0} \quad (Eq\ Ap.\text{VIII})$$

With t_{R_A} the retention time of the solute A, and t_0 the dead time.

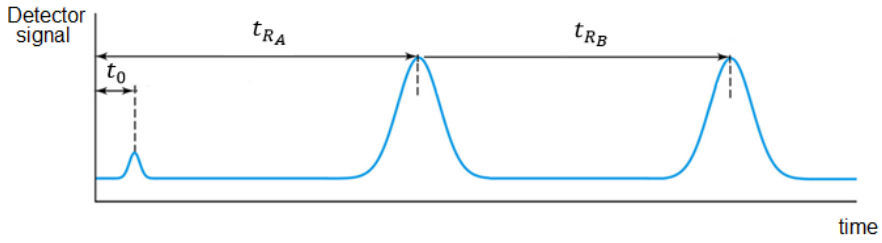

Figure 3: Standard chromatogram of two solutes

A quantitative analysis involves many steps that could be summarized as follows:

- ✓ Knowing the compound to be analyzed (TPH)

- ✓ Establishing a method to analyze samples containing this compound
- ✓ Analyzing a set of calibration solutions of the standard sample (TPH) at known concentrations to obtain the response due to that concentration
- ✓ Analyzing the sample containing an unknown concentration of the compound (TPH in DPL samples) to obtain the response due to the unknown concentration
- ✓ Comparing it to the response of the known concentration of the standard to determine the concentration in the sample

To obtain a valid comparison for the unknown sample response to that of the known standard, the data must be acquired and processed under identical conditions (*i.e.* analytical conditions and integration method). It has to be noticed that if a wide concentration range is to be measured in the samples, a multi-level calibration has to be done to ensure good accuracy in the determination of the amount of the compound in the sample. Also, the accuracy of the quantitation is strongly influenced by the resolution of the peaks (*i.e.* the separation between two consecutive peaks of approximately same magnitude) and the state of the baseline surrounding the peaks of interest. Well separated peaks can be easily and reproducibly integrated because other peaks do not influence the height and area. In our case, it was necessary to find analytical conditions allowing to have a good separation between DPL and TPH in a reasonable analysis time. UV detection was used and the peak areas allowed for obtaining the quantitative calculations.

II) Calibration of TPH

The first step was to analyze TPH at a known concentration to obtain the response due to that concentration. For that purpose, stock solutions at 100 mg/L and 10 mg/L were prepared in water. The standard solutions (from 0.200 to 3.205 mg/L) were obtained by dilution with water, and analyzed at the optimized analytical conditions (Column Luna C18 150 mm × 4.6 mm ×3 µm. Acetonitrile-water with phosphoric acid (0.1 %), (5:95 (*v/v*), pH 3.5, T = 22 °C, UV = 271 nm.). In those conditions, TPH and DPL retention times were found to be 17.4 and 22.3 min, respectively. The results of the calibration are presented in Table 1 and Figure 4.

Table 1. Concentration of TPH and the corresponding absorbance under the analytical conditions: Column Luna C18 150 mm × 4.6 mm ×3 µm. Acetonitrile-water with phosphoric acid (0.1%), (5:95 (v/v), pH 3.5, T = 22 °C, UV = 271 nm.)

X (concentration in mg/L)	Y (Absorbance in mAU)
0.020	0.10000
0.267	0.51160
0.801	1.38375
1.602	2.79165
2.671	4.62940
3.205	5.56720

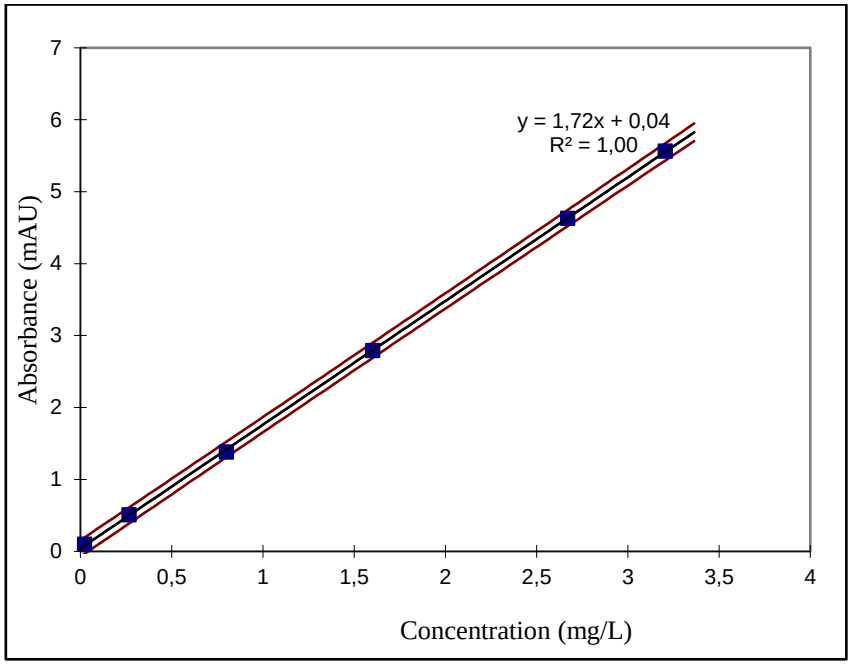

Figure 4: Calibration of TPH. Analytical conditions: Column Luna C18 150 mm × 4.6 mm ×3 µm. Acetonitrile-water with phosphoric acid (0.1 %), (5:95 (v/v), pH 3.5, T = 22 °C, UV = 271 nm).

AI-4. X-Ray Powder Diffraction (XRPD)

Routine XRPD analyses were performed using a D8 diffractometer (Bruker, Germany) equipped with a LinxEye detector and a modified goniometer of reverse-geometry (-θ/-θ). The tube voltage and amperage were 40 kV and 40 mA respectively and the CuKα radiation with λ= 1.54059 Å was used. XRPD analyses were performed with a step of 0.04° (2θ), from 3 to 50° (2θ). For analysis of thin DPL samples recrystallized from the supercooled melts, lamellar samples (with a few µm thickness) were covered with a Kapton film before recording their XRPD patterns.

AI-5. Classical Differential Scanning Calorimetry (DSC)

Routine Classical DSC experiments on crystalline and amorphous samples were performed using a Netzsch DSC 214 Polyma apparatus equipped with an intracooler. Each DSC run was performed with 5-6 mg of a powdered sample in 25 µL aluminum pans with closed lids. The atmosphere of the analyses was regulated by a Nitrogen flux (50 mL/min). The temperature and enthalpy calibration were performed (at the defined heating rate) with certified standards (adamantane, indium, tin, bismuth and zinc). Onset temperatures are calculated from the intersection between the baseline and the slope of the first part of the endotherm. The Netzsch – TA Proteus Software v6.1.0 was used for data processing.

AI-6. Thermogravimetric Analysis coupled with DSC (TG-DSC)

For the preliminary control of thermal stabilities, simultaneous thermogravimetric (TG), and differential scanning calorimetry (DSC) analyses were performed using a Netzsch STA 449 C instrument. Each run was performed with 5−6 mg of a powdered sample in a 25 µL aluminum crucible and heated at a rate of 5 °C/min from 20 to 290 °C, with helium as purging gas.

AI-7. Temperature Modulated Differential Scanning Calorimetry (TM-DSC)

Temperature-modulated (TM-DSC) measurements were performed either with a TA Instrument Q100 DSC or Q2000 DSC coupled with a liquid nitrogen cooling system. The calorimeter was first calibrated in temperature and energy with the standard values of zinc and indium melting points. Then, specific TM-DSC calibration was performed using sapphire as reference to calibrate the specific heat capacity signal. The DPL sample mass was in the range 7-8 mg, and the "heat only protocol" was used with a heating rate of 2 K/min, a modulation amplitude of 0.318 K and a modulation period at 60 seconds. The TA Universal Analysis Software was used for data processing.

AI-8. Hot & Cold Stage Microscopy (HSM, CSM)

Quantities in the range 1-3 mg of powdered samples were first on a microscope slide and heated up to complete melting in a hot stage setup (Mettler FP90). A cover slide (heated at the same temperature) was carefully deposited on the molten sample. After fast cooling of the thin film sample (Liquid nitrogen was used as the refrigerant for cooling ramp down to 15 °C and the nitrogen flux into the cell was regulated via an automatic pump), recrystallization was monitored at controlled temperature using the hot stage coupled to a microscope (Nikon

Optiphot-2, maximum magnification ×40) in cross polarization mode and image captures were performed with a CCD camera (Digital Sight DS Fi2, Nikon).

AI-9. Raman Spectroscopy

Raman analyses were carried out with a Confocal Raman Microscope (LabRam HR by Jobin-Yvon Horiba) coupled to an optical microscope (Model BX41, Olympus) with xyz mapping stage. The excitation of Raman scattering was operated by a He-Ne laser at a wavelength of 632.8 nm. For this study, the laser beam was focused on the sample placed between a glass slide and a cover slide, by a microscope objective ×50 LWF. The Raman signal was analyzed using a confocal pinhole of 400 µm and 600 lines per mm grating. The selected spectral resolution was 4 cm^{-1}. In order to minimize the background signal, the duration of data collection was adjusted in the range 10-20 s. Temperature regulation was ensured by using a linkam TMS 94 programmer with liquid N_2 as a cooling source.

Appendix II:

AII-1. TM-DSC out-of-phase raw data

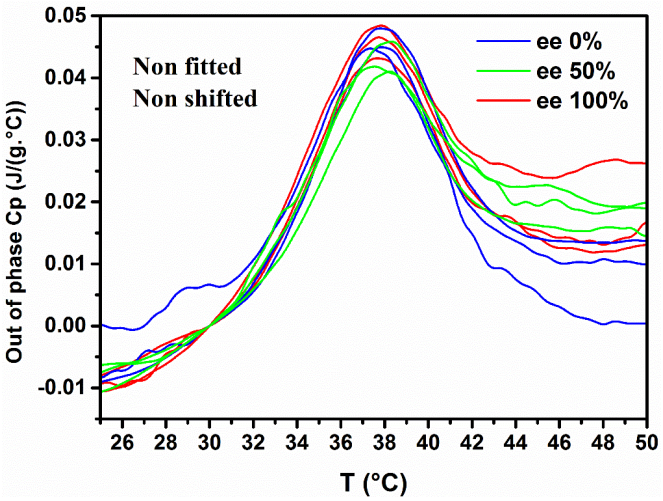

Figure 5. Out-of-phase C_p'' obtained for samples from compositions 0, 50, 100% ee (2 K/min, amp= 0. 318 K, p= 60 s, endo up).

AII-2. Density determination

The displacement method is a procedure for density determination on solids based on the Archimedean Principle. The beaker is placed on the pan of the balance and the sample-holding device is immersed in the liquid, to the same depth that it will later be immersed with the sample on it. The weighing instrument is tared. The sample is placed next to the beaker on the weighing pan. The mass of the sample in air $m(a)$ is determined. The sample is placed in the holding device on the stand and immersed in the liquid. The weight readout shows the mass of the displaced liquid m_{fl}.

The density of the sample ρ is calculated according to the following equation:

$$\rho = \rho_{fl} \frac{m(a)}{m_{fl}} \quad (Eq\ Ap.\ \text{IX})$$

AII-3. Purification procedures

Due to the synthesis procedure, the solid may contain traces of KCl and of impurities such as TPH, which can be removed by means of cooling recrystallization. Racemic DPL was purchased from Sigma Aldrich (USA, purity 99%), anhydrous TPH was purchased from

Acros Organics (Thermo Fisher Scientific, purity > 99%), and all solvents used (Fisher Scientific) were of analytical grade. Purity checks by chromatographic analyses were performed by HPLC. The amount of TPH in as received DPL is 0.14 % wt whereas commercial TPH was found almost free of impurities. For the enantiomer synthesized as for the commercial racemic compound, the same purification procedure was applied. The solid is slurried under magnetic stirring for 24 h in ethanol/water mixture 95:5 (*v/v*) under ambient conditions. After filtration, the pure product is dried in an oven at 50 °C and ground with a mortar and a pestle.

Appendix III: European Pharmacopoeia of Diprophylline

01/2012:0486

DIPROPHYLLINE

Diprophyllinum

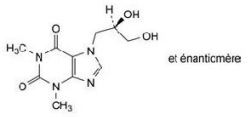

et énanticmère

$C_{10}H_{14}N_4O_4$ M_r 254,2
[479-18-5]

DÉFINITION

7-[(2*RS*)-2,3-Dihydroxypropyl]-1,3-diméthyl-3,7-dihydro-1*H*-purine-2,6-dione.

Teneur : 98,5 pour cent à 101,0 pour cent (substance desséchée).

CARACTÈRES

Aspect : poudre cristalline blanche ou sensiblement blanche.

Solubilité : facilement soluble dans l'eau, peu soluble dans l'éthanol à 96 pour cent.

IDENTIFICATION

Spectrophotométrie d'absorption dans l'infrarouge (*2.2.24*).

Comparaison : *diprophylline SCR*.

ESSAI

Solution S. Dissolvez 2,5 g de diprophylline dans de l'*eau exempte de dioxyde de carbone R* et complétez à 50 mL avec le même solvant.

Aspect de la solution. La solution S est limpide (*2.2.1*) et incolore (*2.2.2, Procédé II*).

Acidité ou alcalinité. A 10 mL de solution S, ajoutez 0,25 mL de *solution de bleu de bromothymol R1*. La solution est jaune ou verte. Le virage au bleu de l'indicateur ne nécessite pas plus de 0,4 mL d'*hydroxyde de sodium 0,01 M*.

Substances apparentées. Chromatographie liquide (*2.2.29*).

Solution à examiner. Dissolvez 50 mg de diprophylline dans de l'*eau R* et complétez à 50,0 mL avec le même solvant.

Solution témoin (a). Prélevez 1,0 mL de solution à examiner et complétez à 100,0 mL avec de l'*eau R*. Prélevez 1,0 mL de cette solution et complétez à 10,0 mL avec de l'*eau R*.

Solution témoin (b). Dissolvez 5 mg d'*étofylline SCR* (impureté C) dans de l'*eau R* et complétez à 50,0 mL avec le même solvant. Prélevez 0,5 mL de solution et complétez à 20,0 mL avec la solution à examiner.

Colonne :

- *dimensions* : *l* = 0,15 m, Ø = 4,6 mm,
- *phase stationnaire* : *gel de silice octadécylsilylé pour chromatographie, à groupements polaires incorporés, postgreffé R* (3 µm),
- *température* : 30 °C.

Phase mobile : *méthanol R, eau R* (10:90 *V/V*).

Débit : 0,7 mL/min.

Détection : spectrophotomètre à 272 nm.

Injection : 10 µL.

Enregistrement : 3 fois le temps de rétention de la diprophylline.

Rétention relative par rapport à la diprophylline (temps de rétention = environ 18 min) : impureté C = environ 1,1.

Conformité du système : solution témoin (b) :

- *rapport pic/vallée* : au minimum 5, avec H_p = hauteur au-dessus de la ligne de base du pic dû à l'impureté C et H_v = hauteur au-dessus de la ligne de base du point le plus bas du tracé entre ce pic et celui dû à la diprophylline.

Limites :

- *impuretés non spécifiées* : pour chaque impureté, au maximum la surface du pic principal du chromatogramme obtenu avec la solution témoin (a) (0,10 pour cent),
- *total* : au maximum 3 fois la surface du pic principal du chromatogramme obtenu avec la solution témoin (a) (0,3 pour cent),
- *limite d'exclusion* : 0,5 fois la surface du pic principal du chromatogramme obtenu avec la solution témoin (a) (0,05 pour cent).

Chlorures (*2.4.4*) : au maximum 400 ppm.

Prélevez 2,5 mL de solution S et complétez à 15 mL avec de l'*eau R*.

Métaux lourds (*2.4.8*) : au maximum 20 ppm.

12 mL de solution S satisfont à l'essai A. Préparez la solution témoin avec la *solution à 1 ppm de plomb (Pb) R*.

Perte à la dessiccation (*2.2.32*) : au maximum 0,5 pour cent, déterminé à l'étuve à 105 °C sur 1,000 g de diprophylline.

Cendres sulfuriques (*2.4.14*) : au maximum 0,1 pour cent, déterminé sur 1,0 g de diprophylline.

DOSAGE

Afin d'éviter un échauffement trop important du milieu réactionnel, mélangez soigneusement pendant le titrage et arrêtez le titrage immédiatement après le point de fin de titrage.

Dissolvez 0,200 g de diprophylline dans 3,0 mL d'*acide formique anhydre R* et ajoutez 50,0 mL d'*anhydride acétique R*. Titrez par l'*acide perchlorique 0,1 M*. Déterminez le point de fin de titrage par potentiométrie (*2.2.20*).

1 mL d'*acide perchlorique 0,1 M* correspond à 25,42 mg de $C_{10}H_{14}N_4O_4$.

CONSERVATION

A l'abri de la lumière.

IMPURETÉS

Autres impuretés décelables (si elles sont présentes à une teneur suffisante, les substances suivantes seront détectées par l'un des essais de la monographie. Elles sont limitées par le critère général d'acceptation applicable aux autres impuretés ou impuretés non spécifiées, ou par les dispositions de la monographie générale *Substances pour usage pharmaceutique (2034)*. Il n'est donc pas nécessaire de les identifier pour démontrer la conformité de la substance. Voir également chapitre *5.10. Contrôle des impuretés dans les substances pour usage pharmaceutique*) : *A, B, C, D*.

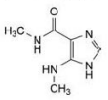

A. *N*-méthyl-5-(méthylamino)-1*H*-imidazole-4-carboxamide (théophyllidine),

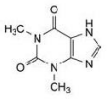

B. 1,3-diméthyl-3,7-dihydro-1*H*-purine-2,6-dione (théophylline),

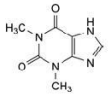

C. 7-(2-hydroxyéthyl)-1,3-diméthyl-3,7-dihydro-1*H*-purine-2,6-dione (étofylline),

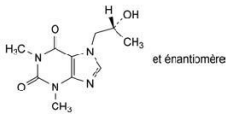

D. 7-[(2*RS*)-2-hydroxypropyl]-1,3-diméthyl-3,7-dihydro-1*H*-purine-2,6-dione (proxyphylline).

References:

[1] Kivelson, S.A.; Tarjus, G. In search of a theory of supercooled liquids. *Nat. Mater.* **2008**, *7* (11), 831-833.

[2] Coquerel, G.; Sanselme, M.; Lafontaine, A. Method and measuring scattering of X-Rays, its applications and implementation device. Patent WO2012/136921 A1, **2012**.

During the last few decades, the field of crystal engineering has gained prominence. Along with the improvement of analytical techniques, the understanding and prediction of crystal structures become more and more accurate. The present work is dedicated to one of the borderline cases encountered that challenge the general understanding of crystallography, polymorphism, phase transition theories and chiral discrimination mechanisms. The chiral pharmaceutical drug diprophylline is one of them, at least for crystallization aspects. Both racemic and enantiopure compositions of this system at the amorphous state have been considered, to carefully study the kinetic transitions with respect to the global molecular mobility. A robust protocol has been established to investigate the molecular mobility by broadband dielectric spectroscopy covering a temperature range of more than 200 °C. The comparative dielectric study of the purified samples proved that the dynamic behaviors of a single enantiomer and of the racemic mixture are very similar; but another secondary relaxation γ was found in samples containing theophylline, the main impurity identified by chromatographic measurements. Additionally, the present study demonstrated that the crystallization from the supercooled melt occurs as a complex multistep process. It involves the homogeneous nucleation and growth of a first population, whose characteristics are highlighted, and which acts as support for the development of secondary populations constituted of metastable solid solutions with higher growth rates. Moreover, the conducted studies demonstrated that at various enantiomeric compositions, the presence of interfaces favored the heterogeneous nucleation of a more stable form.

Au cours des dernières années, le domaine de la cristallisation a pris de l'importance. Avec l'amélioration de techniques analytiques, la compréhension et la prédiction de structures cristallines deviennent plus précises. Ce travail porte sur l'un des cas limites répertoriés, qui défient la compréhension de la cristallographie, du polymorphisme, des théories de transition de phases et des mécanismes de discrimination chirale. La diprophylline est une molécule chirale d'intérêt pharmaceutique, et rentre dans cette catégorie de cas limites, au moins en ce qui concerne le comportement à la cristallisation. Les compositions énantiomérique et racémique de ce système à l'état amorphe ont été traitées, afin de soigneusement étudier les transitions cinétiques en lien avec la mobilité moléculaire globale. Un protocole robuste a été élaboré afin d'étudier la mobilité moléculaire par spectroscopie diélectrique, en couvrant une gamme de température de 200 °C. L'étude comparative des échantillons purifiés a démontré que le comportement dynamique d'un seul énantiomère et du mélange racémique était très similaire. Une autre relaxation secondaire γ a été trouvée pour les échantillons contenant de la théophylline, l'impureté majeure détectée par chromatographie. De plus, cette étude démontre que la cristallisation depuis l'état vitreux se déroule en plusieurs étapes complexes. Il s'agit d'abord de la nucléation homogène et croissance d'une première population de cristaux, dont les caractéristiques sont détaillées, et qui agit comme support pour le développement de populations secondaires constituées de solutions solides métastables ayant des cinétiques de croissance plus élevées. Ces études démontrent également que la présence d'interfaces favorise la nucléation hétérogène de formes plus stables, et ce à différents taux énantiomériques.